

# Fault Detection and Monitoring using an Information-Driven Strategy: Method, Theory, and Application

Camilo Ramírez <sup>a</sup>, Jorge F. Silva <sup>a</sup>, Ferhat Tamssaouet <sup>b</sup>, Tomás Rojas <sup>a</sup>, Marcos E. Orchard <sup>a</sup>

<sup>a</sup>Information and Decision Systems Group, Department of Electrical Engineering, University of Chile, Santiago, Chile

<sup>b</sup>PROMES-CNRS, UPVD, Perpignan, France

---

## Abstract

The ability to detect when a system undergoes an incipient fault is of paramount importance in preventing a critical failure. In this work, we propose an information-driven fault detection method based on a novel concept drift detector. The method is tailored to identifying drifts in input-output relationships of additive noise models – i.e., model drifts – and is based on a distribution-free mutual information (MI) estimator. Our scheme does not require prior faulty examples and can be applied distribution-free over a large class of system models. Our core contributions are twofold. First, we demonstrate the connection between fault detection, model drift detection, and testing independence between two random variables. Second, we prove several theoretical properties of the proposed MI-based fault detection scheme: (i) strong consistency, (ii) exponentially fast detection of the non-faulty case, and (iii) control of both significance levels and power of the test. To conclude, we validate our theory with synthetic data and the benchmark dataset N-CMAPSS of aircraft turbofan engines. These empirical results support the usefulness of our methodology in many practical and realistic settings, and the theoretical results show performance guarantees that other methods cannot offer.

*Keywords:* Fault detection, Concept drift, System monitoring, Mutual information, Independence testing, Turbofan engine

---

## 1. Introduction

The objective of Prognostics and Health Management (PHM) is to provide methodologies and tools for creating tailored maintenance plans based on the specific characteristics, operations, and degradation scenarios of a given asset [1]. This approach aims to achieve optimal system availability while minimizing costs, representing a comprehensive and efficient strategy for system health management. PHM integrates Fault Detection and Isolation (FDI), health management, and prognostic capabilities, including Remaining Useful Life (RUL) prediction, to provide insights into current system conditions [2].

Fault Detection and Isolation (FDI) is primarily concerned with identifying when a fault occurs, understanding its characteristics, and pinpointing its location within a system. Degradations are unavoidable phenomena within systems, which can be divided into incipient failures and critical failures. Incipient failures can be defined as alterations that do not prohibit the system from operating, whereas critical failures occur when degradation levels result in the system not operating as required [3]. As a consequence, the detection of incipient failures is subject to exhaustive study, especially in complex and multivariate systems [4], and is of paramount importance because early detection of incipient failures can enable maintenance plans to be created that prevent the occurrence of a critical failure [2].

The literature offers a diverse range of FDI methods [5], which can be classified into two approaches: model-based and data-driven. Initially, FDI efforts focused on model-based approaches such as eigenstructure assignment [6], parity-based methods [7], parameter identification-based methods [8], observer-based methods [9], and structural graphs (e.g., bond graph [10] and Petri net [11]). These methods are based on the idea of comparing system outputs with failure models and comparing this difference with a threshold; then, a fault is detected when the value of the difference exceeds the threshold [12]. However, in the presence of significant noise or an unknown noise distribution, these methods may have poor performance and make the task of determining the most adequate fault decision threshold difficult [12, 13]. Set-membership methods, where a set of models is generated for the system, emerge to overcome these limitations; in these methods, a fault is detected whenever a measurement is inconsistent with any of the members of this set [14]. However, the computational cost scales exponentially with the number of uncertain parameters [15], which is the case for complex systems. Overall, model-based methods are effective for simple systems whose phenomenology can be understood and represented by explicit mathematical models; although providing accurate and interpretable results, they are challenging to implement for complex systems [16].

Data-driven approaches, which contrast with model-based approaches, are also prevalent in the current literature. These phenomenological-agnostic methods involve performing mathematical or statistical operations on measurements or training neural networks using measurements to extract information

---

*Email addresses:* camilo.ramirez@ug.uchile.cl (Camilo Ramírez ) , josilva@ing.uchile.cl (Jorge F. Silva ) , ferhat.tamssaouet@univ-perp.fr (Ferhat Tamssaouet ) , tomas.rojas.c@ug.uchile.cl (Tomás Rojas ) , morchard@ing.uchile.cl (Marcos E. Orchard )

from the system and predict faults. The information is obtained through measured signals and their conversion into fault-characterizing features through time or frequency transformations, or by leveraging prior knowledge of signal distribution [4, 17]. Machine fault detection and diagnosis, particularly in rotating machinery, employ various methods for data collection, such as vibration monitoring and thermal imaging [18]. The collected data undergoes processing using methods like spectral analysis, wavelet analysis, short-term Fourier transform, and others, contributing to a comprehensive root cause failure analysis. The processed data can then be directly used for fault detection by setting fixed [19] or adaptive thresholds [20]. As the system state is generally not directly measurable from data, two approaches are used for its estimation: statistical and non-statistical. Statistical methods, such as Kalman filter [21], principal component analysis [22], among others, excel in rapid fault detection for linear systems but may not be optimal for diagnosis and for detection in non-linear or non-Gaussian systems. The non-statistical data-driven methods involve using mathematical classification models from supervised learning methods. Techniques like the k-nearest neighbors algorithm (kNN) [23] and Support Vector Machines (SVMs) [24] are employed. Despite their effectiveness, SVMs are sensitive to initial parameters, necessitating a parameter-tuning process for each signal dataset. Artificial Neural Networks (ANNs) are widely utilized for their self-learning capabilities and automatic feature extraction; however, they may tend to over-fit the training set, requiring regularization terms and prior knowledge for enhanced performance [25]. Recent advancements in ANNs and the adoption of deep learning algorithms have led to the development of novel classification models for fault detection and diagnosis [26]. Deep learning architectures such as Convolutional Neural Networks, Deep Belief Networks, Restricted Boltzmann Machines, and Autoencoders have performed successfully in various industrial applications, including gearboxes, mechanical bearings, compressors, wind and gas turbines, and steel plates [27]. These deep learning models offer the ability to learn complex structures from datasets, although they require larger samples and longer processing times to achieve higher accuracy.

Compared to model-based methods, data-driven approaches are generally easier to implement but have disadvantages such as the lack of interpretability and uncertainty management [16]. In addition, it is difficult to obtain data that identifies all possible faulty operations; moreover, conducting run-to-failure experiments is not possible for complex systems where creating a fault database is prohibitively expensive or impossible for safety reasons. To overcome this problem, behavioral models can be used. Indeed, modern systems are increasingly relying on behavioral models, such as AI-based models, for monitoring and control. The emergence of digital twins is notable in this sense [16]. These models are constructed from data gathered with diverse sensors facilitated by the development of the Industrial Internet of Things (IIoT).

Behavioral models are designed to capture the statistical dynamics of the system. These dynamics depend on whether the system is being subjected to a fault or not. In this context,

faults imply an alteration – namely, a drift – of the statistical relationships expressed in the system variables [28]. As a consequence, a link between detecting faults and statistical drifts arises [29, 30]. Concept drift, a widely-used term in the literature, occurs when the distribution of a stochastic phenomenon changes over time [31, 32]. Much work has been done in the area of concept drift [32, 33] but using different names such as data shift [34] and anomaly detection [35]. Approaches for detecting drifts can be supervised or unsupervised. Supervised methods, such as the one described in [35], rely on the availability of anomalous data, which is a restriction in scenarios where this data is scarce or expensive [36]. Unsupervised methods are commonly based on error rates and compute  $p$ -values for the observations as a measure of their abnormality [32]. We highlight DMM [29], ADWIN [37], and STEPD [38] as popular error-based methods, but they have the disadvantage of assuming discrete targets, and consequently, they are not suitable for monitoring continuous variables. In [33], a variety of regression-suited learning methods are shown, but they are used in adaptive scenarios and are restricted to their algorithm category as seen in [33, Table 6]; hence, they cannot be used in already-deployed models or in problems with modeling more complex than their base algorithm.

In the current landscape, behavioral models offer real advantages for FDI. This approach is particularly attractive as it does not assume a history, making it applicable to new or critical systems. However, there are several open challenges, which include (i) the nonexistence or scarcity of faulty data, which makes the supervised methods inoperable, (ii) the lack of decision guarantees for the majority of existing methods, particularly in complex multi-variate non-linear and non-Gaussian systems, and (iii) the inability to work with already-deployed behavioral models not necessarily dedicated to FDI. In addition, one can observe a link in the literature between concept drift detection and FDI, but we do not observe a formal connection between results found in concept drift literature and its applications to FDI.

### 1.1. Contributions of this Work

We propose a novel data-driven fault detection strategy leveraged by a concept drift theory tailored to capture input-output relationship (model) drifts within the system. Remarkably, our method does not require the availability of previous faulty data and is agnostic to learning algorithms, expert modeling, and data distributions, which makes it applicable to a large family of scenarios. Our key contributions are as follows:

- We establish a formal framework that links the fault detection (FD) task with a kind of concept drift (model drift) detection that is especially suited to address alterations in input-output relationships. We develop a theoretical proof demonstrating the equivalence between testing model drift and testing independence between a regression input and its residual for the rich class of additive noise models.
- We introduce the use of a non-parametric mutual information estimator [39, 40] to perform model drift detec-

tion. We prove that the resulting scheme is strongly consistent (asymptotic expressiveness for model drift detection), has finite-length performance guarantees, and has a specific vanishing error convergence rate.

- We complement our theoretical and methodological contributions with numerical analyses on controlled (synthetic) scenarios and in the realistic benchmark dataset of turbofan engines N-CMAPSS [41]. Our empirical findings support the practical capabilities of our method in complex fault detection settings.

### 1.2. Related Works

Some related works use mutual information (MI) in their fault detection pipeline, but most use MI to select features (e.g., [42]) or to circumvent the high-dimensionality of the process (e.g., [43, 44]). An exception is the work of Lv et al. [45]; in that work, they proposed to monitor the statistics of a component-pairwise MI estimation matrix of all variables involved in the system to detect faults and identify the variables associated with the fault by checking deviations, in testing time, from the values of the statistics observed in a healthy scenario.

From the basic fact that MI is used, all the previously mentioned works ([42, 43, 44, 45]) might appear to be related to the method presented in this paper; However, there are essential differences worth mentioning. From a formulation perspective, our work is constructed from a novel theory – developed in this paper – that connects model drift detection with independence testing. Notably, this formal path justifies the adoption of MI to detect input-output deviations within a system and, consequently, the usage of MI features as health indicators, which strongly quantify the fault severity; this is a guarantee that is not present in any of the mentioned methods. Moreover, our methodology offers unique performance guarantees that are not offered by other methods.

### 1.3. Paper Outline

The outline of the remainder of our work is as follows. In Sec. 2, we introduce the model drift detection task, state its link with fault detection, and introduce definitions useful for the rest of the work. In Sec. 3, we formalize model drift and show the equivalence between testing model drift and testing independence (Theorem 1). In Sec. 4, our new methodology to perform model drift detection and, consequently, fault detection is introduced. In Sec. 5, we show a regime of parameters in which our methodology has the following desirable properties: strong consistency (Theorem 2), exponentially-fast decision convergence on healthy systems (Theorem 3), and error convergence guarantees (Theorem 4). In Sec. 6, we discuss our methodology and its properties. In Sec. 7, we apply our method to a diversity of synthetic-defined systems, visualizing and validating our theoretical development, and in Sec. 8, we apply it to the N-CMAPSS dataset, a benchmark dataset of realistic simulations of turbofans; with this, we demonstrate our method’s capability to detect faults in a real-life application. Finally, in Sec. 9, we summarize our contributions and propose directions for future research.

## 2. Preliminaries

In this section, we describe our main decision problem related to fault detection, state general definitions, and introduce the concept of mutual information.

### 2.1. Fault Detection as a Model Drift Detection Task

In this paper, we deal with system monitoring from a behavioral data-driven approach. This means that data obtained from a system is treated as realizations of the random variables that compose the system. In this setting, each variable of the system corresponds to a random variable, and the system as a whole is described by the joint distribution of the random vector built upon all the system’s variables.

Concept drift corresponds to an arbitrary change in the statistical properties of a certain phenomenon over time [32]. Moreover, when considering an explanatory-response relationship between two random vectors  $X$  and  $Y$ , their joint distribution  $(P_{X,Y})$  can be decomposed into the product of the explanatory-marginal distribution  $(P_X)$  and the predictive distribution  $(P_{Y|X})$ , i.e.,  $P_{X,Y} = P_X \cdot P_{Y|X}$ . Then, we can distinguish between *virtual drifts* (changes in  $P_X$ ) and *actual drifts* (changes in  $P_{Y|X}$ ) [46].

A fault event within a system implies an alteration in its inner dynamics, which leads to a disturbance in the predictive distribution of the response given the explanatory variables  $(P_{Y|X})$ ; i.e., a fault is an event that leads to an actual drift. In contrast, a model drift can have different origins, which include changes in operational parameters, replacement of sub-components of a system, and faults. In this context, we can define any unwanted alteration of the inner dynamics of a system as a fault. Therefore, in a setting where no desired alterations are being made to a system, we can establish an equivalence between the existence of a fault and the existence of an actual drift.

In Sec. 3, we show how this drift can be decoupled into drifts on the underlying deterministic explanatory-response relationship (*model drift*) and drifts on the noise model (*noise drift*), and consequently, how the fault-drift equivalence reduces to the equivalence between fault existence and model drift existence. Taking this equivalence into consideration, we propose an information-driven model drift detection method to implement a data-driven fault detector.

### 2.2. Model Drift Detection

Let us consider two random vectors (r.v.s)  $X$  and  $Y$ , whose distributions might change over time, taking values in  $\mathcal{X}$  and  $\mathcal{Y}$ , respectively. Formally, we say that the r.v.  $(X, Y)$  has a *nominal* distribution  $P_{X,Y} \in \mathcal{P}(\mathcal{X} \times \mathcal{Y})$  and an *actual* distribution  $P'_{X,Y} \in \mathcal{P}(\mathcal{X} \times \mathcal{Y})$ .<sup>1</sup> As we are focusing on model drift (MD) detection, we need to distinguish between two statistical hypotheses: The null hypothesis ( $\mathcal{H}_0$  : the absence of MD), under which the actual distribution has the same underlying model

<sup>1</sup>The nominal distribution is the one describing the phenomenon in its nominal, healthy, or desired behavior; the actual distribution describes the phenomenon in its current and potentially unknown behavior.

as the nominal distribution, and the alternative hypothesis ( $\mathcal{H}_1$ : the presence of MD), under which the actual distribution has a different underlying model than the nominal distribution.

To test MD, we require i.i.d. samples from the actual distribution (the evidence) of  $(X, Y)$  and a data-driven decision rule. We denote by  $\mathbf{Z}_n = (Z_j)_{j=1}^n$  the  $n$  i.i.d. realizations from  $(X, Y) \sim P'_{X,Y}$ . A decision rule of length  $n$ , corresponds to a function  $\phi_n : (\mathcal{X} \times \mathcal{Y})^n \rightarrow \{0, 1\}$  from the  $n$ -size sample space  $((\mathcal{X} \times \mathcal{Y})^n)$  to the decision space  $(\{0, 1\})$ , where 0 means accepting  $\mathcal{H}_0$  and 1 means rejecting  $\mathcal{H}_0$ . The collection of the  $n$ -size decision rules is denoted by  $\Pi_n$ . Finally,  $\Phi = (\phi_n(\cdot))_{n \in \mathbb{N}}$  is said to be a decision scheme if  $\phi_n(\cdot) \in \Pi_n, \forall n \in \mathbb{N}$ .

### 2.3. Performance Metrics for Model Drift Detection

We introduce three standard concepts – strong consistency, detection time, and power and significance level – that are widely used by the decision community to measure the quality of an MD detection method, i.e., the quality of a scheme  $\Phi = (\phi_n(\cdot))_{n \in \mathbb{N}}$ . Due to the equivalence between MD detection and fault detection, we can extend these properties to a fault detection scheme.

#### 2.3.1. Strong Consistency

An important concept in hypothesis testing is *strong consistency* [47]. This requirement means that eventually, in the sample size, a scheme converges to the correct decision (almost-surely).

**Definition 1.** A decision scheme  $\Phi = (\phi_n(\cdot))_{n \in \mathbb{N}}$  is said to be *strongly consistent* if for any nominal and actual distributions  $P_{X,Y} \in \mathcal{P}(\mathcal{X} \times \mathcal{Y})$  and  $P'_{X,Y} \in \mathcal{P}(\mathcal{X} \times \mathcal{Y})$ , the following almost-surely convergence holds true:

$$\mathbb{P} \left( \lim_{n \rightarrow \infty} \phi_n(\mathbf{Z}_n) = i \mid \mathcal{H}_i \right) = 1, \forall i \in \{0, 1\}, \quad (1)$$

where  $\mathbb{P}$  represents the process distribution of  $(Z_n)_{n \in \mathbb{N}}$ , being  $Z_n \sim P'_{X,Y}, \forall n \in \mathbb{N}$ .

#### 2.3.2. Finite-Sample Analysis

A refined (non-asymptotic) metric to evaluate a consistent scheme is the number of samples required to converge to the right decision [48]. For this purpose, given a sequence of binary values  $\mathbf{s} = (s_n)_{n=1}^\infty \in \{0, 1\}^\infty$  (decisions) and  $i \in \{0, 1\}$  (the right decision), the collapsing time of  $\mathbf{s}$  is expressed by  $\text{col}(\mathbf{s}, i) \equiv \sup\{n \in \mathbb{N} : s_n = 1 - i\}$ .<sup>2</sup> If  $\text{col}(\mathbf{s}, i) < \infty$ , we say that  $\mathbf{s}$  *collapses to  $i$*  after  $\text{col}(\mathbf{s}, i)$  observations.

Given a sampling sequence  $\mathbf{z} = (z_j)_{j=1}^\infty \in (\mathcal{X} \times \mathcal{Y})^\infty$ , the sequence of decisions obtained by applying a scheme  $\Phi$  in  $\mathbf{z}$  is denoted as  $\mathbf{s}_{\Phi, \mathbf{z}} \equiv (\phi_n((z_j)_{j=1}^n))_{n=1}^\infty$ . Then, for  $i \in \{0, 1\}$ , we are interested in the set  $\mathcal{S}_i^\Phi \equiv \{\mathbf{z} \in (\mathcal{X} \times \mathcal{Y})^\infty : \text{col}(\mathbf{s}_{\Phi, \mathbf{z}}, i) < \infty\}$ .

**Definition 2.** Let  $\Phi = (\phi_n(\cdot))_{n \in \mathbb{N}}$  be a decision scheme and  $i \in \{0, 1\}$ . For any  $\mathbf{z} = (z_j)_{j=1}^\infty \in \mathcal{S}_i^\Phi$ , the  *$i$ -detection time* of  $\Phi$  is

$$\mathcal{T}_i^\Phi(\mathbf{z}) = \text{col}(\mathbf{s}_{\Phi, \mathbf{z}}, i) < \infty, \quad (2)$$

otherwise, i.e., if  $\mathbf{z} \notin \mathcal{S}_i^\Phi$ , we have that  $\mathcal{T}_i^\Phi(\mathbf{z}) = \infty$ .

<sup>2</sup>For any  $i \in \{0, 1\}$ , if  $\mathbf{s} = (i)_{n \in \mathbb{N}}$ , then  $\text{col}(\mathbf{s}, i) = 0$ .

#### 2.3.3. Power and Significance Level

Finally, we introduce the significance level of the test and the power of the test [48]. These are the probability of incurring a type I error (erroneously reject  $\mathcal{H}_0$ ) and the probability of not incurring a type II error (successfully reject  $\mathcal{H}_0$  when  $\mathcal{H}_1$  holds true), respectively.

**Definition 3.** Let  $\phi_n(\cdot)$  be a decision rule of length  $n$ . The *significance level* ( $\alpha_{\phi_n}$ ) and the *power* ( $1 - \beta_{\phi_n}$ ) of  $\phi_n(\cdot)$  are such that

$$\alpha_{\phi_n} = \mathbb{P}(\phi_n(\mathbf{Z}_n) = 1 \mid \mathcal{H}_0), \quad (3)$$

$$\beta_{\phi_n} = \mathbb{P}(\phi_n(\mathbf{Z}_n) = 0 \mid \mathcal{H}_1). \quad (4)$$

### 2.4. Mutual Information

Our work proposes an information-driven method for fault detection; in particular, we base our method on the celebrated *Mutual Information* (MI), which was proposed by Claude Shannon [49] to quantify a higher order dependency between two r.v.s. [50]. We focus on the MI between two continuous r.v.s equipped with a joint density.<sup>3</sup> Let  $X$  and  $Y$  be two continuous r.v.s taking values in  $\mathcal{X}$  and  $\mathcal{Y}$ , with a joint density  $f_{X,Y} : \mathcal{X} \times \mathcal{Y} \rightarrow \mathbb{R}$ . The MI between  $X$  and  $Y$  is

$$I(X; Y) \equiv \int_{\mathcal{X}} \int_{\mathcal{Y}} f_{X,Y}(x, y) \log \left( \frac{f_{X,Y}(x, y)}{f_X(x) \cdot f_Y(y)} \right) dy dx, \quad (5)$$

where  $f_X(\cdot)$  and  $f_Y(\cdot)$  denote the marginal densities of  $X$  and  $Y$ , respectively, induced by  $f_{X,Y}(\cdot)$ .

## 3. Problem Formalization

We address MD, as presented in Sec. 2.2, using the concept of noise outsourcing [51]. By that means, we define a framework of MD detection suitable for monitoring a system in a regression context. The steps of this formalization are shown in Fig. 1.

### 3.1. General Model

Let  $V$  be a continuous r.v. taking values in  $\mathbb{R}^r$  (with  $r \in \mathbb{N}$ ). The system (or phenomenon of interest) is represented by  $V$  and is illustrated in Fig. 1a. In the context of input-output system modeling, it is common to identify an explanatory (input) subset of  $V$  and a response (output) subset of  $V$  [52]. Formally, the input variables are denoted by  $X \equiv f_{\text{in}}(V)$ , and the output variables are denoted by  $Y \equiv f_{\text{out}}(V)$ , taking values in  $\mathcal{X} = \mathbb{R}^p$  and  $\mathcal{Y} = \mathbb{R}^q$ , respectively.<sup>4</sup> Then, we move from the description of the distribution of  $V$  to the description of the input-output joint distribution of  $(X, Y)$  that we consider as our observable system. A special case of this setting is illustrated in Fig. 1b, where a system  $V$  is a collection of variables, and we partition a subset of this set into input ( $X$ ) and output ( $Y$ ) variables.

<sup>3</sup>A probability measure on  $(\mathbb{R}^r, \mathcal{B}(\mathbb{R}^r))$  has a density if it is absolutely continuous with respect to the Lebesgue measure in  $(\mathbb{R}^r, \mathcal{B}(\mathbb{R}^r))$ . For  $\mathbb{R}^r$  with arbitrary  $r \in \mathbb{N}$ ,  $\mathcal{B}(\mathbb{R}^r)$  denotes the Borel  $\sigma$ -field of  $\mathbb{R}^r$ .

<sup>4</sup> $p \in \mathbb{N}$ ,  $q \in \mathbb{N}$ , and  $r \in \mathbb{N}$  are arbitrary natural numbers.

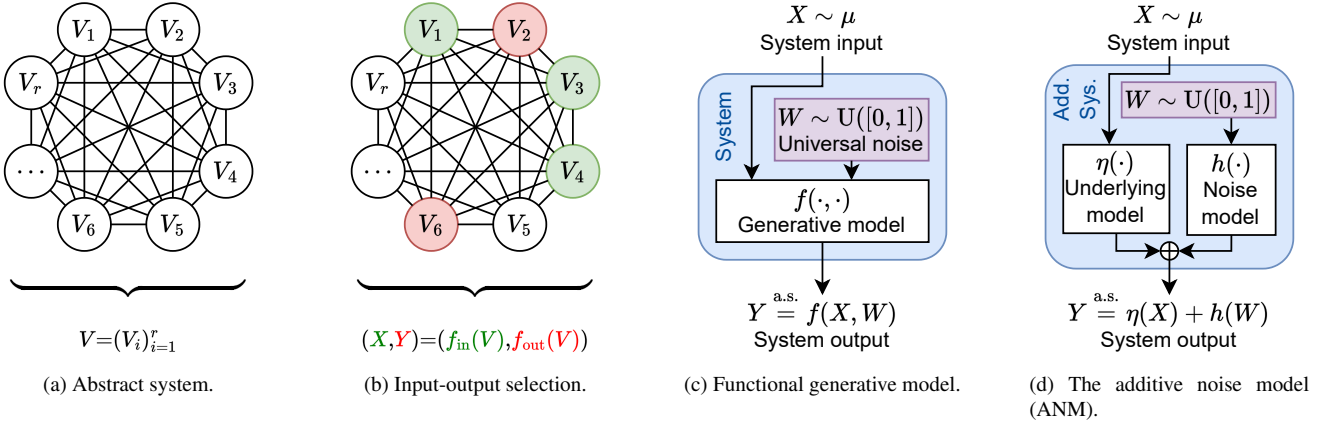


Figure 1: Diagrams of the abstraction stages of our formal framework.

### 3.2. Functional Generative Model via Noise Outsourcing

The following result offers a functional description of the distribution of  $(X, Y)$ .

**Lemma 1** (see [51, Lemma 3.1]<sup>5</sup>). *Let  $X$  and  $Y$  be r.v.s taking values in  $\mathbb{R}^p$  and  $\mathbb{R}^q$ , respectively. There exists a random variable  $W \sim \text{Uniform}([0, 1])$ , independent of  $X$ , and a measurable function  $f : \mathbb{R}^p \times [0, 1] \rightarrow \mathbb{R}^q$ , such that  $(X, Y) \stackrel{\text{a.s.}}{=} (X, f(X, W))$ .*<sup>6</sup>

Importantly, this lemma states that any system  $(X, Y)$  admits the following functional predictive structure:  $Y|X \stackrel{\text{a.s.}}{=} f(X, W)$ . Therefore, if the distribution of the input ( $X$ ) is known or controlled, knowing  $f(\cdot, \cdot)$  is sufficient to fully describe the predictive distribution of  $Y|X$  and the joint distribution of  $(X, Y)$ . In particular,  $f(X, W)$  can be seen as a *generative model* for  $Y|X$ . We illustrate this in Fig. 1c.

### 3.3. The Class of Additive Noise Models

Using Lemma 1, we focus on the expressive family of additive noise models (ANMs; see Fig. 1d), which are widely used in system theory and system monitoring applications [52].

**Definition 4.** A system  $(X, Y)$  is said to follow an additive noise model, denoted by  $(X, Y) \sim \text{add}(\eta, h; \mu)$ , if both following properties hold true:

- (i)  $\mathbb{P}(X \in A) = \mu(A), \forall A \in \mathcal{B}(\mathbb{R}^p)$ ,
- (ii)  $(X, Y) \stackrel{\text{a.s.}}{=} (X, \eta(X) + h(W))$ ,

where  $\mu$  is a probability measure over  $(\mathbb{R}^p, \mathcal{B}(\mathbb{R}^p))$ ,  $W \sim \text{Uniform}([0, 1])$  a r.v. independent of  $X$ , and  $\eta : \mathbb{R}^p \rightarrow \mathbb{R}^q$  and  $h : [0, 1] \rightarrow \mathbb{R}^q$  two measurable functions, which are denominated as the system's *underlying model* and *noise model*, respectively.

<sup>5</sup>The result shown in [51, Lemma 3.1] can be traced back as a straightforward application of [53, Prop. 5.13] by noting that  $X$  and  $Y$  are trivially conditionally independent given  $X$ .

<sup>6</sup>“a.s.” stands for “almost-surely.”  $A \stackrel{\text{a.s.}}{=} B$  means that  $\mathbb{P}(A = B) = 1$ .

Some observations regarding Definition 4:

- For the rest of the exposition, we focus on the rich case where  $\mathbb{E}[h(W)] = \mathbf{0} \in \mathbb{R}^q$ . This assumption induces no loss of generality, as it is simple to embed any noise bias in  $\eta(\cdot)$ .<sup>7</sup> This is further justified in Appendix G.1.
- A system following an ANM is fully defined by its tuple  $(\eta, h, \mu)$ , and its predictive distribution is fully described by the tuple  $(\eta, h)$ ; hence, an actual drift can be decoupled into drifts in  $\eta(\cdot)$  and  $h(\cdot)$ . We denominate these as *model drifts* and *noise drifts*, respectively.
- In system monitoring, we can assume that  $\mu$  is known or controlled, as this is the marginal distribution of the explanatory (input) variable; note that drifts in  $\mu$  are virtual drifts. In addition,  $h(\cdot)$  is the noise model, and its drifts do not alter the underlying deterministic input-output relationship; hence, they cannot be attributed to unwanted alterations of the inner dynamics of a system (faults) but to external disturbances, such as alterations in the measurement procedures. As neither virtual nor noise drifts can be attributed to system faults and as faults do not necessarily imply either of those drifts, they are out of the scope of our study.
- As a consequence of the above, the focus of our study is to detect model drifts, i.e., disturbances on the underlying deterministic input-output relationship  $\eta(\cdot)$ . As disturbances in the underlying model are a proxy for unwanted alterations in the system's inner dynamics (faults), and faults induce model drifts, we establish an equivalence between fault detection and model drift detection.

### 3.4. Model Equivalence

For the class of ANMs (Def. 4), it is crucial to have an equivalence relationship that can be used to represent the idea of MD.

<sup>7</sup>If  $\mathbb{E}[h(W)] = \mathbf{b} \neq \mathbf{0}$ , then we can define  $\bar{\eta}(\cdot)$  and  $\bar{h}(\cdot)$  such that  $\bar{\eta}(x) = \eta(x) + \mathbf{b}, \forall x \in \mathbb{R}^p$ , and  $\bar{h}(w) = h(w) - \mathbf{b}, \forall w \in [0, 1]$ , with the consequence that  $\mathbb{E}[\bar{h}(W)] = \mathbb{E}[h(W)] - \mathbf{b} = \mathbf{0} \in \mathbb{R}^q$ .

**Definition 5.** Let  $\eta_1 : \mathbb{R}^p \rightarrow \mathbb{R}^q$  and  $\eta_2 : \mathbb{R}^p \rightarrow \mathbb{R}^q$  be measurable functions.  $\eta_1(\cdot)$  and  $\eta_2(\cdot)$  are said to be *almost-surely equivalent* w.r.t.  $\mu$ , denoted by  $\eta_1 \simeq_\mu \eta_2$ , if for every r.v.  $X \sim \mu$  it holds that  $\eta_1(X) \stackrel{\text{a.s.}}{=} \eta_2(X)$ . If  $\eta_1 \simeq_\mu \eta_2$  does not hold, it is denoted as  $\eta_1 \not\simeq_\mu \eta_2$ .

**Remark 1.** It is worth noting that for an arbitrary system  $(X, Y) \sim \text{add}(\eta, h; \mu)$ , the minimum mean square error (MMSE) estimation of  $Y$  given  $X$  is  $\mathbb{E}[Y|X] = \eta(X) + \mathbb{E}[h(W)] = \eta(X)$  [54, Th. 13-1]. Hence, it follows for the optimal (MMSE) estimator that  $\hat{Y} \simeq_\mu \eta$ , for any input distribution  $\mu \in \mathcal{P}(\mathbb{R}^p)$ . Equipped with Def. 5, in the following sections, we show that MD over this class of ANMs can be observed by using the MMSE estimator of the reference (nominal) scenario  $\mathcal{H}_0$ .

### 3.5. Model Drift Detection

Within our class of models from Def. 4 and using the almost-surely equivalence definition introduced in Def. 5, we can state the hypothesis test required for dealing with model drift. Let us consider a system with nominal distribution  $\text{add}(\eta, h; \mu)$  and actual distribution  $\text{add}(\tilde{\eta}, \tilde{h}; \mu)$ . We define the absence of model drift as our null hypothesis  $\mathcal{H}_0$ , and the presence of model drift as our alternative hypothesis  $\mathcal{H}_1$ . Then, formally, we have that

$$\begin{aligned} \mathcal{H}_0 : \eta &\simeq_\mu \tilde{\eta}, \\ \mathcal{H}_1 : \eta &\not\simeq_\mu \tilde{\eta}. \end{aligned} \quad (6)$$

As a consequence of Remark 1, if  $\eta_{\text{nominal}}(\cdot)$  is the MMSE estimator built from the nominal distribution, then  $\eta \simeq_\mu \tilde{\eta} \Leftrightarrow \eta_{\text{nominal}} \simeq_\mu \tilde{\eta}$  holds true for every  $\mu \in \mathcal{P}(\mathbb{R}^p)$ . Hence,  $\eta_{\text{nominal}}(\cdot)$  can be used as a snapshot of the nominal system to be tested with the actual underlying model via samples  $\mathbf{Z}_n = (Z_j)_{j=1}^n$  collected from the actual system with distribution  $\text{add}(\tilde{\eta}, \tilde{h}; \mu)$ .

### 3.6. Model Drift and Input-Residual Dependency

The first main contribution of our work formalizes a link between MD and input-residual dependency. From this point on, the following assumptions will be considered:<sup>8</sup>

- (i)  $\mathbb{E}[\tilde{h}(W)] = \mathbf{0} \in \mathbb{R}^q$ .
- (ii)  $\mathbb{E}[Y - \eta(X)] = \mathbf{0} \in \mathbb{R}^q$ .
- (iii) Both r.v.s  $(X, Y - \eta(X))$  and  $(X, \tilde{h}(W))$  have densities.

We name these as our “*standard assumptions*.”<sup>9</sup>

<sup>8</sup>Although assumptions (i) and (ii) might seem equivalent and both r.v.s in assumption (iii) might seem the same, neither of those statements is necessarily true; this is because  $Y - \eta(X)$  is a.s. equal to  $\tilde{\eta}(X) - \eta(X) + \tilde{h}(W)$  and not  $\tilde{h}(W)$  when  $(X, Y) \sim \text{add}(\tilde{\eta}, \tilde{h}; \mu)$ .

<sup>9</sup>Assumption (i) was already discussed in the observations regarding Def. 4. Both assumptions (i) and (ii) are formally justified in Appendix G.1 and Appendix G.2, respectively. Assumption (iii) emerges from the continuous nature of our setup. All these assumptions can be relaxed but are taken into consideration for the sake of clarity and simplicity of our presentation.

**Theorem 1.** Let  $X$  and  $Y$  be r.v.s with values in  $\mathbb{R}^p$  and  $\mathbb{R}^q$ , respectively, such that  $(X, Y) \sim \text{add}(\tilde{\eta}, \tilde{h}; \mu)$ , and let  $\eta : \mathbb{R}^p \rightarrow \mathbb{R}^q$  be a measurable function. Under the standard assumptions, the following statements are equivalent:

- (i)  $\tilde{\eta} \simeq_\mu \eta$ , i.e.,  $\mathcal{H}_0$  in (6).
- (ii)  $X$  and  $Y - \eta(X)$  are independent.

The proof of Theorem 1 is presented in Appendix C. As shown in the proof, Theorem 1 is a consequence of a generalized version of this result – Theorem 5, see Appendix B – which relaxes assumptions (i) and (ii).

Importantly, Theorem 1 shows that testing the possibility of model drift (see Sec. 3.5) reduces to analyzing the statistical dependency (or higher order dependency) between the input  $X$  and  $Y - \eta(X)$ . This last variable, which we denominate as *residual*, can be seen as the regression error obtained from the MMSE estimator built from  $\mathcal{H}_0$  (the nominal model).

## 4. Information-Driven Model Drift Detection

In this section, we show our core methodological contribution: a novel MI-based pipeline for testing model drift. Mutual information can be used to determine if two arbitrary r.v.s. ( $A$  and  $B$ ) are independent or not. In fact,  $I(A; B) = 0$  if, and only if,  $A$  and  $B$  are independent [39]. Using this expressive property and driven by Theorem 1, we propose the adoption of a data-driven consistent estimation of the MI between  $Y - \eta(X)$  and  $X$  to inform the decision about  $\mathcal{H}_0$  and  $\mathcal{H}_1$ . To implement this idea (in the form of a decision scheme – see Sec. 2.2 –), we adopt a distribution-free MI estimator [40] and extend its statistical properties into our MD detection problem expressed in (6).

### 4.1. Data-Driven Decision Strategy — The Residual Information Value (RIV) Pipeline

Returning to the problem formulated in Sec. 3.5, let  $(X, Y) \sim \text{add}(\tilde{\eta}, \tilde{h}; \mu)$  be a system and  $\eta : \mathbb{R}^p \rightarrow \mathbb{R}^q$  be the function that models its reference (nominal) scenario ( $\mathcal{H}_0$ ; in other words, under  $\mathcal{H}_0$ :  $\tilde{\eta} \simeq_\mu \eta$  and under  $\mathcal{H}_1$ :  $\tilde{\eta} \not\simeq_\mu \eta$ ), and let  $\mathbf{Z}_n = (X_j, Y_j)_{j=1}^n$  be  $n$  i.i.d. samples of  $(X, Y) \sim \text{add}(\tilde{\eta}, \tilde{h}; \mu)$ . Our MI-based decision rule of length  $n$ , which we denote by  $\psi_{b_n, d_n, a_n}^{\lambda, n} : (\mathbb{R}^{p+q})^n \rightarrow \{0, 1\}$ , is computed as follows:

1. From  $\mathbf{Z}_n$ , a sampling of the residual  $R \equiv Y - \eta(X)$  is built:  $\mathbf{R}_n \equiv (R_j)_{j=1}^n \equiv (Y_j - \eta(X_j))_{j=1}^n$ .
2. The value of  $I(X; R)$  – see (5) – is estimated using an MI estimator presented in Sec. 4.2. In particular, we denote  $\hat{I}_n(X; R) \equiv I_{b_n, d_n}^{\lambda, n}(\mathbf{J}_n)$  as the estimated MI (EMI) between  $X$  and  $R$  – which we denominate the *residual information value* (RIV) –, being  $\mathbf{J}_n \equiv (X_j, R_j)_{j=1}^n$  the data and  $I_{b_n, d_n}^{\lambda, n}(\cdot)$  the MI estimator. The estimator parameters are  $(\lambda, b_n, d_n)$ , and their roles are explained in Sec. 4.2.
3. Reject  $\mathcal{H}_0$  if the RIV,  $\hat{I}_n(X; R)$ , is above or equal to a threshold  $a_n > 0$ ; otherwise, do not reject  $\mathcal{H}_0$ .

The pipeline induced by our family of decision rules is illustrated in Fig. 2.

In summary, the decision rule corresponds to  $\psi_{b_n, d_n, a_n}^{\lambda, n}(\mathbf{Z}_n) = 1_{[a_n, \infty)}(\hat{I}_n(X; R))$ , where all  $(b_n)_{n \in \mathbb{N}} \equiv \mathbf{b}$ ,  $(d_n)_{n \in \mathbb{N}} \equiv \mathbf{d}$  and  $(a_n)_{n \in \mathbb{N}} \equiv \mathbf{a}$  are sequences of positive numbers, and  $\lambda \in (0, \infty)$ . Then, we can define our proposed decision scheme as a sequence of decision rules  $\Psi_{\mathbf{b}, \mathbf{d}, \mathbf{a}}^\lambda \equiv (\psi_{b_n, d_n, a_n}^{\lambda, n}(\cdot))_{n \in \mathbb{N}}$  parametrized by  $(\lambda, \mathbf{b}, \mathbf{d}, \mathbf{a})$ .

#### 4.2. The Distribution-Free Mutual Information Estimator

In this subsection, we show the basic structure of the MI estimator adopted for our scheme, i.e.,  $I_{b_n, d_n}^{\lambda, n} : (\mathbb{R}^{p+q})^n \rightarrow [0, \infty)$ , introduced in Sec. 4.1. This non-parametric estimator is presented in full detail in [40].

The adopted MI estimator uses the data in three stages:

**Stage one (Data-driven partition):** it builds a partition of the sample space  $(\mathbb{R}^{p+q})$  using axis-parallel hyperplanes, which perform a statistical equivalent division of the data [40, Sec. III.A]. This produces a set of (data-driven) cells  $\mathcal{A} \equiv \{A_\ell\}_{\ell \in \Lambda} \subseteq \mathcal{B}(\mathbb{R}^{p+q})$ , indexed by the nodes of a binary tree. This tree is grown until each cell has at most  $n \cdot b_n$  samples [40, Eq. (8)]. Then, the resulting tree is pruned to achieve a complexity regularized optimum with a factor  $\lambda$ . This pruning (regularization) stage is designed to ensure that the estimation is within a confidence interval shown in [40, Corollary 2] with a probability of at least  $1 - \delta_n$ .<sup>10</sup>

**Stage two (Distribution estimation):** it estimates (from data) both the joint distribution and the marginal distributions over the cells of  $\mathcal{A}$  (the empirical probability), exploiting the fact that the axis-parallel construction implies that for every  $\ell \in \Lambda$ , there exist  $A_\ell^{(1)} \in \mathcal{B}(\mathbb{R}^p)$  and  $A_\ell^{(2)} \in \mathcal{B}(\mathbb{R}^q)$  such that  $A_\ell = A_\ell^{(1)} \times A_\ell^{(2)}$ . The empirical probability is defined as  $P_n(A) \equiv \frac{1}{n} \sum_{j=1}^n 1_A(J_j)$ ,  $\forall A \in \mathcal{B}(\mathbb{R}^{p+q})$ .

**Stage three (MI estimation):** it estimates the MI using an empirical expression of (5). This corresponds to

$$\hat{I}_n(X; R) = I_{b_n, d_n}^{\lambda, n}(\mathbf{J}_n) \equiv \sum_{\ell \in \Lambda} P_n(A_\ell) \cdot \log \left( \frac{P_n(A_\ell)}{Q_n(A_\ell)} \right), \quad (7)$$

where  $Q_n(A_\ell) \equiv P_n(A_\ell^{(1)} \times \mathbb{R}^q) \cdot P_n(\mathbb{R}^p \times A_\ell^{(2)})$ .

## 5. Performance Results

In this section, we state the theoretical properties of our method illustrated in Fig. 2. We show concrete performance results, from asymptotic to important finite-sample properties. These results support the capacity of our scheme to reach the right decision once sufficient evidence is collected from the input-output data observed in the system:  $\mathbf{Z}_n = (X_j, Y_j)_{j=1}^n$ .

Before stating our results, we need to introduce the following notation: Let  $\mathbf{u} = (u_n)_{n \in \mathbb{N}}$  and  $\mathbf{v} = (v_n)_{n \in \mathbb{N}}$  be two sequences of non-negative numbers; first, we define  $1/\mathbf{u} \equiv (1/u_n)_{n \in \mathbb{N}}$ ; second,  $\mathbf{u} \approx \mathbf{v} \Leftrightarrow \exists C \in (0, \infty) : \lim_{n \rightarrow \infty} u_n/v_n = C$ ; third,  $\mathbf{u} \in O(v_n) \Leftrightarrow \exists C \in (0, \infty), \exists n_0 \in \mathbb{N} : \forall n \geq n_0, u_n \leq C v_n$ ; fourth,  $\mathbf{u} \in \ell_1(\mathbb{N}) \Leftrightarrow \sum_{n \in \mathbb{N}} |u_n| < \infty$ ; and lastly, that  $\mathbf{u} \in o(1) \Leftrightarrow \lim_{n \rightarrow \infty} u_n = 0$ .

<sup>10</sup>What we denote as  $d_n$  is denoted as  $\delta$  and  $\delta_n$  in [40].

### 5.1. Strong Consistency

**Theorem 2.** Under the standard assumptions (see Sec. 3.6), any decision scheme (see Sec. 4.1) in the family  $\Psi_{\text{SC}}$  expressed by

$$\Psi_{\text{SC}} \equiv \left\{ \Psi_{\mathbf{b}, \mathbf{d}, \mathbf{a}}^\lambda : \begin{array}{l} \mathbf{b} \approx (n^{-l})_{n \in \mathbb{N}}, \\ 1/\mathbf{d} \in O(\exp(n^{1/3})), \mathbf{d} \in \ell_1(\mathbb{N}), \\ \mathbf{a} \in o(1), \lambda \in (0, \infty), l \in (0, 1/3) \end{array} \right\} \quad (8)$$

is strongly consistent for detecting model drift (Def. 1).

The proof of Theorem 2 is presented in Appendix D. This result shows a large regime of parameters in (8), where our scheme converges (with the number of samples) to the right decision almost-surely with respect to the process distribution of  $(Z_n)_{n \in \mathbb{N}}$ .

### 5.2. Exponentially-Fast Decision Under $\mathcal{H}_0$

**Theorem 3.** Under the standard assumptions (see Sec. 3.6), for any decision scheme  $\Psi$  in the family  $\Psi_{\text{FL}}$  expressed by

$$\Psi_{\text{FL}} \equiv \left\{ \Psi_{\mathbf{b}, \mathbf{d}, \mathbf{a}}^\lambda : \begin{array}{l} \mathbf{b} \approx (n^{-l})_{n \in \mathbb{N}}, \mathbf{d} \approx (\exp(n^{-1/3}))_{n \in \mathbb{N}}, \\ \mathbf{a} \in o(1), \lambda \in (0, \infty), l \in (0, 1/3) \end{array} \right\}, \quad (9)$$

we have that  $\forall m \in \mathbb{N}$ ,

$$\mathbb{P}(\mathcal{T}_0^\Psi((Z_n)_{n=1}^\infty) < m | \mathcal{H}_0) \geq 1 - K \exp(-m^{1/3}), \quad (10)$$

for a universal (distribution-free) constant  $K > 0$ .<sup>11</sup>

The proof of Theorem 3 is presented in Appendix E. This result refines Theorem 2 and says that under  $\mathcal{H}_0$ , the probability of arriving to the right decision (with less than  $m$  samples) converges exponentially fast to 1.

### 5.3. Power and Significance Level

**Theorem 4.** Under the standard assumptions (see Sec. 3.6), for any decision scheme  $\Psi = (\psi_n(\cdot))_{n \in \mathbb{N}}$  in the family expressed in (9), i.e.,  $\forall \Psi \in \Psi_{\text{FL}}$ , it follows that

$$\lim_{n \rightarrow \infty} (1 - \beta_{\psi_n}) = 1, \quad (11)$$

$$\alpha_{\psi_n} \leq K \cdot \exp(-n^{1/3}), \forall n \in \mathbb{N}, \quad (12)$$

with  $K > 0$ , a universal (distribution-free) constant.

The proof of Theorem 4 is presented in Appendix F.

## 6. Discussion of the Methodology and Results

Regarding our methodological contribution and the significance of our results, we can highlight the following:

- Our method, illustrated in Fig. 2, works over the rich family of ANMs. Importantly, beyond our standard assumptions, we do not require any special distribution for the r.v.s that determine the system, and we do not impose any restriction on the underlying model (i.e., on  $\eta(\cdot)$ ) and the noise distribution (induced by  $h(\cdot)$  in the ANM).

<sup>11</sup>See Def. 2 for further details on the notation  $\mathcal{T}_0^\Psi(\cdot)$ .

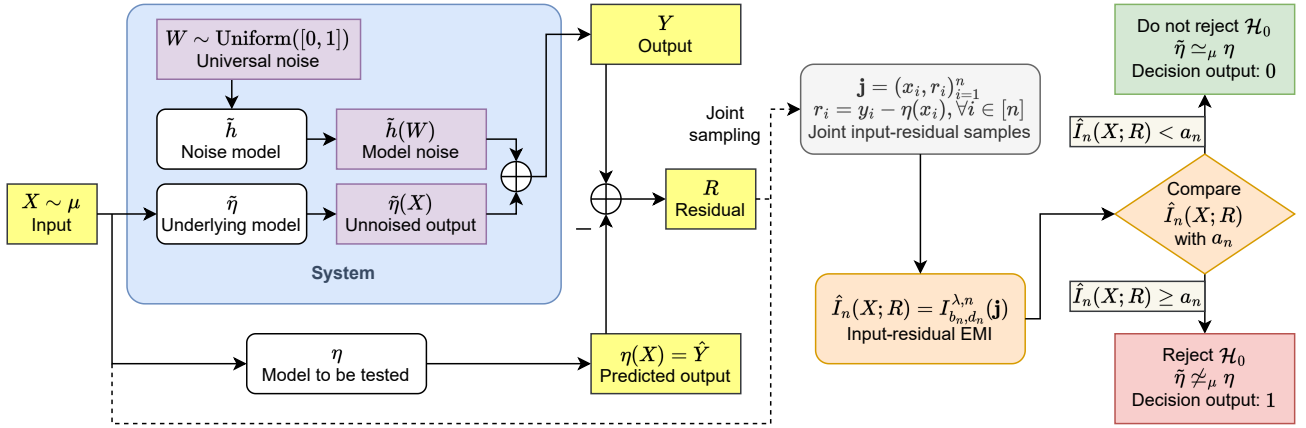


Figure 2: Block diagram for the pipeline induced by our family of decision rules:  $\psi_{b_n, d_n, a_n}^{\lambda, n}(\cdot)$ .

- From  $\Psi_{\text{FL}}$ , we provide a concrete parameter regime to practitioners – see (9) – to ensure strong consistency, an exponentially-fast decision on  $\mathcal{H}_0$ , and error convergence to 0 in the sample size.
- Any decision scheme  $\Psi \in \Psi_{\text{FL}}$  has an exponentially-fast decision convergence under  $\mathcal{H}_0$  (see Theorem 3). This finite-sample size behavior is remarkable and distinctive from other existing methods. To the best of our knowledge, this exponential velocity for detecting  $\mathcal{H}_0$  is not observed in other methods for fault detection.
- Our method is unsupervised in the sense that it does not require examples from failure scenarios to be implemented. In practice, we only need healthy data or a phenomenological insight about the system to start monitoring it and detect its faults via model drift detections.

In the following two sections, we apply our method to practical scenarios, starting with systems that have synthetic distributions (see Sec. 7) and finishing with a benchmark dataset of turbofan engines (see Sec. 8).

## 7. Numerical Analysis on Synthetic Distributions

In this section, we perform a numerical analysis to validate our pipeline by applying our methodology to several synthetic parametric systems. All experiments in this section are subjected to an error-bar analysis in Appendix I. We consider systems within the family of ANMs (see Def. 4) determined by a parametric function expressed by  $\eta_{\theta} : \mathbb{R}^p \rightarrow \mathbb{R}^q$  and  $h : [0, 1] \rightarrow \mathbb{R}^q$ . The parameter for  $\eta_{\theta}(\cdot)$  is  $\theta \in \Theta \subseteq \mathbb{R}^v$ , where  $v \in \mathbb{N}$  is the dimensionality of  $\Theta$ , which varies according to the system in consideration. For these parametric constructions, we consider a nominal system to be determined by its nominal parameters  $\theta$ , i.e.,  $(X, Y) \sim \text{add}(\eta_{\theta}, h; \mu)$ . On the other hand, a drifted system is described by its nominal parameters ( $\theta$ ) and its drift; the latter is expressed as a perturbation  $\delta = (\delta_{\ell})_{\ell=1}^v \in \mathbb{R}^v$ . In consequence, a drifted system is expressed by  $(X, Y) \sim \text{add}(\eta_{\theta, \delta}, h; \mu)$ . In particular,  $\delta = \mathbf{0} \in \mathbb{R}^v$  implies

Table 1: Expressions for  $\eta_{\theta, \delta}(x_1, x_2)$  in the explored systems.

System	Value of $\eta_{\theta, \delta}(x_1, x_2)$
Linear	$(c_1 + \delta_1)x_1 + (c_2 + \delta_2)x_2$
Polynomial	$(c_1 + \delta_1)x_1^2 + (c_2 + \delta_2)x_2^3$
Trigonometric	$(A + \delta_1) \sin(x_1 x_2 + \phi + \delta_2)$
MLP	$f_{\theta, \delta}^{\text{MLP}}(x_1, x_2)$

that the system is non-drifted from its reference scenario, i.e.,  $\text{add}(\eta_{\theta, \mathbf{0}}, h; \mu) = \text{add}(\eta_{\theta}, h; \mu)$ .

### 7.1. Experimental Setup

Our setup for analyzing MD detection considers a parametric system  $(X, Y)$  with an un-drifted nominal distribution  $\text{add}(\eta_{\theta}, h; \mu)$  and a potentially drifted distribution  $\text{add}(\eta_{\theta, \delta}, h; \mu)$ . In this setting, the nominal model for  $Y$  given  $X$  corresponds to  $\eta_{\theta}(\cdot)$ , and the value of  $\delta$  quantifies the model drift. The MD detector uses actual data  $\mathbf{Z}_n$ , i.e.,  $n$  i.i.d. samples from the actual distribution  $(X, Y) \sim \text{add}(\eta_{\theta, \delta}, h; \mu)$  to test the actual underlying model ( $\eta_{\theta, \delta}(\cdot)$ ) with the nominal model ( $\eta_{\theta}(\cdot)$ ).

For simplicity, in this section, we restrict our analysis to a 2-dimensional input space, a univariate output space, and a 2-dimensional  $\delta$ -space, i.e.,  $p = 2$ ,  $q = 1$ , and  $v = 2$ . We explore four systems, denominated as *Linear*, *Polynomial*, *Trigonometric* and *MLP*; their expressions for  $\eta_{\theta, \delta}(\cdot)$  are shown in Table 1.<sup>12</sup> Additional details for all the distributions and functions used in our experimental setup, including marginal distributions, noise models, and the values of the coefficients that make up the nominal parameters ( $\theta$ ), are contained in Appendix H.

For all cases, the nominal system ( $\mathcal{H}_0$ ) corresponds to  $\eta_{\theta, \mathbf{0}}(\cdot)$ . In our experiments, we range  $\delta_1$  and  $\delta_2$  from  $-0.15$  to  $0.15$

<sup>12</sup>  $f_{\theta, \delta}^{\text{MLP}}$  is the function defined by a simple multi-layer perceptron with a single hidden layer of two units and parameters  $\theta$  disturbed by  $\delta$ . In particular,  $\delta_1$  and  $\delta_2$  disturb additively the weights from the first and second input unit to the first hidden unit. We fix  $\delta_{\ell} = 0, \forall \ell > 2$ , in our experiments over the MLP system.

with a step of 0.0015. Within this range, it holds that  $\delta = \mathbf{0} \Leftrightarrow \eta_\theta \simeq_\mu \eta_{\theta,\delta}$ . Consequently, applying our method to observations from  $(X, Y) \sim \text{add}(\eta_{\theta,\delta}, h; \mu)$  will raise an MD detection ( $\mathcal{H}_1$ ) if, and only if,  $\delta \neq (0, 0)$ .

To better visualize our method, we compute the RIV, i.e., the input-residual EMI ( $\hat{I}_n(X; R)$ ), and show its value prior to thresholding it. This is done for every  $\delta$  within the aforementioned range. These MI estimations are made using parameters from the range expressed in (9); therefore, each decision scheme  $\Psi_{\mathbf{b},\mathbf{d},\mathbf{a}}^l \in \Psi_{\text{FL}} \subseteq \Psi_{\text{SC}}$  satisfies the hypotheses of Theorem 2, 3, and 4. In particular, we choose  $\lambda = 2.3 \cdot 10^{-5} \in (0, \infty)$ ,  $\mathbf{d} = (\exp(n^{-1/3}))_{n \in \mathbb{N}} \approx (\exp(n^{-1/3}))_{n \in \mathbb{N}}$ , and  $\mathbf{b} = (wn^{-l})_{n \in \mathbb{N}} \approx (n^{-l})_{n \in \mathbb{N}}$  with  $w = 5 \cdot 10^{-2}$  and  $l = 0.167 \in (0, 1/3)$ . As we simulated a fixed amount of  $n = 2000$  samples, the reported EMIs are computed with  $b_n \approx 0.014051$  and  $d_n \approx 1.082605$ .

Finally, we consider two baseline strategies with which to compare our method. The first, which we denote as the *Correlation method*, is the maximum absolute value of the Pearson correlation coefficients between the residual and each input coordinate;<sup>13</sup> we select this method, as the input-error correlation is used as a common validation measure for system identification [55, Ch. 9]. The second strategy, which we denote as the *RMSE method*, is the root mean squared error computed from the residual; supporting this selection, there are different works based on thresholding RMSE, both in FDI (e.g., [7, 9, 10]) and concept drift detection applied to regression [33].

## 7.2. Numerical Results and Discussions about our Method

Figure 3 shows the values obtained for all four systems using our method and both baseline methods. Every single cell of every colormap has the average value over 10 different seeds for that specific  $\delta$  value, method, and system. We can see that for all systems, the residual information value (RIV) reaches 0 when  $\delta = (0, 0)$ . In consequence, for any threshold sequence  $\mathbf{a} \in o(1)$ , our method returns the right decision on  $\mathcal{H}_0$ . In addition, we can see in every model a region of  $\delta$  values around the  $\mathcal{H}_0$  point, which would raise false negatives as their RIVs are 0; this is due to the difficulty of detecting dependency in slightly non-independent r.v.s. In general, as  $\delta$  is farther from  $(0, 0)$ , it is easier to identify input-residual dependencies.

In addition, we can see that each RIV colormap gives us an insight into the underlying model subjected to the drift. For example, the Linear and Trigonometric systems have colormaps where the RIV increases monotonically with  $\|\delta\|$  following no privileged directions (isotropic monotonicity); hence, if we weight equally drifts in  $\delta_1$  and  $\delta_2$ , the RIV is a clear indicator of the drift's magnitude. The greater RIV values in the Linear system, in contrast with the Trigonometric system, express that it is simpler to detect model drift in the Linear system. In regard to the Polynomial system, we can see a privileged direction of RIV increment (anisotropic monotonicity); this is the  $\delta_1 = 0$  axis. The reason for this privilege is the cubic relationship of  $Y$

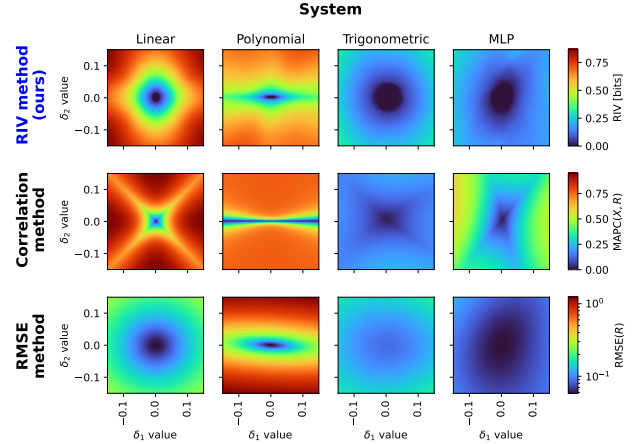


Figure 3: Numerical results for our MI-based model drift detection method and baselines on parametrized drifts.

with  $X_2$  (whose weight is disturbed by  $\delta_2$ ) in contrast with the quadratic dependence of  $Y$  with  $X_1$  (whose weight is disturbed by  $\delta_1$ ). This implies that  $\delta_2$ -disturbances induce stronger input-residual dependencies (cubic) than  $\delta_1$ -disturbances (quadratic). Finally, regarding the MLP system, we can see oblique privilege directions; this pattern is due to asymmetric non-linearities induced by the activation function of the system. We remark that these colormaps, or high-dimensional versions of them, can be built for any system that can be identified with a white-box model to have a clear phenomenological interpretation of its possible drifts.

### 7.2.1. Comparison

Contrasting our method with the baselines, we can make the following observations. Regarding correlation, for the Polynomial system, the MAPC approximates zero across the region defined by  $\delta_2 = 0$ . This means that this method is unable to detect a drift caused by  $\delta_1 \neq 0$  when  $\delta_2 = 0$ . This lack of MD observability is a consequence of the quadratic dependency between the input and the residuals when  $\delta_2 = 0$  because the correlation is unable to capture high-order dependencies. This is in clear contrast with the capacity of our MI-based residual analysis, as the MI captures high-order dependencies. As for the RMSE, we can see a local minimum at  $\delta = (0, 0)$  for all colormaps. However, the value of the local minimum is system-dependent, which implies the necessity of a system-dependent threshold. This design is not straightforward and is a limitation of this error-based strategy.<sup>14</sup> In contrast, our RIVs reach zero under  $\mathcal{H}_0$  independently of the system. This is expressed in the exponentially fast convergence of the decision under  $\mathcal{H}_0$  as shown in Theorem 3.

### 7.3. Complementary Analysis — Autoregressive Systems

We complement our results by applying our method and both baselines on autoregressive (AR) systems. These AR sys-

<sup>13</sup>We denote this as  $\text{MAPC}(X, R) \equiv \max\{|\text{corr}(X_1, R)|, |\text{corr}(X_2, R)|\}$ ; MAPC stands for *Maximum Absolute Pearson Correlation*.

<sup>14</sup>There exists a systematic study for error-based drift detection methods [33].

Table 2: Expressions for  $\eta_{\theta,\delta}(d, u)$  in autoregressive systems.

System	Value of $\eta_{\theta,\delta}(d, u)$
ARX	$(c_1 + \delta_1)d + (c_2 + \delta_2)u$
NARX	$(c_3 + \delta_1 + c_4 \exp(-d^2)) \cdot d + (c_5 + \delta_2) \cdot u^2$

tems are described by

$$D_j = \eta_{\theta,\delta}(D_{j-1}, U_j) + H_j, \quad (13)$$

$$Y_j = D_j + W_j, \quad (14)$$

where all  $U$ ,  $H$ , and  $W$  are independent univariate r.v.s. representing the exogenous input, the model noise, and the measurement noise, respectively. In these systems, the nominal model is still  $\eta_{\theta,0}(\cdot, \cdot)$ . We perform experiments on a linear AR system (ARX) and a non-linear AR system (NARX); their expressions for  $\eta_{\theta,\delta}(\cdot, \cdot)$  are presented in Table 2.<sup>15</sup> For these AR systems, an input sampling corresponds to  $(X_j)_{j=1}^n = (Y_{j-1}, U_j)_{j=1}^n$ ; hence, the temporal dependency between instances of the input implies that  $\mathbf{Z}_n$  is not an i.i.d. sequence. We experimented with these systems to analyze the capabilities of our method beyond its formal hypotheses.

In Fig. 4, we show the results of applying our method and both baselines using the same amount of samples ( $n$ ) and parameters of the MI estimator ( $\lambda$ ,  $\mathbf{b}$ , and  $\mathbf{d}$ ; shown in Sec. 7.1) to both ARX and NARX systems. We can see that the main observations discussed in Sec. 7.2 remain valid for both systems. In particular, we get zero RIV under  $\mathcal{H}_0$  and an increase of the RIV when moving away from  $\delta = (0, 0)$ . We also observe an approximately isotropic monotonicity of the RIV for the ARX system; this is in contrast with the clear asymmetric pattern for the NARX system. This last asymmetric information pattern can be attributed to the non-linearities of the system. Moreover, we can still observe the inability of the Correlation method to identify non-trivial drifts (attributed to quadratic input-residual dependencies; see MAPC values for the NARX system at  $\delta_1 = 0$ ) and the system-dependent non-zero minima of the RMSE method.

Our results for the AR systems demonstrate the practical potential of our method in realistic scenarios. This capability is especially useful for controlled systems, as they have an inherent temporal dependence embedded in their signals due to the control loop.

## 8. Study Case — N-CMAPSS Dataset

In this section, we apply our data-driven fault detection strategy to the N-CMAPSS dataset [41]. This dataset corresponds to aircraft engine (turbofan) run-to-failure simulations under realistic flight scenarios; these simulations are run under the *Commercial Modular Aero-Propulsion System Simulation*

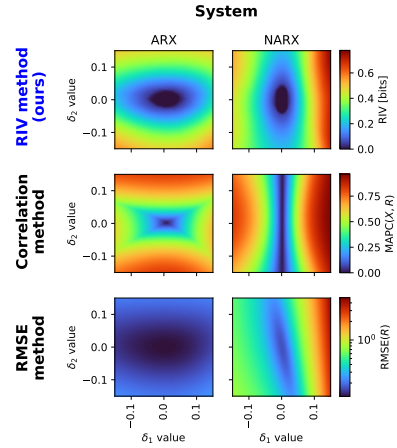


Figure 4: Numerical results for the RIV method and baselines on parametrized drifts over AR systems.

(CMAPSS) turbofan model developed at NASA [56] using as input real recordings of environmental variables obtained in real commercial flights. The N-CMAPSS dataset is widely used as a benchmark in the PHM community.

### 8.1. Dataset Description

The N-CMAPSS dataset provides 8 sub-datasets denominated from DS01 to DS08; our work focuses on DS04. Each sub-dataset contains simulations for a number of turbofan units that varies according to the sub-dataset. These units are already divided and specified as train or test units. Each turbofan unit is simulated in a sequence of flights of the same class — short-length, medium-length, and long-length flights; in DS04, there are only units with medium and long-length flights. Each complete flight is referred to as a *cycle* of the unit, which corresponds with the recording of a simulated flight. Each recording is a multivariate series sampled at 1 Hz during the time interval where the altitude of the unit is above 10 000 ft (3048 m). The attributes of these recordings are divided into 4 scenario descriptors, 14 sensor measurements, and 14 virtual measurements. In addition, the dataset provides the ground-truth model health parameters, the remaining useful life (RUL), and auxiliary data such as the flight class and health state.

We discarded the virtual measurements to ensure a realistic application of our methodology; consequently, we built our nominal models and computed the RIVs only with the scenario descriptors and the sensor measurements. In Table 3, we detail the variables we consider in our pipeline.<sup>16</sup> To describe the application of our methodology, we refer to each variable by either its number ID or its symbol as a subscript of  $V$ ; e.g., we refer to the fuel flow by either  $V_{Wf}$  or  $V_5$ .

All units start with a random small degradation and are subjected to increasing noisy degradation throughout their cycles. This degradation can evolve in a normal or abnormal way, following a linear or exponential fashion respectively. The latter

<sup>15</sup>In-depth details for these constructions are in Appendix H.

<sup>16</sup>LPC, HPC, LPT, and HPT stand for *low pressure compressor*, *high pressure compressor*, *low pressure turbine*, and *high pressure turbine*, respectively.

Table 3: Variables of interest in the N-CMAPSS dataset.

Category	Number ID	Symbol	Description	Unit
Scenario descriptor	1	alt	Altitude	ft
	2	Mach	Flight Mach number	–
	3	TRA	Throttle-resolver angle	%
	4	T2	Total temperature at fan inlet	°R
Sensor measurements	5	Wf	Fuel flow	pps
	6	Nf	Physical fan speed	rpm
	7	Nc	Physical core speed	rpm
	8	T24	Total temperature at LPC outlet	°R
	9	T30	Total temperature at HPC outlet	°R
	10	T48	Total temperature at HPT outlet	°R
	11	T50	Total temperature at LPT outlet	°R
	12	P15	Total pressure in bypass-duct	psia
	13	P2	Total pressure at fan inlet	psia
	14	P21	Total pressure at fan outlet	psia
	15	P24	Total pressure at LPC outlet	psia
	16	Ps30	Static pressure at HPC outlet	psia
	17	P40	Total pressure at burner outlet	psia
	18	P50	Total pressure at LPT outlet	psia

starts at some number of cycles determined by the simulation following criteria regarding energy usage of the unit’s subcomponent. In Table 4, we summarize the characteristics of the units simulated in DS04. We refer to the number of cycles occurring prior to the onset of the exponential evolution for the degradation as *healthy flights*.

The degradation is parametrized with the *model health parameters* (MHPs). In Table 5, we detail the available MHPs in the N-CMAPSS dataset (all MHPs are adimensional). We can observe that these MHPs are analogous to the drift parameters ( $\delta$ ) described in Sec. 7. Hence, we refer to each MHP by its number ID as a subscript of  $\delta$ , e.g., we refer to the LPT efficiency modifier by  $\delta_9$ .

The units of a particular sub-dataset are only subjected to a particular kind of degradation. Units in DS04 are subjected only to fan degradations, i.e., alterations on only fan efficiency and fan flow modifiers. This means that in DS04, all from  $\delta_3$  to  $\delta_{10}$  are fixed to 0, and only  $\delta_1$  and  $\delta_2$  are able to have non-zero values, implying that  $(\delta_1, \delta_2) = (0, 0)$  represents a perfectly healthy turbofan. In Fig. 5, we show the trajectory of fan modifiers as the unit’s number of cycles increases. We can see a noisy degradation close to  $\delta = (0, 0)$  over the first flights and a drift away from point  $(0, 0)$  as the number of cycles increases. In all sub-datasets, the degradation remains constant during the course of a cycle. For the sake of realism, we note that each unit follows its own trajectory, that the degradation is noisy, and that there is no perfectly healthy turbofan in any case.

## 8.2. Methodology Specifics for N-CMAPSS

The first step in applying our methodology is to define the system. We will consider that a turbofan is a system composed

of all variables shown in Table 3, i.e.,  $V \equiv (V_\ell)_{\ell=1}^{18}$  (taking values in  $\mathbb{R}^{18}$ ) is the r.v. representing the system (see Fig. 1a). Next, we define the input and output. As this selection is left to the user, we will choose an arbitrary variable from Table 3 with ID number  $k \in \{1, 2, \dots, 18\}$  as the target (response or output) and will consider all the rest as explanatory (input). This means that considering  $V_k$  as the target, the output is the r.v.  $Y_{[k]} \equiv V_k$  (taking values in  $\mathbb{R}$ ), and the input is the r.v.  $X_{[k]} \equiv (X_{j,[k]})_{j=1}^{17} \equiv (V_\ell)_{\ell \in \{1, 2, \dots, 18\} \setminus \{k\}}$  (taking values in  $\mathbb{R}^{17}$ ) – see Fig. 1b.

The next step is to build a nominal model for  $Y_{[k]}|X_{[k]}$ . For that, we need to obtain an approximation of the MMSE estimator of  $Y_{[k]}$  given  $X_{[k]}$ ; we denominate the optimal model as  $\eta_{[k]} : \mathbb{R}^{17} \rightarrow \mathbb{R}$ . We approximate  $\eta_{[k]}(\cdot)$  with a multilayer perceptron (MLP) using data from the first flights of the train units, specifically, the first 15 cycles of units with medium-length flights (IDs 1 and 3) and the first 10 cycles of units with long-length flights (IDs 2, 4, 5, and 6). We used the first cycles to ensure data came from non-abnormal degraded units (see Fig. 5).

The 18 MLPs used to model each possible target share the same properties and training hyperparameters: each MLP has 4 hidden layers with 1024 hidden units per layer. The input attributes are normalized with a standard scaler. The loss function is the MSE loss. The optimizer is ADAM [57] with a learning rate of  $10^{-6}$  and values of  $\beta_1 = 0.9$  and  $\beta_2 = 0.999$ . The training is done with a batch size of 256 samples and early stopping with 32 tolerance epochs and a maximum of 256 epochs using 30% of the nominal data as validation.

Building a nominal model is the only prerequisite of our method. This nominal model is built only with healthy flights of train units; hence, the unsupervised capability of our method-

Table 4: Summary of the units simulated in sub-dataset DS04.

Division	Flight class	Unit ID	Healthy flights	Total flights
Train	Medium-length	1	21	87
		3	21	100
	Long-length	2	16	73
		4	15	69
		5	16	100
		6	16	83
Test	Medium-length	7	21	87
		8	21	99
	Long-length	9	21	73
		10	16	85

Table 5: Model health parameters in the N-CMAPSS dataset.

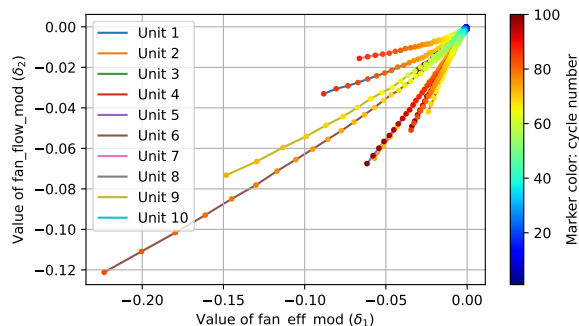
# ID	Symbol	Description
1	fan_eff_mod	Fan efficiency modifier
2	fan_flow_mod	Fan flow modifier
3	LPC_eff_mod	LPC efficiency modifier
4	LPC_flow_mod	LPC flow modifier
5	HPC_eff_mod	HPC efficiency modifier
6	HPC_flow_mod	HPC flow modifier
7	HPT_eff_mod	HPT efficiency modifier
8	HPT_flow_mod	HPT flow modifier
9	LPT_eff_mod	LPT efficiency modifier
10	LPT_flow_mod	LPT flow modifier

ology to detect faults is clear, as there is no data coming from degraded units involved prior to the actual test. This is especially useful in scenarios with a scarcity of faulty observations.

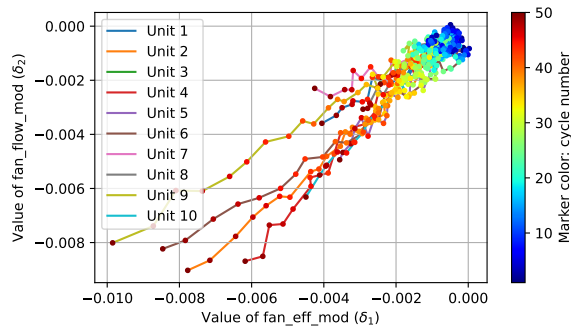
### 8.3. Numerical Results — RIV and Degradation

We are interested in analyzing how the residual information value (RIV) evolves as the degradation of the units evolves. For this reason, we associate a RIV to each cycle of each unit. This can be done by using the whole recording of that particular cycle and unit to obtain the input and output (which depend on the targeted variable) as a sampling of the system in that particular state. The sampled input is fed to the MLP model to compute the residuals and then to obtain the input-residual EMI, i.e., the RIV (see Fig. 2) of that particular unit and cycle.

In Fig. 6, we show how the RIV evolves in each test unit for a model with P24 ( $k = 15$ ) as its target. We also show how the fault magnitude ( $\|\delta\|$ ) evolves in comparison. In these examples, a detection is raised when the RIV goes above 0. This occurs in the neighborhood of cycle number 50 of each unit when the fault magnitude goes above approximately 0.01. Importantly, we observe a clear correlation between the RIV and  $\|\delta\|$ .



(a) Trajectories for the complete usage of the units.



(b) Trajectories for the first 50 cycles.

Figure 5: Trajectories of the fan modifiers ( $\delta_1$  and  $\delta_2$ ) over units' usage.

To complement this analysis, in Fig. 7, we show how RIVs correlate with fault magnitudes for the different possible models and different units. In Fig. 7a, we show the RIV-degradation correlation for each unit and each possible targeted variable. The white cells in Fig. 7a are undetermined correlations caused by a 0 RIV signal for all cycles of that specific targeted variable and unit. In Fig. 7b, we group the correlations by train and test units and show their sorted average; we remove the models for T24, T30, and Nc of this analysis due to their undetermined correlation at unit ID 3. It is easy to see that the election of the

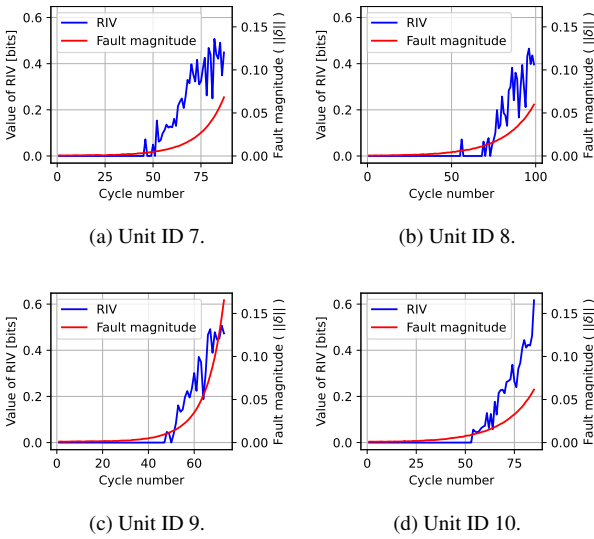


Figure 6: Degradation magnitude ( $\|\delta\|$ ) and RIV ( $k = 15$ ) evolution over usage for test units.

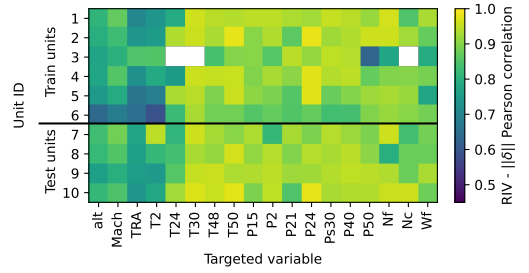
target variable is crucial to obtain better RIVs in terms of their correlation with the fault magnitude; in this case, P24 ( $k = 15$ ) is the best variable to target as an output. These correlations show the potential of the RIV values to estimate the health state of the system.

#### 8.4. Beyond Detection — Residual Information Features (RIF)

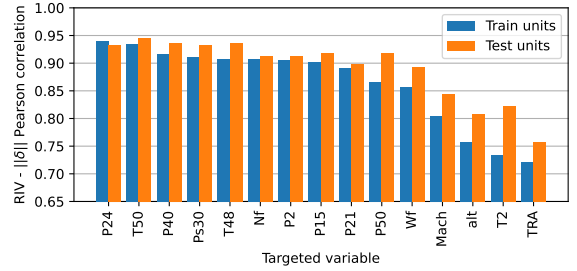
Although the results shown in Sec. 8.3 validate our methodology in a realistic benchmark dataset, these results can be improved. The RIVs are estimations of the MI between  $X_{[k]}$  and  $R_{[k]} \equiv Y_{[k]} - \hat{\eta}_{[k]}(X_{[k]})$ ; i.e., an EMI between a 17-dimensional ( $X_{[k]}$ ) and a unidimensional ( $R_{[k]}$ ) r.v. The estimator we are using is tailored for low dimensionalities (see [58]); hence, a straightforward way to enrich our analysis is not to compute  $\hat{I}_n(X_{[k]}; R_{[k]})$  but to compute  $\hat{I}_n(X_{j,[k]}; R_{[k]})$  for each  $j \in \{1, 2, \dots, 17\}$ . This means computing 17 estimations of MI of univariate pairs instead of a single value of EMI involving a high-dimensionality variable. In practical terms, instead of obtaining a single value, we are obtaining a rich vector; we name this vector as the *residual information feature* (RIF).

In Fig. 8, we show how the RIFs evolve in each test unit for a model with T50 ( $k = 11$ ) as its target. We can see a clear correlation between the RIF coordinates and the degradation. In Fig. 9, we show how RIF magnitudes ( $\|\text{RIF}\|$ ) correlate with fault magnitudes ( $\|\delta\|$ ) for the different possible models and different units. In Fig. 9a, we show the  $\|\text{RIF}\| - \|\delta\|$  correlation for each unit and each possible targeted variable, and in Fig. 9b, we show the same correlation grouped by train and test units sorted by average. We can make the same observations about these results as in Sec. 8.3 with two main differences: We are getting better correlations when computing component-wise EMIs, and we obtain a more detailed description of the fault when computing a feature (RIF) instead of a single value (RIV).

It should be noted that for each particular unit and cycle, we have 18 (one per targeted variable) possible RIFs, i.e., 18



(a) Detailed correlation for all models and units.



(b) Train and test units' average correlation.

Figure 7: Pearson correlation between the RIVs and the fault magnitude ( $\|\delta\|$ ).

vectors of 17 components; if we concatenate these RIFs, we obtain a 306-dimensional vector describing the fault, i.e., a signature vector. To evaluate the signature capability to describe the fault, we train an MLP regressor using the vector of concatenated RIFs as the input and  $\|\delta\|$  as the target; for this objective, we use all data available from training units. The MLP used in the signature- $\|\delta\|$  regression has 4 hidden layers with 128 hidden units per layer. The signature coordinates are normalized with a min-max scaler. The loss function is the MSE loss. The optimizer is ADAM with a learning rate of  $10^{-6}$ , and values of  $\beta_1 = 0.9$  and  $\beta_2 = 0.999$ . The training is done with a batch size of 256 samples and early stopping with 1024 tolerance epochs and a maximum of 32 768 epochs using 30% of the data from the training units as validation.

In Fig. 10, we show the true (real) and estimated fault magnitude ( $\|\delta\|$ ) over each test unit usage and the root mean squared error (RMSE) of the estimation. These estimations are made with the signature-to-magnitude MLP regressor mentioned above. Remarkably, here, we can observe the predictive power of our information signatures to describe and estimate the hidden degradation profile of a test turbofan.

#### 8.5. Final Discussion

The results in this section validate our formal contributions and synthetic analysis in a realistic benchmark scenario: N-CMAPSS. Moreover, we have built an observable value to describe hidden degradation and incipient faults in turbofans. Better models, such as physics-informed ones, a better tuning of hyperparameters, and a consideration of the time dynamics of the fault could significantly improve these results. This means that even with simple data-driven models and no knowledge of the system dynamics or degradation mechanisms, it is possible

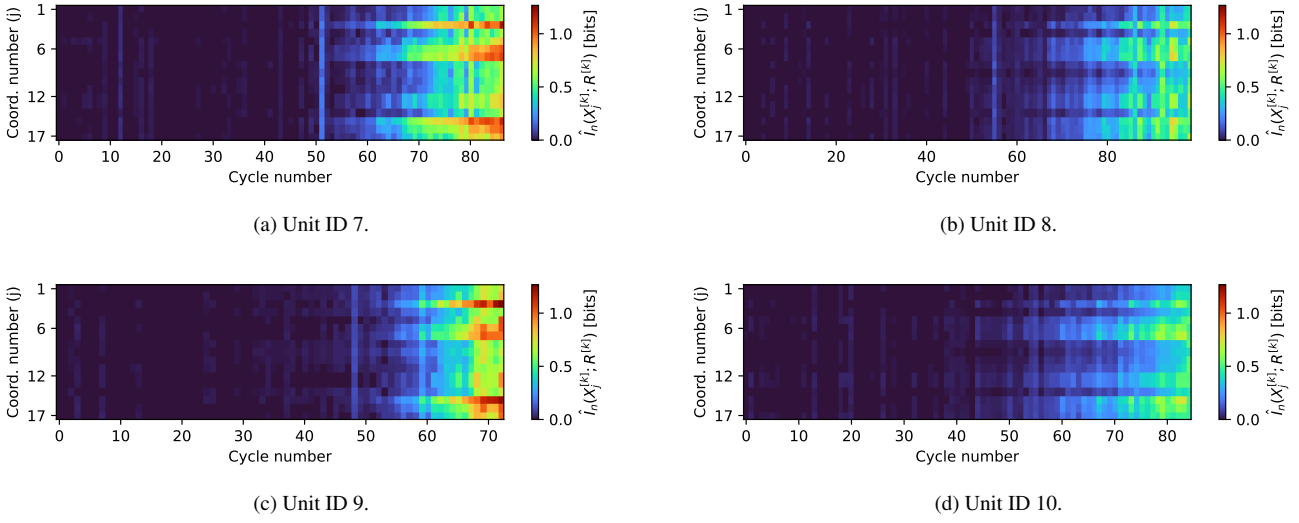
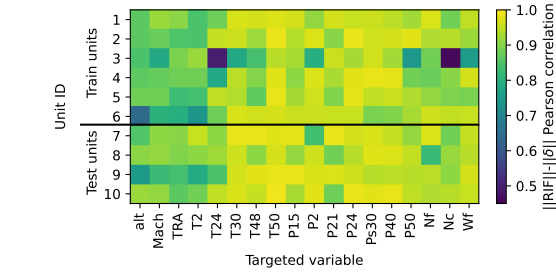
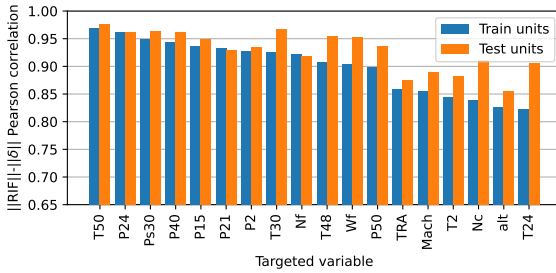


Figure 8: RIF  $(\hat{I}_n(X_{j_i[k]}; R^{[k]}))_{j=1}^{17}$  evolution for  $k = 11$  over usage for test units.



(a) Detailed correlation for all models and units.



(b) Train and test units' average correlation.

Figure 9: Pearson correlation between RIF magnitudes and the fault magnitudes.

to build a successful fault descriptor. To summarize, in addition to fault detection, our methodology can be used to develop diagnosis and prognostic approaches for complex input-output systems.

## 9. Summary and Future Perspectives

In this work, we introduce a novel information-driven fault detection (FD) method and a new theory for model drift detection tailored to systems with continuous input-output rela-

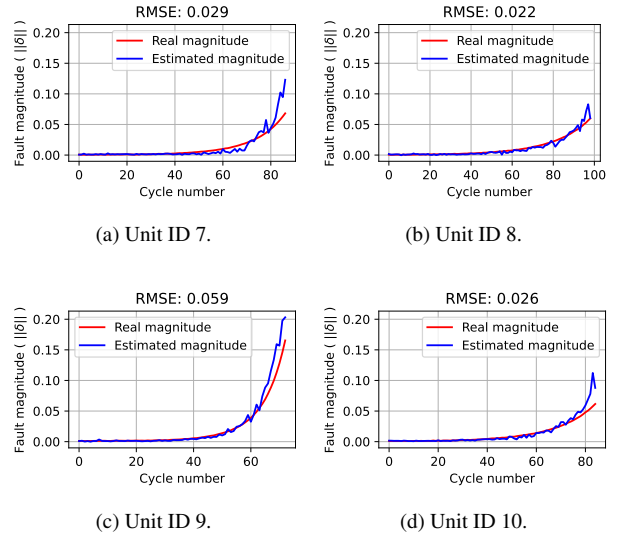


Figure 10: Real and estimated values of  $\|\delta\|$  using RIF's signatures.

tionships within the ANM family. On the theoretical side, we formally state the link between faults and model drift and prove the equivalence between the latter and an independence test. On the practical side, our proposed FD method does not require prior knowledge of faulty data to make accurate decisions and can be applied to continuous phenomena with no restrictions on the regression learning algorithm or expert knowledge used to capture its healthy dynamics. The following points summarize the key contributions of our work.

- We show that the fault detection task over the rich class of additive noise models can be equivalent to the machine learning problem of testing independence (distribution-free) between a regression input and its correspondent regression residual.

- We propose a new decision scheme for fault detection using the residual information values (RIVs), which are mutual information estimations.
- We state a range of parameters for the MI estimator to make our method strongly consistent, able to achieve exponentially fast decision under  $\mathcal{H}_0$ , and able to achieve both test power convergence to 1 and significance level exponential convergence to 0.
- We perform numerous experiments on synthetic systems for which we show the discrimination ability of our method for fault detection. Importantly, we observe that our method even works for systems outside the i.i.d. sampling assumption.
- We validate our method in the benchmark N-CMAPSS dataset, evidencing its usability in realistic scenarios. In this context, we also show our method's capability of describing the state of health (diagnosis) of the turbopumps in terms of information-driven features (RIFs).

These formal, numerical, and empirical results lead us to explore further practical applications for our method, such as benchmarking its capacity to estimate the state of health of other realistic time series systems and working in real-world scenarios. The ability of the residual information features (RIFs) to describe the state of health suggests a variety of next steps to study their practical usage in fault diagnosis and system prognostics.

## Appendix A. Appendix Outline

In these appendices, we present the proofs for all our theoretical claims, describe the details of the systems involved in the numerical analysis performed on synthetic distributions, and provide further insight into our theoretical assumptions and the experimental results on the synthetic scenarios. On the theoretics, in [Appendix B](#), we show and prove [Theorem 5](#), a generalized version of [Theorem 1](#), which establishes the relationship between model drift and input-residual dependency; this proof is supported with the aid of [Lemma 2](#), whose proof is shown in [Appendix J](#). In [Appendix C](#), we prove [Theorem 1](#) as a corollary of its extended version. In [Appendix D](#), [Appendix E](#), and [Appendix F](#), we prove [Theorem 2](#) (strong consistency), [3](#) (exponentially-fast decision), and [4](#) (error rate guarantees), respectively, and in [Appendix G](#), we justify the generality of our assumptions. On the numerical analysis, in [Appendix H](#), we provide a full description of the systems and methods employed in the results shown in [Sec. 7](#); and in [Appendix I](#), to enhance our analysis, we provide an error-bar analysis that showcases the consistency of the asymptotic and finite-length properties proved for our method.

## Appendix B. Generalized Link between Model Drift and Input-Residual Dependency

In this section, we show a generalized version of [Theorem 1](#). This generalized theorem links model drift and input-

residual dependency even outside our assumptions of the absence of bias, i.e., assumptions (i) and (ii) of our *standard assumptions* (see [Sec. 3.6](#)). Before making the statement of this generalized theorem, we need to introduce a broader version of [Def. 5](#), which enables us to work with the class of equivalence we denote as *perfectly biased almost-surely equivalent* models. This definition captures the idea of models that are equivalent in the sense of [Def. 5](#) but have a *perfect bias* between them, i.e., an offset.

**Definition 6.** Let  $\eta_1 : \mathbb{R}^p \rightarrow \mathbb{R}^q$  and  $\eta_2 : \mathbb{R}^p \rightarrow \mathbb{R}^q$  be measurable functions, and  $\mathbf{c} \in \mathbb{R}^q$ .  $\eta_1(\cdot)$  and  $\eta_2(\cdot)$  are said to be *almost-surely equivalent w.r.t.  $\mu$  with a bias  $\mathbf{c}$* , denoted by  $\eta_1 \approx_{\mu}^{\mathbf{c}} \eta_2$ , if for every r.v.  $X \sim \mu$  it holds that  $\eta_1(X) \stackrel{\text{a.s.}}{=} \eta_2(X) + \mathbf{c}$ . If there does not exist any  $\mathbf{c} \in \mathbb{R}^q$  such that  $\eta_1 \approx_{\mu}^{\mathbf{c}} \eta_2$ , it is denoted as  $\eta_1 \not\approx_{\mu} \eta_2$ .

Now, equipped with [Def. 6](#), we can state the general version of [Theorem 1](#) as follows.

**Theorem 5.** Let  $X$  and  $Y$  be random variables with values in  $\mathbb{R}^p$  and  $\mathbb{R}^q$ , respectively, such that  $(X, Y) \sim \text{add}(\tilde{\eta}, \tilde{h}; \mu)$ , and let  $\eta : \mathbb{R}^p \rightarrow \mathbb{R}^q$  be a measurable function. The following properties are true:

- (i) If there exists  $\mathbf{c} \in \mathbb{R}^q$  such that  $\tilde{\eta} \approx_{\mu}^{\mathbf{c}} \eta$ , then  $X$  and  $Y - \eta(X)$  are independent.
- (ii) If  $\tilde{\eta} \not\approx_{\mu} \eta$ , and both r.v.s.  $(X, Y - \eta(X))$  and  $(X, \tilde{h}(W))$  have densities, then  $X$  and  $Y - \eta(X)$  are not independent.

**Remark 2.** We highlight that property (i) of [Theorem 5](#) does not require any r.v. to have densities. Then, it would remain true even in a classification context where  $Y$  is a discrete random variable. The extension of our theory to discrete-output systems would require rethinking the properties of the MMSE estimator we exploited in this work to consider the properties of a classifier that optimizes a classification loss, such as the cross-entropy. The idea is to use this classifier to capture the nominal dynamics of the discrete-output system.

**PROOF OF THEOREM 5.** We divide this proof into proving each property (i) and (ii) that constitute [Theorem 5](#).

- **PROOF OF TH. 5 (i):** This proof relies on the definition of independence between r.v.s, this means, that we prove independence between  $X$  and  $Y - \eta(X)$  by proving that  $\forall A \in \mathcal{B}(\mathbb{R}^p), \forall B \in \mathcal{B}(\mathbb{R}^q)$ ,

$$\mathbb{P}(X \in A, Y - \eta(X) \in B) = \mathbb{P}(X \in A) \cdot \mathbb{P}(Y - \eta(X) \in B). \quad (\text{B.1})$$

Let us start this proof by noting that  $\tilde{\eta} \approx_{\mu}^{\mathbf{c}} \eta$ , from [Def. 6](#), implies that for every random variable  $\tilde{X} \sim \mu$ , it holds that  $\tilde{\eta}(\tilde{X}) \stackrel{\text{a.s.}}{=} \eta(\tilde{X}) + \mathbf{c}$ . This, in particular, is true for the marginal input of  $(X, Y) \sim \text{add}(\tilde{\eta}, \tilde{h}; \mu)$ ; i.e.,  $X \sim \mu$  satisfies that  $\tilde{\eta}(X) \stackrel{\text{a.s.}}{=} \eta(X) + \mathbf{c}$ .

To continue this proof, we define the following events in  $\Sigma$ :<sup>17,18</sup>

$$\mathcal{E}^{\text{add}} \equiv \{\omega \in \Omega : Y(\omega) = \tilde{\eta}(X(\omega)) + \tilde{h}(W(\omega))\}, \quad (\text{B.2})$$

$$\mathcal{E}_c^{\text{eq}} \equiv \{\omega \in \Omega : \tilde{\eta}(X(\omega)) = \eta(X(\omega)) + \mathbf{c}\}, \quad (\text{B.3})$$

and then, we have the following sequence of equalities for any arbitrary sets  $A \in \mathcal{B}(\mathbb{R}^p)$  and  $B \in \mathcal{B}(\mathbb{R}^q)$ :

$$\begin{aligned} & \mathbb{P}(X \in A, Y - \eta(X) \in B) \\ &= \mathbb{P}(X \in A, Y - \eta(X) \in B, \mathcal{E}^{\text{add}}) \end{aligned} \quad (\text{B.4})$$

$$= \mathbb{P}(X \in A, \tilde{\eta}(X) + \tilde{h}(W) - \eta(X) \in B, \mathcal{E}^{\text{add}}) \quad (\text{B.5})$$

$$= \mathbb{P}(X \in A, \tilde{\eta}(X) + \tilde{h}(W) - \eta(X) \in B) \quad (\text{B.6})$$

$$= \mathbb{P}(X \in A, \tilde{\eta}(X) + \tilde{h}(W) - \eta(X) \in B, \mathcal{E}_c^{\text{eq}}) \quad (\text{B.7})$$

$$= \mathbb{P}(X \in A, \eta(X) + \mathbf{c} + \tilde{h}(W) - \eta(X) \in B, \mathcal{E}_c^{\text{eq}}) \quad (\text{B.8})$$

$$= \mathbb{P}(X \in A, \tilde{h}(W) + \mathbf{c} \in B), \quad (\text{B.9})$$

where (B.4), (B.6), (B.7), and (B.9) are a consequence of the following property:

$$\forall \mathcal{E}_1 \in \Sigma, \forall \mathcal{E}_2 \in \Sigma, \mathbb{P}(\mathcal{E}_1) = 1 \Rightarrow \mathbb{P}(\mathcal{E}_1, \mathcal{E}_2) = \mathbb{P}(\mathcal{E}_2); \quad (\text{B.10})$$

Equation (B.5) and (B.8) are consequences of (B.2) and (B.3), respectively. As  $X$  and  $W$  are independent, we have that  $X$  and  $\tilde{h}(W)$  are independent. Moreover, if we define the set  $B_{-\mathbf{c}} \equiv \{\mathbf{x} \in \mathbb{R}^q : \mathbf{x} + \mathbf{c} \in B\}$ , we can see that

$$\begin{aligned} & \mathbb{P}(X \in A, Y - \eta(X) \in B) \\ &= \mathbb{P}(X \in A, \tilde{h}(W) + \mathbf{c} \in B) \end{aligned} \quad (\text{B.11})$$

$$= \mathbb{P}(X \in A, \tilde{h}(W) \in B_{-\mathbf{c}}) \quad (\text{B.12})$$

$$= \mathbb{P}(X \in A) \cdot \mathbb{P}(\tilde{h}(W) \in B_{-\mathbf{c}}), \quad (\text{B.13})$$

where (B.11), (B.12), and (B.13) come from (B.9), the definition of  $B_{-\mathbf{c}}$ , and the independence between  $X$  and  $\tilde{h}(W)$ , respectively. Developing further  $\mathbb{P}(\tilde{h}(W) \in B_{-\mathbf{c}})$ , we can see that

$$\begin{aligned} & \mathbb{P}(\tilde{h}(W) \in B_{-\mathbf{c}}) \\ &= \mathbb{P}(\tilde{h}(W) + \mathbf{c} \in B) \end{aligned} \quad (\text{B.14})$$

$$= \mathbb{P}(\tilde{h}(W) + \mathbf{c} \in B, \mathcal{E}_c^{\text{eq}}) \quad (\text{B.15})$$

$$= \mathbb{P}(\tilde{h}(W) + \tilde{\eta}(X) - \eta(X) \in B, \mathcal{E}_c^{\text{eq}}) \quad (\text{B.16})$$

$$= \mathbb{P}(\tilde{\eta}(X) + \tilde{h}(W) - \eta(X) \in B) \quad (\text{B.17})$$

$$= \mathbb{P}(\tilde{\eta}(X) + \tilde{h}(W) - \eta(X) \in B, \mathcal{E}^{\text{add}}) \quad (\text{B.18})$$

$$= \mathbb{P}(Y - \eta(X) \in B, \mathcal{E}^{\text{add}}) \quad (\text{B.19})$$

$$= \mathbb{P}(Y - \eta(X) \in B), \quad (\text{B.20})$$

where (B.15), (B.17), (B.18), and (B.20) are a consequence of (B.10); Equation (B.16) and (B.19) come from

(B.3) and (B.2), respectively; Equation (B.14) is a consequence of the definition of  $B_{-\mathbf{c}}$ . Then, from (B.13) and (B.20), we get that

$$\begin{aligned} & \mathbb{P}(X \in A, Y - \eta(X) \in B) \\ &= \mathbb{P}(X \in A) \cdot \mathbb{P}(\tilde{h}(W) \in B_{-\mathbf{c}}) \end{aligned} \quad (\text{B.21})$$

$$= \mathbb{P}(X \in A) \cdot \mathbb{P}(Y - \eta(X) \in B). \quad (\text{B.22})$$

Finally, we can see that (B.22) is precisely what we wanted to show, as stated in (B.1), proving in this way the property (i) of Theorem 5.

- **PROOF OF TH. 5 (ii):** We prove point (ii) by contradiction; in particular, we show how assuming both  $\tilde{\eta} \neq_{\mu} \eta$  and the independence between  $X$  and  $Y - \eta(X)$  leads to a contradiction. This contradiction has to do with the impossibility of the existence of probability density functions (pdfs) for the continuous r.v.s  $(X, Y - \eta(X))$  and  $(X, \tilde{h}(W))$  under the stated assumptions.

Let us start this proof by considering the mappings  $f_{X,R} : \mathbb{R}^{p+q} \rightarrow [0, \infty)$  and  $f_{X,\tilde{h}(W)} : \mathbb{R}^{p+q} \rightarrow [0, \infty]$  as pdfs of  $(X, Y - \eta(X))$  and  $(X, \tilde{h}(W))$ , respectively, and let us consider  $f_R : \mathbb{R}^q \rightarrow [0, \infty)$  as the marginal pdf of  $Y - \eta(X)$  induced from  $f_{X,R}(\cdot)$  and  $f_{\tilde{h}(W)} : \mathbb{R}^q \rightarrow [0, \infty)$  as the marginal pdf of  $\tilde{h}(W)$  induced from  $f_{X,\tilde{h}(W)}(\cdot, \cdot)$ .

Let us define a function  $D_{\eta,\tilde{\eta}} : \mathbb{R}^p \rightarrow \mathbb{R}^q$  in a way that  $D_{\eta,\tilde{\eta}}(\mathbf{x}) = \eta(\mathbf{x}) - \tilde{\eta}(\mathbf{x}), \forall \mathbf{x} \in \mathbb{R}^p$ . From Def. 4, we get that  $(X, Y) \sim \text{add}(\tilde{\eta}, \tilde{h}; \mu)$  implies  $(X, Y) \stackrel{\text{a.s.}}{=} (X, \tilde{\eta}(X) + \tilde{h}(W))$ , in turn implying  $(X, Y - \eta(X)) \stackrel{\text{a.s.}}{=} (X, \tilde{\eta}(X) + \tilde{h}(W) - \eta(X))$ ; as the latter r.v. is equal to  $(X, \tilde{h}(W) - D_{\eta,\tilde{\eta}}(X))$ , we get that  $(X, Y - \eta(X)) \stackrel{\text{a.s.}}{=} (X, \tilde{h}(W) - D_{\eta,\tilde{\eta}}(X))$ . Then, as  $f_{X,R}(\cdot, \cdot)$  is a pdf of  $(X, Y - \eta(X))$ , it also is a pdf of  $(X, \tilde{h}(W) - D_{\eta,\tilde{\eta}}(X))$ .

Let us consider an arbitrary set  $C \in \mathcal{B}(\mathbb{R}^{p+q})$ , then we can define a set  $\tilde{C}$  expressed by

$$\tilde{C} \equiv \{(\mathbf{x}, \mathbf{r} + D_{\eta,\tilde{\eta}}(\mathbf{x})) : \mathbf{x} \in \mathbb{R}^p, \mathbf{r} \in \mathbb{R}^q, (\mathbf{x}, \mathbf{r}) \in C\}. \quad (\text{B.23})$$

This definition satisfies that  $\forall \mathbf{x} \in \mathbb{R}^p, \forall \mathbf{r} \in \mathbb{R}^q$ , the equivalence  $[(\mathbf{x}, \mathbf{r}) \in C \Leftrightarrow (\mathbf{x}, \mathbf{r} + D_{\eta,\tilde{\eta}}(\mathbf{x})) \in \tilde{C}]$  holds; then, we have the following event equality:

$$\begin{aligned} & \{\omega \in \Omega : (X(\omega), \tilde{h}(W(\omega)) - D_{\eta,\tilde{\eta}}(X(\omega))) \in C\} \\ &= \{\omega \in \Omega : (X(\omega), \tilde{h}(W(\omega))) \in \tilde{C}\} \end{aligned} \quad (\text{B.24})$$

and, as a consequence,

$$\mathbb{P}((X, \tilde{h}(W) - D_{\eta,\tilde{\eta}}(X)) \in C) = \mathbb{P}((X, \tilde{h}(W)) \in \tilde{C}). \quad (\text{B.25})$$

Hence, if we define  $\tilde{f} : \mathbb{R}^{p+q} \rightarrow [0, \infty)$  as a function such that  $\tilde{f}(\mathbf{x}, \mathbf{r}) = f_{X,\tilde{h}(W)}(\mathbf{x}, \mathbf{r} + D_{\eta,\tilde{\eta}}(\mathbf{x})), \forall \mathbf{x} \in \mathbb{R}^p, \forall \mathbf{r} \in \mathbb{R}^q$ ,

<sup>17</sup>We are denoting the probability space of all the r.v.s involved in this work as  $(\Omega, \Sigma, \mathbb{P})$ .

<sup>18</sup>We highlight for these events that  $(X, Y) \sim \text{add}(\tilde{\eta}, \tilde{h}; \mu) \Leftrightarrow \mathbb{P}(\mathcal{E}^{\text{add}}) = 1$  and  $\tilde{\eta} \approx_{\mu}^c \eta \Leftrightarrow \mathbb{P}(\mathcal{E}_c^{\text{eq}}) = 1$ .

we can see that

$$\begin{aligned} & \mathbb{P}((X, \tilde{h}(W) - D_{\eta, \tilde{\eta}}(X)) \in C) \\ &= \mathbb{P}((X, \tilde{h}(W)) \in \tilde{C}) \end{aligned} \quad (\text{B.26})$$

$$= \int_{\tilde{C}} f_{X, \tilde{h}(W)}(\mathbf{x}, \mathbf{h}) \, d(\mathbf{x}, \mathbf{h}) \quad (\text{B.27})$$

$$= \int_{\tilde{C}} \tilde{f}(\mathbf{x}, \mathbf{h} - D_{\eta, \tilde{\eta}}(\mathbf{x})) \, d(\mathbf{x}, \mathbf{h}) \quad (\text{B.28})$$

$$= \int_C \tilde{f}(\mathbf{x}, \mathbf{r}) \, d(\mathbf{x}, \mathbf{r}), \quad (\text{B.29})$$

where (B.26) and (B.28) come from (B.25) and the definition of  $\tilde{f}(\cdot, \cdot)$ , respectively; hence,  $\tilde{f}(\cdot, \cdot)$  is a pdf of  $(X, \tilde{h}(W) - D_{\eta, \tilde{\eta}}(X))$ , and in consequence, it is a pdf of  $(X, Y - \eta(X))$ . This lets us state that the following equalities hold  $\lambda^{p+q}$ -almost everywhere:<sup>19</sup>

$$\begin{aligned} & f_{X,R}(\mathbf{x}, \mathbf{r}) \\ &= \tilde{f}(\mathbf{x}, \mathbf{r}) \end{aligned} \quad (\text{B.30})$$

$$= f_{X, \tilde{h}(W)}(\mathbf{x}, \mathbf{r} + D_{\eta, \tilde{\eta}}(\mathbf{x})), \quad (\text{B.31})$$

where (B.30) and (B.31) come from both  $f_{X,R}(\cdot, \cdot)$  and  $\tilde{f}(\cdot, \cdot)$  being pdfs of  $(X, Y - \eta(X))$ , and the definition of  $\tilde{f}(\cdot, \cdot)$ , respectively. This means that if we define the set of points where the pdfs are equal as  $E \subseteq \mathbb{R}^{p+q}$ , this is

$$E \equiv \left\{ (\mathbf{x}, \mathbf{r}) \in \mathbb{R}^{p+q} : \begin{array}{l} \mathbf{x} \in \mathbb{R}^p, \mathbf{r} \in \mathbb{R}^q, \\ f_{X,R}(\mathbf{x}, \mathbf{r}) = f_{X, \tilde{h}(W)}(\mathbf{x}, \mathbf{r} + D_{\eta, \tilde{\eta}}(\mathbf{x})) \end{array} \right\}, \quad (\text{B.32})$$

we get that  $E^c \equiv \mathbb{R}^{p+q} \setminus E \in \mathcal{B}(\mathbb{R}^{p+q})$  is a  $\lambda^{p+q}$ -null set, i.e.,  $\lambda^{p+q}(E^c) = 0$ .

One of the assumptions that lead to a contradiction is the independence between  $X$  and  $Y - \eta(X)$ ; this independence implies that

$$\forall \mathbf{x} \in \mathbb{R}^p, \forall \mathbf{r} \in \mathbb{R}^q, f_{X,R}(\mathbf{x}, \mathbf{r}) = f_X(\mathbf{x}) \cdot f_R(\mathbf{r}). \quad (\text{B.33})$$

Then, we get the following  $\forall (\mathbf{x}, \mathbf{r}) \in E$ :

$$\begin{aligned} & f_X(\mathbf{x}) \cdot f_R(\mathbf{r}) \\ &= f_{X,R}(\mathbf{x}, \mathbf{r}) \end{aligned} \quad (\text{B.34})$$

$$= f_{X, \tilde{h}(W)}(\mathbf{x}, \mathbf{r} + D_{\eta, \tilde{\eta}}(\mathbf{x})) \quad (\text{B.35})$$

$$= f_X(\mathbf{x}) \cdot \tilde{f}_{\tilde{h}(W)}(\mathbf{r} + D_{\eta, \tilde{\eta}}(\mathbf{x})), \quad (\text{B.36})$$

where (B.34), (B.35), and (B.36) are a consequence of (B.33), (B.31), and the independence between the r.v.s  $X$  and  $\tilde{h}(W)$ , respectively. Moreover, let us define  $\forall \mathbf{x} \in \mathbb{R}^p$ , the sets  $E_{\mathbf{x}} \equiv \{\mathbf{r} \in \mathbb{R}^q : (\mathbf{x}, \mathbf{r}) \in E\}$  and  $E_{\mathbf{x}}^c \equiv \mathbb{R}^q \setminus E_{\mathbf{x}}$ . We can see that  $E_{\mathbf{x}}^c \equiv \{\mathbf{r} \in \mathbb{R}^q : (\mathbf{x}, \mathbf{r}) \in E^c\}$ ,  $\forall \mathbf{x} \in \mathbb{R}^p$ . Then, as  $E^c$  is a  $\lambda^{p+q}$ -measurable set, from Fubini's theorem (see [59, Th. 3.4.1.]), we get that  $\lambda^p$ -almost every set  $E_{\mathbf{x}}^c$  is  $\lambda^q$ -measurable and that

$$\lambda^{p+q}(E^c) = \int_{\mathbb{R}^p} \lambda^q(E_{\mathbf{x}}^c) \, d\mathbf{x}, \quad (\text{B.37})$$

where  $\lambda^p$  and  $\lambda^q$  are the Lebesgue measures of  $(\mathbb{R}^p, \mathcal{B}(\mathbb{R}^p))$  and  $(\mathbb{R}^q, \mathcal{B}(\mathbb{R}^q))$ , respectively.

In addition, as  $\lambda^{p+q}(E^c) = 0$ , if we define a set

$$M \equiv \{\mathbf{x} \in \mathbb{R}^p : \lambda^q(E_{\mathbf{x}}^c) = 0\} \in \mathcal{B}(\mathbb{R}^p), \quad (\text{B.38})$$

we get from (B.37) that  $\lambda^p(M^c) = 0$ , for the complement set  $M^c \equiv \mathbb{R}^p \setminus M = \{\mathbf{x} \in \mathbb{R}^p : \lambda^q(E_{\mathbf{x}}^c) > 0\} \in \mathcal{B}(\mathbb{R}^p)$ . This means that there are  $\lambda^p$ -almost none points  $\mathbf{x} \in \mathbb{R}^p$  such that the set of points  $\mathbf{r} \in \mathbb{R}^q$  where (B.36) does not hold has a  $\lambda^q$ -measure greater than 0.

Before continuing this proof, we need to state the following lemma about degenerated random variable distributions. This lemma is related to the concept of *perfectly biased* equivalence we introduce in Def. 6.

**Lemma 2.**<sup>20</sup> *Let  $U$  be a random variable taking values in  $\mathbb{R}^r$  with  $r \in \mathbb{N}$ . If for every  $S \in \mathcal{B}(\mathbb{R}^r)$  it is satisfied that  $\mathbb{P}(U \in S) \in \{0, 1\}$ , then there exists  $\mathbf{c} \in \mathbb{R}^r$  such that  $\mathbb{P}(U = \mathbf{c}) = 1$ .*

Regarding the other assumption that leads to a contradiction, let us note that  $\tilde{\eta} \not\approx_{\mu} \eta$ , from Def. 6, corresponds to the non-existence of  $\mathbf{c}$  such that  $\tilde{\eta} \approx_{\mu}^c \eta$ , or which is equivalent, that  $\forall \mathbf{c} \in \mathbb{R}^q$ , there exists a r.v.  $\tilde{X} \sim \mu$  such that  $\mathbb{P}(\tilde{\eta}(\tilde{X}) = \eta(\tilde{X}) + \mathbf{c}) < 1$ . Then, since  $X$  has the same distribution as  $\tilde{X}$ , we have that  $\mathbb{P}(\tilde{\eta}(X) = \eta(X) + \mathbf{c}) < 1$ ,  $\forall \mathbf{c} \in \mathbb{R}^q$ , or equivalently, that  $\nexists \mathbf{c} \in \mathbb{R}^q : D_{\eta, \tilde{\eta}}(X) \stackrel{\text{a.s.}}{=} \mathbf{c}$ . Due to the contrapositive of Lemma 2, the nonexistence of  $\mathbf{c} \in \mathbb{R}^q$  such that  $\mathbb{P}(D_{\eta, \tilde{\eta}}(X) = \mathbf{c}) = 1$  implies that the proposition  $[\mathbb{P}(D_{\eta, \tilde{\eta}}(X) \in S) \in \{0, 1\}, \forall S \in \mathcal{B}(\mathbb{R}^q)]$  is false, or which is equivalent, that there exists  $G \in \mathcal{B}(\mathbb{R}^q)$  such that  $\mathbb{P}(D_{\eta, \tilde{\eta}}(X) \in G) \in (0, 1)$ , which in turn, implies the existence of  $H = \mathbb{R}^q \setminus G \in \mathcal{B}(\mathbb{R}^q)$  which also satisfies that  $\mathbb{P}(D_{\eta, \tilde{\eta}}(X) \in H) = 1 - \mathbb{P}(D_{\eta, \tilde{\eta}}(X) \in G) \in (0, 1)$ .

In addition, let us note the following event equality:

$$\{\omega \in \Omega : D_{\eta, \tilde{\eta}}(X(\omega)) \in G\} = \{\omega \in \Omega : X(\omega) \in D_{\eta, \tilde{\eta}}^{-1}(G)\}; \quad (\text{B.39})$$

this enables us to state that  $\exists A = D_{\eta, \tilde{\eta}}^{-1}(G) \in \mathcal{B}(\mathbb{R}^p) : \mathbb{P}(X \in A) = \mathbb{P}(D_{\eta, \tilde{\eta}}(X) \in G) > 0$  and, analogously, it is possible to state that  $\exists B = D_{\eta, \tilde{\eta}}^{-1}(H) \in \mathcal{B}(\mathbb{R}^p) : \mathbb{P}(X \in B) = \mathbb{P}(D_{\eta, \tilde{\eta}}(X) \in H) > 0$ .

Let us retrieve set  $M$  from (B.38), we can see that  $\lambda^p(M^c) = 0$  implies that  $\mathbb{P}(X \in M^c) = 0$ . In consequence, as  $A \cap M^c \subseteq M^c$ , it holds that  $\mathbb{P}(X \in A \cap M^c) = 0$ , and therefore, it is possible to conclude the following:  $\mathbb{P}(X \in A \cap M) = \mathbb{P}(X \in A) - \mathbb{P}(X \in A \cap M^c) = \mathbb{P}(X \in A) > 0$ ; analogously,  $\mathbb{P}(X \in B \cap M) = \mathbb{P}(X \in B) > 0$ .

Furthermore, let us consider  $f_X : \mathbb{R}^p \rightarrow [0, \infty)$  as a pdf induced by the marginalization of  $X$  from either a density of  $(X, Y - \eta(X))$  or  $(X, h(W))$ . We can see that  $\exists \mathbf{a} \in A \cap M$

<sup>19</sup> $\lambda^{p+q}$  corresponds to the Lebesgue measure of  $(\mathbb{R}^{p+q}, \mathcal{B}(\mathbb{R}^{p+q}))$ .

<sup>20</sup>The proof of Lemma 2 is presented in Appendix J.

such that  $f_X(\mathbf{a}) > 0$ .<sup>21</sup> Moreover, it is possible to see that evaluating  $\mathbf{x} = \mathbf{a}$  in (B.36) and dividing the terms of the equality by  $f_X(\mathbf{a}) > 0$ , we get that

$$\forall \mathbf{r} \in E_{\mathbf{a}}, f_R(\mathbf{r}) = f_{\tilde{h}(W)}(\mathbf{r} + D_{\eta, \tilde{\eta}}(\mathbf{a})). \quad (\text{B.40})$$

Analogously, we can see that  $\exists \mathbf{b} \in B \cap M$ , such that  $f_X(\mathbf{b}) > 0$  and

$$\forall \mathbf{r} \in E_{\mathbf{b}}, f_R(\mathbf{r}) = f_{\tilde{h}(W)}(\mathbf{r} + D_{\eta, \tilde{\eta}}(\mathbf{b})). \quad (\text{B.41})$$

From (B.40) and (B.41), we get the following:

$$\forall \mathbf{r} \in E_{\mathbf{a}, \mathbf{b}}, f_{\tilde{h}(W)}(\mathbf{r} + D_{\eta, \tilde{\eta}}(\mathbf{a})) = f_{\tilde{h}(W)}(\mathbf{r} + D_{\eta, \tilde{\eta}}(\mathbf{b})), \quad (\text{B.42})$$

where  $E_{\mathbf{a}, \mathbf{b}} \equiv E_{\mathbf{a}} \cap E_{\mathbf{b}} \in \mathcal{B}(\mathbb{R}^q)$ . Since  $\mathbf{a} \in M$  and  $\mathbf{b} \in M$ , we get that  $\lambda^q(E_{\mathbf{a}}^c) = \lambda^q(E_{\mathbf{b}}^c) = 0$ . Then, for  $E_{\mathbf{a}, \mathbf{b}}^c \equiv \mathbb{R}^q \setminus E_{\mathbf{a}, \mathbf{b}} = E_{\mathbf{a}}^c \cup E_{\mathbf{b}}^c \in \mathcal{B}(\mathbb{R}^q)$ , we get that  $\lambda^q(E_{\mathbf{a}, \mathbf{b}}^c) = 0$ ; this is because of the inequality  $\lambda^q(E_{\mathbf{a}, \mathbf{b}}^c) \leq \lambda^q(E_{\mathbf{a}}^c) + \lambda^q(E_{\mathbf{b}}^c) = 0$ . In consequence, the equality shown in (B.42), i.e., a periodicity for the pdf  $f_{\tilde{h}(W)}(\cdot)$ , is true  $\lambda^q$ -almost everywhere.

Let us define  $\mathbf{p} = (p_j)_{j=1}^q \in \mathbb{R}^q$  as  $\mathbf{p} \equiv D_{\eta, \tilde{\eta}}(\mathbf{a}) - D_{\eta, \tilde{\eta}}(\mathbf{b})$ . Due to  $\mathbf{a} \in A = D_{\eta, \tilde{\eta}}^{-1}(G)$  and  $\mathbf{b} \in B = D_{\eta, \tilde{\eta}}^{-1}(H)$ , we have that  $D_{\eta, \tilde{\eta}}(\mathbf{a}) \in G$  and  $D_{\eta, \tilde{\eta}}(\mathbf{b}) \in H$ ; then, as  $G \cap H = \emptyset$ , we have that  $D_{\eta, \tilde{\eta}}(\mathbf{a}) \neq D_{\eta, \tilde{\eta}}(\mathbf{b})$ ; hence,  $\mathbf{p} \neq \mathbf{0} \in \mathbb{R}^q$ . If we define the set  $\tilde{E} \equiv \{\mathbf{h} \in \mathbb{R}^q : \mathbf{h} - D_{\eta, \tilde{\eta}}(\mathbf{b}) \in E_{\mathbf{a}, \mathbf{b}}\} \in \mathcal{B}(\mathbb{R}^q)$ , we get that  $\forall \mathbf{h} \in \tilde{E}, \mathbf{h} - D_{\eta, \tilde{\eta}}(\mathbf{b}) \in E_{\mathbf{a}, \mathbf{b}}$ ; hence,

$$\forall \mathbf{h} \in \tilde{E}, f_{\tilde{h}(W)}(\mathbf{h}) = f_{\tilde{h}(W)}(\mathbf{h} + \mathbf{p}). \quad (\text{B.43})$$

For  $\tilde{E}^c \equiv \mathbb{R}^q \setminus \tilde{E} = \{\mathbf{h} \in \mathbb{R}^q : \mathbf{h} - D_{\eta, \tilde{\eta}}(\mathbf{b}) \in E_{\mathbf{a}, \mathbf{b}}^c\} \in \mathcal{B}(\mathbb{R}^q)$ , we can observe that  $\lambda^q(\tilde{E}^c) = \lambda^q(E_{\mathbf{a}, \mathbf{b}}^c) = 0$ .

In addition, if for an arbitrary  $j \in \mathbb{Z}$  we define a set  $\tilde{E}_j \equiv \{\mathbf{h} \in \mathbb{R}^q : \mathbf{h} + j\mathbf{p} \in \tilde{E}\} \in \mathcal{B}(\mathbb{R}^q)$ , we can see that  $\tilde{E}_j^c \equiv \mathbb{R}^q \setminus \tilde{E}_j = \{\mathbf{h} \in \mathbb{R}^q : \mathbf{h} + j\mathbf{p} \in \tilde{E}^c\} \in \mathcal{B}(\mathbb{R}^q)$  has a  $\lambda^q$ -measure of  $\lambda^q(\tilde{E}_j^c) = \lambda^q(\tilde{E}^c) = 0$  and that  $\forall \mathbf{h} \in \tilde{E}_j, \mathbf{h} + j\mathbf{p} \in \tilde{E}$ ; hence,

$$\forall \mathbf{h} \in \tilde{E}_j, f_{\tilde{h}(W)}(\mathbf{h} + j\mathbf{p}) = f_{\tilde{h}(W)}(\mathbf{h} + (j+1)\mathbf{p}). \quad (\text{B.44})$$

Moreover, if we define  $\tilde{E}_{\mathbb{Z}} \equiv \bigcap_{k \in \mathbb{Z}} \tilde{E}_k \in \mathcal{B}(\mathbb{R}^q)$ , its complement is  $\tilde{E}_{\mathbb{Z}}^c \equiv \mathbb{R}^q \setminus \tilde{E}_{\mathbb{Z}} = \bigcup_{k \in \mathbb{Z}} \tilde{E}_k^c \in \mathcal{B}(\mathbb{R}^q)$ . As  $\tilde{E}_{\mathbb{Z}}^c$  is the result of a countable union, we get that its  $\lambda^q$ -measure is  $\lambda^q(\tilde{E}_{\mathbb{Z}}^c) = 0$ ; this is due to the inequality  $\lambda^q(\tilde{E}_{\mathbb{Z}}^c) \leq \sum_{k \in \mathbb{Z}} \lambda^q(\tilde{E}_k^c) = \sum_{k \in \mathbb{Z}} 0 = 0$ . Now, we can apply (B.44) inductively to obtain the following property:

$$\forall \mathbf{h} \in \tilde{E}_{\mathbb{Z}}, [\forall k \in \mathbb{Z}, f_{\tilde{h}(W)}(\mathbf{h}) = f_{\tilde{h}(W)}(\mathbf{h} + k\mathbf{p})]. \quad (\text{B.45})$$

Let us note that  $\mathbf{p} = (p_j)_{j=1}^q \neq \mathbf{0} \in \mathbb{R}^q$  implies the existence of  $\ell \in \{1, 2, \dots, q\}$ , a dimension index, such that  $p_\ell \neq 0 \in \mathbb{R}$ . Then, according to  $\ell$ , it is possible to define

a partition  $\mathcal{R} \equiv \{r_k\}_{k \in \mathbb{Z}} \subseteq \mathcal{B}(\mathbb{R}^q)$  of  $\mathbb{R}^q$  such that  $\forall k \in \mathbb{Z}, r_k \equiv \{\mathbf{h} = (h_j)_{j=1}^q \in \mathbb{R}^q : h_\ell \in [kp_\ell, (k+1)p_\ell)\}$ . We can observe that  $\forall k \in \mathbb{Z}, [\forall \mathbf{h} \in r_0, \mathbf{h} + k\mathbf{p} \in r_k]$ ; hence, we obtain the following property for every  $k \in \mathbb{Z}$ :

$$\begin{aligned} & \mathbb{P}(\tilde{h}(W) \in r_k) \\ &= \int_{r_k} f_{\tilde{h}(W)}(\tilde{\mathbf{h}}) d\tilde{\mathbf{h}} \end{aligned} \quad (\text{B.46})$$

$$= \int_{r_0} f_{\tilde{h}(W)}(\mathbf{h} + k\mathbf{p}) d\mathbf{h} \quad (\text{B.47})$$

$$= \int_{r_0 \cap \tilde{E}_{\mathbb{Z}}} f_{\tilde{h}(W)}(\mathbf{h} + k\mathbf{p}) d\mathbf{h} + \int_{r_0 \cap \tilde{E}_{\mathbb{Z}}^c} f_{\tilde{h}(W)}(\mathbf{h} + k\mathbf{p}) d\mathbf{h} \quad (\text{B.48})$$

$$= 0 + \int_{r_0 \cap \tilde{E}_{\mathbb{Z}}} f_{\tilde{h}(W)}(\mathbf{h}) d\mathbf{h} \quad (\text{B.49})$$

$$= \int_{r_0 \cap \tilde{E}_{\mathbb{Z}}} f_{\tilde{h}(W)}(\mathbf{h}) d\mathbf{h} + \int_{r_0 \cap \tilde{E}_{\mathbb{Z}}^c} f_{\tilde{h}(W)}(\mathbf{h}) d\mathbf{h} \quad (\text{B.50})$$

$$= \int_{r_0} f_{\tilde{h}(W)}(\mathbf{h}) d\mathbf{h} \quad (\text{B.51})$$

$$= \mathbb{P}(\tilde{h}(W) \in r_0) \quad (\text{B.52})$$

where (B.46) and (B.52) come from  $f_{\tilde{h}(W)}(\cdot)$  being a pdf of  $\tilde{h}(W)$ , (B.48) and (B.51) come from the disjoint union  $r_0 = (r_0 \cap \tilde{E}_{\mathbb{Z}}) \cup (r_0 \cap \tilde{E}_{\mathbb{Z}}^c)$ , (B.49) and (B.50) come from  $\lambda^q(\tilde{E}_{\mathbb{Z}}^c) = 0$ , and (B.47) comes from a change of variable.

Let us note that

$$\begin{aligned} & \mathbb{P}(\tilde{h}(W) \in \mathbb{R}^q) \\ &= \sum_{k \in \mathbb{Z}} \mathbb{P}(\tilde{h}(W) \in r_k) \end{aligned} \quad (\text{B.53})$$

$$= \sum_{k \in \mathbb{Z}} \mathbb{P}(\tilde{h}(W) \in r_0), \quad (\text{B.54})$$

where (B.53) and (B.54) are a consequence of  $\mathcal{R}$  being a partition of  $\mathbb{R}^q$  and (B.52), respectively. Then, there are only two possible cases, and both lead to a contradiction.

In the first case,  $\mathbb{P}(\tilde{h}(W) \in r_0) = 0$ ; this implies that  $\sum_{k \in \mathbb{Z}} \mathbb{P}(\tilde{h}(W) \in r_0) = 0$ , which contradicts the fact that  $\mathbb{P}(\tilde{h}(W) \in \mathbb{R}^q) = 1$ . In the second case  $\mathbb{P}(\tilde{h}(W) \in r_0) > 0$ ; this implies that  $\sum_{k \in \mathbb{Z}} \mathbb{P}(\tilde{h}(W) \in r_k)$  diverges, which also contradicts that  $\mathbb{P}(\tilde{h}(W) \in \mathbb{R}^q) = 1$ .

In conclusion, we have shown that under the hypotheses of property (ii) of Theorem 5, assuming both  $\tilde{\eta} \neq_\mu \eta$  and the independence between  $X$  and  $Y - \eta(X)$  leads to a contradiction. This leads us to prove that under the mentioned hypotheses,  $\tilde{\eta} \neq_\mu \eta$  implies that  $X$  and  $Y - \eta(X)$  are not independent, proving in this way the property (ii) of Theorem 5.

Having demonstrated both properties (i) and (ii) of Theorem 5, we conclude our proof for Theorem 5.  $\square$

<sup>21</sup>  $\exists \mathbf{a} \in A \cap M : f_X(\mathbf{a}) > 0$  is true; otherwise, it would hold that  $f_X(\mathbf{x}) = 0, \forall \mathbf{x} \in A \cap M$ , implying  $\mathbb{P}(X \in A \cap M) = \int_{A \cap M} f_X(\mathbf{x}) d\mathbf{x} = \int_{A \cap M} 0 d\mathbf{x} = 0$ . I.e.,  $\nexists \mathbf{a} \in A \cap M : f_X(\mathbf{a}) > 0$  would contradict that  $\mathbb{P}(X \in A \cap M) > 0$ .

### Appendix C. Proof of Theorem 1 — Model Drift and Input-Residual Dependency Equivalence

In this section, we prove Theorem 1. Within this proof, we can observe that Theorem 1 is a corollary of Theorem 5, which corresponds to a broader version of Theorem 1.

**PROOF OF THEOREM 1.** As Theorem 1 states an equivalence relationship, in this proof, we will prove both implications that constitute the equivalence.

For the first implication (i.e.,  $[\tilde{\eta} \approx_\mu \eta]$  implies  $[X$  and  $Y - \eta(X)$  are independent]), the proof is straightforward. We can see that  $\tilde{\eta} \approx_\mu \eta$  (Def. 5) is equivalent to  $\tilde{\eta} \approx_\mu^0 \eta$  (Def. 6); then, there exists  $\mathbf{c} = \mathbf{0} \in \mathbb{R}^q$  such that  $\tilde{\eta} \approx_\mu^{\mathbf{c}} \eta$  and, in consequence, due to Theorem 5 point (i),  $X$  and  $Y - \eta(X)$  are independent.

For the second implication (i.e.,  $[X$  and  $Y - \eta(X)$  are independent] implies  $[\tilde{\eta} \approx_\mu \eta]$ ), we need to look at the contrapositive of Theorem 5 point (ii); this is, that the independence between  $X$  and  $Y - \eta(X)$  implies that either  $\tilde{\eta} \approx_\mu \eta$  is false or that the existence of the densities of  $(X, Y - \eta(X))$  and  $(X, \tilde{h}(W))$  is false. As the existence of the densities is ensured by our *standard assumptions* – point (iii) – we are only left with the fact that  $\tilde{\eta} \not\approx_\mu \eta$  is false.

The falsehood of  $\tilde{\eta} \approx_\mu \eta$  implies that there exists a value  $\mathbf{c} \in \mathbb{R}^q$  such that  $\tilde{\eta} \approx_\mu^{\mathbf{c}} \eta$ . Then, as  $X \sim \mu$ , we have that  $\tilde{\eta}(X) \stackrel{\text{a.s.}}{=} \eta(X) + \mathbf{c}$ . Moreover, as  $(X, Y) \sim \text{add}(\tilde{\eta}, \tilde{h}; \mu)$ , we have that  $(X, Y) \stackrel{\text{a.s.}}{=} (X, \tilde{\eta}(X) + \tilde{h}(W))$ ; hence

$$\begin{aligned} & [\tilde{\eta}(X) \stackrel{\text{a.s.}}{=} \eta(X) + \mathbf{c}] \wedge [(X, Y) \stackrel{\text{a.s.}}{=} (X, \tilde{\eta}(X) + \tilde{h}(W))] \\ \Rightarrow & (X, Y) \stackrel{\text{a.s.}}{=} (X, \eta(X) + \tilde{h}(W) + \mathbf{c}). \end{aligned} \quad (\text{C.1})$$

Then, let us note the following:

$$\begin{aligned} & \mathbb{E}[Y - \eta(X)] \\ &= \mathbb{E}[\eta(X) + \tilde{h}(W) + \mathbf{c} - \eta(X)] \end{aligned} \quad (\text{C.2})$$

$$= \mathbb{E}[\tilde{h}(W)] + \mathbf{c}. \quad (\text{C.3})$$

Since our *standard assumptions* consider  $\mathbb{E}[\tilde{h}(W)] = \mathbf{0} \in \mathbb{R}^q$  and  $\mathbb{E}[Y - \eta(X)] = \mathbf{0} \in \mathbb{R}^q$  (points (i) and (ii), respectively), by replacing these values in (C.3), we get that  $\mathbf{c} = \mathbf{0}$ . This, in turn, implies that  $\tilde{\eta} \approx_\mu^0 \eta$  (Def. 6) or, equivalently, that  $\tilde{\eta} \approx_\mu \eta$  (Def. 5).

Finally, we can see that our proof concludes at this point, as we have proven the equivalence relationship stated in Theorem 1 by proving the two implications that constitute it.  $\square$

### Appendix D. Proof of Theorem 2 — Strong Consistency

**PROOF OF THEOREM 2.** Let us note that every decision scheme  $\Psi_{\mathbf{b}, \mathbf{d}, \mathbf{a}}^\lambda = (\psi_{b_n, d_n, a_n}^{\lambda, n}(\cdot))_{n \in \mathbb{N}} \in \Psi_{\text{SC}}$  follows the construction shown in Sec. 4.1; in consequence,  $\Psi_{\mathbf{b}, \mathbf{d}, \mathbf{a}}^\lambda$  is a sequence of decision rules such that  $\forall n \in \mathbb{N}, \forall \mathbf{z}_n = (x_j, y_j)_{j=1}^n \in (\mathbb{R}^{p+q})^n$ ,

$$\psi_{b_n, d_n, a_n}^{\lambda, n}(\mathbf{z}_n) = 1_{[a_n, \infty)}(I_{b_n, d_n}^{\lambda, n}(\mathbf{j}_n)), \quad (\text{D.1})$$

where  $\mathbf{j}_n \equiv (x_j, y_j - \eta(x_j))_{j=1}^n$ . Let us recall that  $I_{b_n, d_n}^{\lambda, n}(\mathbf{j}_n)$  is an estimation of the MI between  $X$  and  $Y - \eta(X)$  as  $\mathbf{j}_n$  consists of

$n$  i.i.d. realizations of  $(X, Y - \eta(X))$ . Hence,  $\psi_{b_n, d_n, a_n}^{\lambda, n}(\mathbf{z}_n)$  is the output of a decision rule of length  $n$  for testing independence between  $X$  and  $Y - \eta(X)$ , and consequently,  $\Psi_{\mathbf{b}, \mathbf{d}, \mathbf{a}}^\lambda$  is a decision scheme for testing independence between the mentioned r.v.s. The usage of the estimator presented in [40] for testing independence was studied by [58].

From (8), let us notice that any  $\Psi_{\mathbf{b}, \mathbf{d}, \mathbf{a}}^\lambda \in \Psi_{\text{SC}}$  satisfies that  $\mathbf{b} \approx (n^{-l})_{n \in \mathbb{N}}$  for  $l \in (0, 1/3)$ ,  $\mathbf{d} \in \ell_1(\mathbb{N})$ ,  $1/\mathbf{d} \in O(\exp(n^{1/3}))$ ,  $\mathbf{a} \in o(1)$ , and  $\lambda \in (0, \infty)$ . Hence, from [58, Th. 3],  $\Psi_{\mathbf{b}, \mathbf{d}, \mathbf{a}}^\lambda$  is strongly consistent (see [58, Def. 1]) for detecting independence between  $X$  and  $Y - \eta(X)$ , which means that

$$X \text{ and } Y - \eta(X) \text{ are independent} \quad (\text{D.2})$$

$$\Rightarrow \mathbb{P}\left(\lim_{n \rightarrow \infty} \psi_{b_n, d_n, a_n}^{\lambda, n}(\mathbf{Z}_n) = 0\right) = 1 \quad (\text{D.3})$$

and

$$X \text{ and } Y - \eta(X) \text{ are not independent} \quad (\text{D.4})$$

$$\Rightarrow \mathbb{P}\left(\lim_{n \rightarrow \infty} \psi_{b_n, d_n, a_n}^{\lambda, n}(\mathbf{Z}_n) = 1\right) = 1. \quad (\text{D.5})$$

Moreover, as we are under our *standard assumptions* and  $(X, Y) \sim \text{add}(\tilde{\eta}, \tilde{h}; \mu)$ , we get from Theorem 1 the equivalence

$$[\tilde{\eta} \approx_\mu \eta] \Leftrightarrow [X \text{ and } Y - \eta(X) \text{ are independent}]; \quad (\text{D.6})$$

hence, as we can see in (6), Sec. 3.5, our null hypothesis ( $\mathcal{H}_0 : \tilde{\eta} \approx_\mu \eta$ ) is equivalent to the input-residual independence hypothesis, and our alternate hypothesis ( $\mathcal{H}_1 : \tilde{\eta} \not\approx_\mu \eta$ ) is equivalent to the input-residual non-independence hypothesis. In consequence, from (D.3), (D.5), and (D.6),

$$\mathbb{P}\left(\lim_{n \rightarrow \infty} \psi_{b_n, d_n, a_n}^{\lambda, n}(\mathbf{Z}_n) = i \mid \mathcal{H}_i\right) = 1, \forall i \in \{0, 1\}. \quad (\text{D.7})$$

Equation (D.7) shows that any  $\Psi_{\mathbf{b}, \mathbf{d}, \mathbf{a}}^\lambda \in \Psi_{\text{SC}}$  satisfies (1), i.e., Def. 1; hence, any decision scheme in  $\Psi_{\text{SC}}$  is strongly consistent in detecting model drift. This concludes our proof for Theorem 2.  $\square$

### Appendix E. Proof of Theorem 3 — Exponentially-Fast Decision under $\mathcal{H}_0$

**PROOF OF THEOREM 3.** Every decision scheme  $\Psi \in \Psi_{\text{FL}}$  follows the construction shown in Sec. 4.1; consequently, its parameters can be written explicitly as  $\Psi \equiv \Psi_{\mathbf{b}, \mathbf{d}, \mathbf{a}}^\lambda = (\psi_{b_n, d_n, a_n}^{\lambda, n}(\cdot))_{n \in \mathbb{N}}$ , and as shown in the proof of Theorem 2 (see Appendix D), it corresponds to a decision scheme for testing independence between  $X$  and  $Y - \eta(X)$ .

From (10), let us notice that any  $\Psi \equiv \Psi_{\mathbf{b}, \mathbf{d}, \mathbf{a}}^\lambda \in \Psi_{\text{FL}}$  satisfies that  $\mathbf{b} \approx (n^{-l})_{n \in \mathbb{N}}$  for  $l \in (0, 1/3)$ ,  $\mathbf{d} \approx (\exp(n^{-1/3}))_{n \in \mathbb{N}}$ ,  $\mathbf{a} \in o(1)$ , and  $\lambda \in (0, \infty)$ . Hence, from [58, Th. 4], we can see that

$$\begin{aligned} & X \text{ and } Y - \eta(X) \text{ are independent} \\ \Rightarrow & \forall m \in \mathbb{N}, \mathbb{P}(C_0^\Psi(\mathbf{J}_\infty) \geq m) \leq K \exp(-m^{1/3}), \end{aligned} \quad (\text{E.1})$$

for some universal constant  $K \in (0, \infty)$ , where  $\mathbf{J}_\infty$  denotes  $(X_j, Y_j - \eta(X_j))_{j=1}^\infty$  and, from [58, Def. 3],  $C_0^\Psi(\mathbf{J}_\infty)$  corresponds

to the random value that expresses when the tree-structured partition used for estimating the MI between  $X$  and  $Y - \eta(X)$  using the parameters of  $\Psi \equiv \Psi_{\mathbf{b}, \mathbf{d}, \mathbf{a}}^\lambda$  ( $\mathcal{A} = \{A_\ell\}_{\ell \in \Lambda}$ ; see Sec. 4.2, Stage one) collapses to the trivial partition  $\{\mathbb{R}^{p+q}\}$ ,<sup>22,23</sup> which in turn implies an MI estimation of 0.

As we have shown in the proof of Theorem 2, both  $(X, Y) \sim \text{add}(\tilde{\eta}, \tilde{h}; \mu)$  and being under our *standard assumptions*, imply from Theorem 1 that  $[\tilde{\eta} \simeq_\mu \eta] \Leftrightarrow [X \text{ and } Y - \eta(X) \text{ are independent}]$ . Hence, as our null hypothesis ( $\mathcal{H}_0$ ) corresponds to  $\tilde{\eta} \simeq_\mu \eta$  (see (6), Sec. 3.5), the consequence of the implication shown in (E.1) reduces to

$$\forall m \in \mathbb{N}, \mathbb{P}(C_0^\Psi(\mathbf{J}_\infty) \geq m | \mathcal{H}_0) \leq K \exp(-m^{1/3}). \quad (\text{E.2})$$

Let us consider an arbitrary  $m \in \mathbb{N}$ , then we have that  $C_0^\Psi(\mathbf{j}_\infty) = m \Rightarrow \forall n > m, I_{b_n, d_n}^{\lambda, n}(\mathbf{j}_n) = 0$ ;<sup>24</sup> hence,  $\forall n > m, \forall \mathbf{a} = (a_n)_{n \in \mathbb{N}} \in o(1), I_{b_n, d_n}^{\lambda, n}(\mathbf{j}_n) < a_n$ . Furthermore, if we observe the sequence of outputs from the decision rule, we have that  $\forall n > m = C_0^\Psi(\mathbf{j}_\infty), \psi_{b_n, d_n, a_n}^{\lambda, n}(\mathbf{z}_n) = 0$ . As this last statement is satisfied  $\forall m \in \mathbb{N}$ , we get the following relationship:

$$\mathcal{T}_0^\Psi(\mathbf{z}_\infty) = \sup \left\{ n \in \mathbb{N} : \psi_{b_n, d_n, a_n}^{\lambda, n}(\mathbf{z}_n) = 1 \right\} \leq C_0^\Psi(\mathbf{j}_\infty). \quad (\text{E.3})$$

From (E.3), we get the following relationship between events  $\forall m \in \mathbb{N}$ :

$$\{\omega \in \Omega : C_0^\Psi(\mathbf{J}_\infty(\omega)) < m\} \subseteq \{\omega \in \Omega : \mathcal{T}_0^\Psi(\mathbf{Z}_\infty(\omega)) < m\}, \quad (\text{E.4})$$

and consequently,  $\mathbb{P}(C_0^\Psi(\mathbf{J}_\infty) < m | \mathcal{H}_0) \leq \mathbb{P}(\mathcal{T}_0^\Psi(\mathbf{Z}_\infty) < m | \mathcal{H}_0)$ , or equivalently,

$$\mathbb{P}(\mathcal{T}_0^\Psi(\mathbf{Z}_\infty) \geq m | \mathcal{H}_0) \leq \mathbb{P}(C_0(\mathbf{J}_\infty) \geq m | \mathcal{H}_0). \quad (\text{E.5})$$

From (E.2) and (E.5), we get that for every  $\Psi \in \Psi_{\text{FL}}$ , it is satisfied that

$$\forall m \in \mathbb{N}, \mathbb{P}(\mathcal{T}_0^\Psi(\mathbf{Z}_\infty) \geq m | \mathcal{H}_0) \leq K \exp(-m^{1/3}), \quad (\text{E.6})$$

or which is equivalent, that

$$\forall m \in \mathbb{N}, \mathbb{P}(\mathcal{T}_0^\Psi(\mathbf{Z}_\infty) < m | \mathcal{H}_0) \geq 1 - K \exp(-m^{1/3}), \quad (\text{E.7})$$

for some universal constant  $K \in (0, \infty)$ . Equation (E.7) shows that  $\forall \Psi \in \Psi_{\text{FL}}$ , (10) is satisfied; hence, it concludes our proof for Theorem 3.  $\square$

## Appendix F. Proof of Theorem 4 — Power and Significance Level

**PROOF OF THEOREM 4.** Let us recall that every decision scheme  $\Psi \in \Psi_{\text{FL}}$  follows the construction shown in Sec. 4.1; consequently, the parameters of the decision scheme and each decision rule can be written explicitly, i.e.,  $\Psi \equiv \Psi_{\mathbf{b}, \mathbf{d}, \mathbf{a}}^\lambda$  and  $\forall n \in \mathbb{N}$ ,

<sup>22</sup>This collapsing time functional we denote as  $C_0^\Phi(\cdot)$  is denoted as  $\mathcal{T}_0(\cdot)$  in [58] (let us recall that we are denoting arbitrary decision schemes and as  $\Phi$  and the decision schemes induced by our pipeline introduced in Sec. 4.1 as  $\Psi$ ). We use the notation  $C_0^\Phi(\cdot)$  to avoid confusion with our functional  $\mathcal{T}_0^\Phi$  (Def. 2).

<sup>23</sup>Let us note that  $[C_0(\mathbf{J}_\infty) \geq m]$  denotes an event in which either  $C_0(\mathbf{J}_\infty)$  exists and is greater or equal than  $m$ , or  $C_0(\mathbf{J}_\infty)$  does not exist; this same idea applies to the notation  $[\mathcal{T}_0^\Phi(\mathbf{Z}_\infty) \geq m]$ .

<sup>24</sup>Here, we denote by  $\mathbf{z}_n$  and  $\mathbf{j}_n$ , the realizations of  $\mathbf{Z}_n = (X_j, Y_j)_{j=1}^n$  and  $\mathbf{J}_n = (X_j, Y_j - \eta(X_j))_{j=1}^n$ , respectively. We extend this notation to  $n = \infty$ .

$\psi_n(\cdot) \equiv \psi_{b_n, d_n, a_n}^{\lambda, n}(\cdot)$ . Theorem 4 states two assertions expressed in (11) and (12); hence, we divide this proof into two parts, one for each equation.

- **PROOF OF EQ. (11):** Let us observe that for every  $\Psi \equiv \Psi_{\mathbf{b}, \mathbf{d}, \mathbf{a}}^\lambda \in \Psi_{\text{FL}}$ , it is satisfied that  $\mathbf{b} \approx (n^{-l})_{n \in \mathbb{N}}$  with  $l \in (0, 1/3)$ ,  $\mathbf{a} \in o(1)$ ,  $\lambda \in (0, \infty)$ , and  $\mathbf{d} \approx (\exp(n^{1/3}))_{n \in \mathbb{N}}$ . The latter asymptotic equivalence implies that  $1/\mathbf{d} \approx (\exp(n^{1/3}))_{n \in \mathbb{N}}$ , and consequently, it implies that  $1/\mathbf{d} \in O(\exp(n^{1/3}))$ , and on the other hand, it implies that  $\sum_{n=1}^\infty d_n$  converges due to the convergence of  $\sum_{n=1}^\infty \exp(n^{-1/3})$ , which in turn, due to the non-negativity of  $\mathbf{d}$ , implies that  $\sum_{n=1}^\infty |d_n| < \infty$ ; this last property is equivalent to  $\mathbf{d} \in \ell_1(\mathbb{N})$ . Consequently, we get that  $\Psi \in \Psi_{\text{FL}} \Rightarrow \Psi \in \Psi_{\text{SC}}$ , i.e.,

$$\Psi_{\text{FL}} \subseteq \Psi_{\text{SC}}. \quad (\text{F.1})$$

From (F.1) and as we are under the *standard assumptions*, we get, from Theorem 2, that any  $\Psi \in \Psi_{\text{FL}} \subseteq \Psi_{\text{SC}}$  is strongly consistent for detecting model drift, i.e.,

$$\mathbb{P}\left(\lim_{n \rightarrow \infty} \psi_n(\mathbf{Z}_n) = i \mid \mathcal{H}_i\right) = 1, \forall i \in \{0, 1\}, \quad (\text{F.2})$$

which, in particular, implies that

$$\mathbb{P}\left(\lim_{n \rightarrow \infty} \psi_n(\mathbf{Z}_n) = 0 \mid \mathcal{H}_1\right) = 0. \quad (\text{F.3})$$

Moreover, we can develop the following sequence of equalities:

$$\begin{aligned} & \mathbb{P}\left(\lim_{n \rightarrow \infty} \psi_n(\mathbf{Z}_n) = 0\right) \\ &= \mathbb{P}\left(\lim_{n \rightarrow \infty} \{\omega \in \Omega : \psi_n(\mathbf{Z}_n(\omega)) = 0\}\right) \end{aligned} \quad (\text{F.4})$$

$$\begin{aligned} &= \mathbb{P}\left(\limsup_{n \rightarrow \infty} \{\omega \in \Omega : \psi_n(\mathbf{Z}_n(\omega)) = 0\}\right) \\ &= \mathbb{P}(\{\omega \in \Omega : [\forall m \in \mathbb{N}, \exists n \geq m : \psi_n(\mathbf{Z}_n(\omega)) = 0]\}) \end{aligned} \quad (\text{F.5})$$

$$\begin{aligned} &= \mathbb{P}\left(\lim_{k \rightarrow \infty} \{\omega \in \Omega : [\forall m \leq k, \exists n \geq m : \psi_n(\mathbf{Z}_n(\omega)) = 0]\}\right) \end{aligned} \quad (\text{F.6})$$

$$\begin{aligned} &= \mathbb{P}\left(\lim_{k \rightarrow \infty} \{\omega \in \Omega : [\exists n \geq k : \psi_n(\mathbf{Z}_n(\omega)) = 0]\}\right) \end{aligned} \quad (\text{F.7})$$

$$\begin{aligned} &= \lim_{k \rightarrow \infty} \mathbb{P}(\{\omega \in \Omega : [\exists n \geq k : \psi_n(\mathbf{Z}_n(\omega)) = 0]\}). \end{aligned} \quad (\text{F.8})$$

Equation (F.4) comes from the definition of the event subject to the limit  $[\psi_n(\mathbf{Z}_n) = 0]$ , and (F.6) and (F.5) come from the definition of the limit superior (limsup) of a set sequence and the existence of its limit superior given the existence of its limit, respectively [60]. To obtain (F.7) and (F.8), if we define the event  $\mathcal{E}_n \equiv \{\omega \in \Omega : \psi_n(\mathbf{Z}_n(\omega)) = 0\}$ , we can see that (F.7) and (F.8) come from  $\bigcap_{m=1}^\infty \bigcup_{n=m}^\infty \mathcal{E}_n = \lim_{k \rightarrow \infty} \bigcap_{m=1}^k \bigcup_{n=m}^\infty \mathcal{E}_n$  and  $\bigcap_{m=1}^k \bigcup_{n=m}^\infty \mathcal{E}_n = \bigcup_{n=k}^\infty \mathcal{E}_n$ , respectively. The last equality, (F.9), is a consequence of the continuity of the probability measure  $\mathbb{P}$ .

Let us observe that for any  $k \in \mathbb{N}$  and sampling realization  $\mathbf{z}_k \in (\mathbb{R}^{p+q})^k$ ,<sup>25</sup> it is satisfied that  $\psi_k(\mathbf{z}_k) = 0$  implies that  $\exists n \geq k : \psi_n(\mathbf{z}_n) = 0$ ; then, we get that  $\forall k \in \mathbb{N}$ ,

$$\{\omega \in \Omega : \psi_k(\mathbf{Z}_k(\omega)) = 0\} \quad (\text{F.10})$$

$$\subseteq \{\omega \in \Omega : [\exists n \geq k : \psi_n(\mathbf{Z}_n) = 0]\}, \quad (\text{F.11})$$

which implies that  $\forall k \in \mathbb{N}$ ,

$$\mathbb{P}(\psi_k(\mathbf{Z}_k) = 0 | \mathcal{H}_1) \leq \mathbb{P}(\exists n \geq k : \psi_n(\mathbf{Z}_n) = 0 | \mathcal{H}_1). \quad (\text{F.12})$$

If we take the limit when  $k$  tends to infinity, we get that

$$\begin{aligned} & \lim_{k \rightarrow \infty} \mathbb{P}(\psi_k(\mathbf{Z}_k) = 0 | \mathcal{H}_1) \\ & \leq \lim_{k \rightarrow \infty} \mathbb{P}(\exists n \geq k : \psi_n(\mathbf{Z}_n) = 0 | \mathcal{H}_1) \end{aligned} \quad (\text{F.13})$$

$$= \mathbb{P}\left(\lim_{n \rightarrow \infty} \psi_n(\mathbf{Z}_n) = 0 \mid \mathcal{H}_1\right) \quad (\text{F.14})$$

$$= 0, \quad (\text{F.15})$$

where (F.13) comes from taking the limit of  $k$  to infinity on (F.12), (F.14) is a consequence of conditioning (F.9) on  $\mathcal{H}_1$ , and (F.15) comes from (F.3). Moreover, from the non-negativity of the probability measure, we get that

$$\lim_{k \rightarrow \infty} \mathbb{P}(\psi_k(\mathbf{Z}_k) = 0 | \mathcal{H}_1) = 0. \quad (\text{F.16})$$

In consequence, recalling that  $\beta_{\psi_n} = \mathbb{P}(\psi_n(\mathbf{Z}_n) = 0 | \mathcal{H}_1)$  from Def. 3, we can see that

$$\begin{aligned} & \lim_{n \rightarrow \infty} (1 - \beta_{\psi_n}) \\ & = 1 - \lim_{n \rightarrow \infty} \beta_{\psi_n} \end{aligned} \quad (\text{F.17})$$

$$= 1 - \lim_{n \rightarrow \infty} \mathbb{P}(\psi_n(\mathbf{Z}_n) = 0 | \mathcal{H}_1) \quad (\text{F.18})$$

$$= 1, \quad (\text{F.19})$$

which proves (11), concluding this part of the proof.

- **PROOF OF EQ. (12):** Let us observe that under the *standard assumptions*, it is satisfied due to Theorem 3, that for every  $\Psi \in \Psi_{\text{FL}}$ ,

$$\mathbb{P}(\mathcal{T}_0^\Psi((\mathbf{Z}_n)_{n=1}^\infty) < m | \mathcal{H}_0) \geq 1 - K \exp(-m^{-1/3}), \forall m \in \mathbb{N}, \quad (\text{F.20})$$

for a universal constant  $K > 0$ , and in consequence,

$$\mathbb{P}(\mathcal{T}_0^\Psi((\mathbf{Z}_n)_{n=1}^\infty) \geq m | \mathcal{H}_0) \leq K \exp(-m^{1/3}). \quad (\text{F.21})$$

In addition, let us note that for an arbitrary sample size  $n \in \mathbb{N}$  and an arbitrary sampling realization  $\mathbf{z}_\infty \in (\mathbb{R}^{p+q})^\infty$ , we have that  $\psi_n(\mathbf{z}_n) = 1 \Rightarrow \mathcal{T}_0^\Psi(\mathbf{z}_\infty) \geq n$ , and in consequence

$$\{\omega \in \Omega : \psi_n(\mathbf{Z}_n(\omega)) = 1\} \subseteq \{\omega \in \Omega : \mathcal{T}_0^\Psi(\mathbf{Z}_\infty(\omega)) \geq n\}, \quad (\text{F.22})$$

which in turn implies that

$$\mathbb{P}(\psi_n(\mathbf{Z}_n) = 1 | \mathcal{H}_0) \leq \mathbb{P}(\mathcal{T}_0^\Psi(\mathbf{Z}_\infty) \geq n | \mathcal{H}_0). \quad (\text{F.23})$$

Recalling  $\alpha_{\psi_n}$  from Def. 3, we can see, from (F.23) and (F.21), that  $\forall n \in \mathbb{N}$ ,

$$\begin{aligned} & \alpha_{\psi_n} \\ & = \mathbb{P}(\psi_n(\mathbf{Z}_n) = 1 | \mathcal{H}_0) \end{aligned} \quad (\text{F.24})$$

$$\leq \mathbb{P}(\mathcal{T}_0^\Psi(\mathbf{Z}_\infty) \geq n | \mathcal{H}_0) \quad (\text{F.25})$$

$$\leq K \exp(-n^{1/3}), \quad (\text{F.26})$$

which proves (12), concluding this part of the proof.

As we have proven both (11) and (12), we conclude our proof for Theorem 4.  $\square$

## Appendix G. Generality of the Non-Bias Assumptions and the Uniform Universal Noise

In this section, we show how the assumptions (i) and (ii) of the *standard assumptions* (see Sec. 3.6) and the uniform distribution for the (*universal*) noise term ( $W$ ) in Def. 4 do not imply a loss of generality.

### Appendix G.1. Assumption of Unbiased Noise

The assumption of unbiased noise corresponds to assumption (i) of our *standard assumptions*, this is that  $\mathbb{E}[\tilde{h}(W)] = \mathbf{0} \in \mathbb{R}^q$ . This does not imply a loss of generality, as if  $(X, Y) \sim \text{add}(\tilde{\eta}, \tilde{h}; \mu)$  with  $\mathbb{E}[\tilde{h}(W)] = \mathbf{b} \in \mathbb{R}^q$  and  $\mathbf{b} \neq \mathbf{0} \in \mathbb{R}^q$ , it is possible to embed the bias ( $\mathbf{b}$ ) into  $\tilde{\eta}(\cdot)$ . Embedding the noise bias into  $\tilde{\eta}(\cdot)$  can be done by considering the mappings  $\tilde{\eta} : \mathbb{R}^p \rightarrow \mathbb{R}^q$  and  $\tilde{h} : [0, 1] \rightarrow \mathbb{R}^q$  such that  $\forall x \in \mathbb{R}^p, \tilde{\eta}(x) = \tilde{\eta}(x) + \mathbf{b}$  and  $\forall w \in [0, 1], \tilde{h}(w) = \tilde{h}(w) - \mathbf{b}$ , respectively. Then, we have that

$$\begin{aligned} & (X, Y) \\ & \stackrel{\text{a.s.}}{=} (X, \tilde{\eta}(X) + \tilde{h}(W)) \end{aligned} \quad (\text{G.1})$$

$$= (X, (\tilde{\eta}(X) + \mathbf{b}) + (\tilde{h}(W) - \mathbf{b})) \quad (\text{G.2})$$

$$= (X, \tilde{\eta}(X) + \tilde{h}(W)). \quad (\text{G.3})$$

This implies that

$$(X, Y) \stackrel{\text{a.s.}}{=} (X, \tilde{\eta}(X) + \tilde{h}(W)) \Leftrightarrow (X, Y) \stackrel{\text{a.s.}}{=} (X, \tilde{\eta}(X) + \tilde{h}(W)). \quad (\text{G.4})$$

Hence, the following equivalence holds

$$[(X, Y) \sim \text{add}(\tilde{\eta}, \tilde{h}; \mu)] \Leftrightarrow [(X, Y) \sim \text{add}(\tilde{\eta}, \tilde{h}; \mu)] \quad (\text{G.5})$$

as a consequence of (G.4) – i.e., equivalence on point (ii) of Def. 4 – and the fact that  $X \sim \mu$  holds for both terms equivalent in (G.5) – i.e., equivalence on point (i) of Def. 4.<sup>26</sup> The equivalence stated in (G.5) lets us know that no generality is lost when assuming  $\mathbb{E}[\tilde{h}(W)] = \mathbf{0} \in \mathbb{R}^q$ .

<sup>25</sup>For more details on the notation of random samplings and their realizations, we refer the reader to the proof of Theorem 3 in Appendix E.

<sup>26</sup> $X \sim \mu$  denotes that  $\mathbb{P}(X \in A) = \mu(A), \forall A \in \mathcal{B}(\mathbb{R}^p)$ .

## Appendix G.2. Assumption of Unbiased Estimator

The assumption of unbiased estimator corresponds to assumption (ii) of our *standard assumptions*, this is that  $\mathbb{E}[Y - \eta(X)] = \mathbf{0} \in \mathbb{R}^q$  for a system  $(X, Y) \sim \text{add}(\tilde{\eta}, \tilde{h}; \mu)$ . This does not imply a loss of generality, as if  $\eta(\cdot)$  is a biased estimator such that  $\mathbb{E}[Y - \eta(X)] = \mathbf{b} \in \mathbb{R}^q$  with  $\mathbf{b} \neq \mathbf{0} \in \mathbb{R}^q$ , it is possible to correct it to build an unbiased one. This correction can be made by considering a mapping  $\tilde{\eta} : \mathbb{R}^p \rightarrow \mathbb{R}^q$  such that  $\tilde{\eta}(x) = \eta(x) + \mathbf{b}, \forall x \in \mathbb{R}^p$ . Then, we can observe that  $\mathbb{E}[Y - \tilde{\eta}(X)] = \mathbb{E}[Y - \eta(X) - \mathbf{b}] = \mathbb{E}[Y - \eta(X)] - \mathbf{b} = \mathbf{b} - \mathbf{b} = \mathbf{0}$ .<sup>27</sup> Hence, no generality is lost when assuming  $\mathbb{E}[Y - \eta(X)] = \mathbf{0}$ .

## Appendix G.3. Generality of the Uniform Universal Noise

Here, we clarify the generality of Def. 4 in terms of using a universal noise with uniform distribution, i.e., the usage of  $W \sim \text{Uniform}([0, 1])$ ; this generality is a consequence of noise outsourcing (see Lemma 1).

Let us consider a r.v. – i.e., a system –  $(X, Y)$  such that  $X \sim \mu$  and  $(X, Y) \stackrel{\text{a.s.}}{=} (X, \eta(X) + h(\tilde{W}))$  with  $\eta : \mathbb{R}^p \rightarrow \mathbb{R}^q$  and  $h : \mathbb{R}^s \rightarrow \mathbb{R}^q$ , where  $\tilde{W}$  takes values in  $(\mathbb{R}^s, \mathcal{B}(\mathbb{R}^s))$  with an arbitrary  $s \in \mathbb{N}$  and an arbitrary distribution. If we consider  $K$  as a constant random variable, i.e.,  $K : \Omega \rightarrow \mathbb{R}$ , where  $\forall \omega \in \Omega, K(\omega) = 0$ ; then, for the r.v.  $(K, \tilde{W})$ , Lemma 1 ensures the existence of the mapping  $f : \mathbb{R} \times [0, 1] \rightarrow \mathbb{R}^s$  such that  $(K, \tilde{W}) \stackrel{\text{a.s.}}{=} (K, f(K, W))$  with  $W \sim \text{Uniform}([0, 1])$  independent of  $K$ . Moreover, as  $[\forall \omega \in \Omega, K(\omega) = 0]$  implies that  $K \stackrel{\text{a.s.}}{=} 0$ , we obtain the following sequence of implications:

$$\begin{aligned} (K, \tilde{W}) &\stackrel{\text{a.s.}}{=} (K, f(K, W)) \wedge K \stackrel{\text{a.s.}}{=} 0 \\ \Rightarrow \mathbb{P}((K, \tilde{W}) = (K, f(K, W)), K = 0) &= 1 \end{aligned} \quad (\text{G.6})$$

$$\Rightarrow \mathbb{P}((0, \tilde{W}) = (0, f(0, W))) = 1 \quad (\text{G.7})$$

$$\Rightarrow \tilde{W} \stackrel{\text{a.s.}}{=} f(0, W), \quad (\text{G.8})$$

where (G.6) is a consequence of intersecting almost-surely events – see (B.10) in Appendix B – (G.7) comes from 0 being the only possible value for the r.v.  $K$ , and (G.8) is a consequence of decoupling the a.s. r.v.s in (G.7) into their two constitutive coordinates and considering the second ones.

Let us note that it is possible to define a mapping  $\tilde{h} : [0, 1] \rightarrow \mathbb{R}^q$  such that  $\forall w \in [0, 1], \tilde{h}(w) = h(f(0, w))$ . From (G.8), we get that  $\tilde{h}(W) = h(f(0, W)) \stackrel{\text{a.s.}}{=} h(\tilde{W})$ . This last relationship implies  $(X, Y) \stackrel{\text{a.s.}}{=} (X, \eta(X) + h(\tilde{W})) \stackrel{\text{a.s.}}{=} (X, \eta(X) + \tilde{h}(W))$ . Consequently, recalling Def. 4 (and that  $X \sim \mu$ ), we get that  $(X, Y) \sim \text{add}(\eta, \tilde{h}; \mu)$ .

The fact that for any system  $(X, Y)$  with  $X \sim \mu$  and  $(X, Y) \stackrel{\text{a.s.}}{=} (X, \eta(X) + h(\tilde{W}))$  where  $\tilde{W}$  follows an arbitrary distribution, there exists a function  $\tilde{h}(\cdot)$  such that  $(X, Y) \sim \text{add}(\eta, \tilde{h}; \mu)$  shows the generality of Def. 4.

<sup>27</sup>Even though  $\mathbf{b}$  may be unknown, it can be easily estimated from a sampling of the system:  $\mathbf{Z}_n = (X_j, Y_j)_{j=1}^n$ , as  $\hat{\mathbf{b}} = \frac{1}{n} \sum_{j=1}^n Y_j - \eta(X_j)$ .

## Appendix H. Experiment Description — Synthetic Distribution Drifts

This section extends the experiment description presented in Sec. 7 regarding the numerical analysis performed on synthetic distributions to make our results reproducible. The core idea of these experiments is to show how our method and baselines behave when ranging a parametrized drift  $\delta \in \mathbb{R}^2$ . For this purpose, we consider a nominal model  $\eta_\theta(\cdot)$  and a system with unknown drift  $(X^{[\delta]}, Y^{[\delta]}) \sim \text{add}(\eta_{\theta, \delta}, h; \mu)$ .<sup>28</sup> Let us note that the nominal model is the MMSE estimator of  $Y$  given  $X$  assuming a nominal system distributes as  $\text{add}(\eta_{\theta, \mathbf{0}}, h; \mu)$ .

Our numeric analysis consists of, first, obtaining a sampling  $\mathbf{Z}_n^{[\delta]} = (X_j^{[\delta]}, Y_j^{[\delta]})_{j=1}^n$  of  $n$  samples from the  $\delta$ -drifted system  $(X^{[\delta]}, Y^{[\delta]}) \sim \text{add}(\eta_{\theta, \delta}, h; \mu)$ , then, building a joint input-residual sampling as expressed in points 1 and 2 of Sec. 4.1:  $\mathbf{J}_n^{[\delta]} = (X_j^{[\delta]}, Y_j^{[\delta]} - \eta_\theta(X_j^{[\delta]}))_{j=1}^n$ , and finally, obtaining a quantification of the model drift using our method and two baseline methods.

### Appendix H.1. Description of Synthetic Systems

Here, we describe the six systems used in our experiments: four forward and two autoregressive systems. Before going into the details of each system, we show that all of them (independent of their drift) share the following common random variables:

$$U \sim \text{Uniform}([a_U, b_U]), \quad (\text{H.1})$$

$$S \sim \mathcal{N}(\mu_S, \sigma_S^2), \quad (\text{H.2})$$

$$H \sim \mathcal{N}(\mu_H, \sigma_H^2), \quad (\text{H.3})$$

$$W \sim \text{Uniform}([a_W, b_W]), \quad (\text{H.4})$$

where all  $U, S, H$ , and  $W$  are independent with each other. We denote the samplings of each r.v. as  $(U_j)_{j=1}^n, (S_j)_{j=1}^n, (H_j)_{j=1}^n$ , and  $(W_j)_{j=1}^n$ , respectively. In Table H.2 (at the end of this subsection), we show the values of all constant coefficients used in our analysis, including the distribution parameters of the mentioned r.v.s.

#### Appendix H.1.1. Forward Systems

The input of these models corresponds to  $X^{[\delta]} \equiv X = (U, S)$ , and in consequence, a sampling of the input corresponds to  $(X_j)_{j=1}^n = (U_j, S_j)_{j=1}^n$ .<sup>29</sup> The generative model of the output corresponds  $\forall j \in \{1, 2, \dots, n\}$  to

$$Y_j^{[\delta]} = \eta_{\theta, \delta}(X_j) + h(W_j). \quad (\text{H.5})$$

The nominal model corresponds to  $\eta_\theta(\cdot) = \eta_{\theta, \mathbf{0}}(\cdot)$ ; hence, the residual is as follows  $\forall j \in \{1, 2, \dots, n\}$ :

$$R_j^{[\delta]} \equiv Y_j^{[\delta]} - \eta_{\theta, \mathbf{0}}(X_j) = \eta_{\theta, \delta}(X_j) - \eta_\theta(X_j) + h(W_j). \quad (\text{H.6})$$

<sup>28</sup>Although in Sec. 7, a potentially drifted system is expressed as  $(X, Y) \sim \text{add}(\eta_{\theta, \delta}, h; \mu)$ , in this description, we express it with the notation  $(X^{[\delta]}, Y^{[\delta]}) \sim \text{add}(\eta_{\theta, \delta}, h; \mu)$  to make explicit the effects of  $\delta$  in the random variables.

<sup>29</sup>Note that  $X$  does not depend on  $\delta$ ; according to our notation, this can be written as  $X_j^{[\delta]} = X_j, \forall \delta \in \mathbb{R}^2$ .

*Linear System.* The linear systems are determined by a simple linear combination of the input coordinates. The expressions for  $\eta_{\theta,\delta}(\cdot)$  and  $h(\cdot)$  are as follows  $\forall (u, s) \in \mathbb{R}^2$  and  $\forall w \in \mathbb{R}$ :

$$\eta_{\theta,\delta}(u, s) = (c_1 + \delta_1)u + (c_2 + \delta_2)s, \quad (\text{H.7})$$

$$h(w) = kw. \quad (\text{H.8})$$

In consequence, the (actual) output (H.9), nominal output (H.10), and residual (H.11), correspond  $\forall j \in \{1, 2, \dots, n\}$  to

$$Y_j^{[\delta]} = (c_1 + \delta_1)U_j + (c_2 + \delta_2)S_j + kW_j, \quad (\text{H.9})$$

$$\eta_{\theta}(X_j) = c_1U_j + c_2S_j, \quad (\text{H.10})$$

$$R_j^{[\delta]} = \delta_1U_j + \delta_2S_j + kW_j. \quad (\text{H.11})$$

*Polynomial System.* The polynomial systems are determined by a linear combination of non-linear transformations of the input coordinates. The expressions for  $\eta_{\theta,\delta}(\cdot)$  and  $h(\cdot)$  are as follows  $\forall (u, s) \in \mathbb{R}^2$  and  $\forall w \in \mathbb{R}$ :

$$\eta_{\theta,\delta}(u, s) = (c_1 + \delta_1)u^2 + (c_2 + \delta_2)s^3, \quad (\text{H.12})$$

$$h(w) = kw. \quad (\text{H.13})$$

In consequence, the (actual) output (H.14), nominal output (H.15), and residual (H.16), correspond  $\forall j \in \{1, 2, \dots, n\}$  to

$$Y_j^{[\delta]} = (c_1 + \delta_1)U_j^2 + (c_2 + \delta_2)S_j^3 + kW_j, \quad (\text{H.14})$$

$$\eta_{\theta}(X_j) = c_1U_j^2 + c_2S_j^3, \quad (\text{H.15})$$

$$R_j^{[\delta]} = \delta_1U_j^2 + \delta_2S_j^3 + kW_j. \quad (\text{H.16})$$

*Trigonometric System.* The trigonometric systems are determined by an input-output relationship expressed by trigonometric functions. The expressions for  $\eta_{\theta,\delta}(\cdot)$  and  $h(\cdot)$  are as follows  $\forall (u, s) \in \mathbb{R}^2$  and  $\forall w \in \mathbb{R}$ :

$$\eta_{\theta,\delta}(u, s) = (A + \delta_1) \sin(u \cdot s + \phi + \delta_2), \quad (\text{H.17})$$

$$h(w) = A_W \sin(f_W \cdot w + \phi_W). \quad (\text{H.18})$$

In consequence, the (actual) output (H.19) and nominal output (H.20), correspond  $\forall j \in \{1, 2, \dots, n\}$  to

$$Y_j^{[\delta]} = (A + \delta_1) \sin(U_j \cdot S_j + \phi + \delta_2) + A_W \sin(f_W \cdot W_j + \phi_W), \quad (\text{H.19})$$

$$\eta_{\theta}(X_j) = A \sin(U_j \cdot S_j + \phi). \quad (\text{H.20})$$

The residual expression ( $R_j^{[\delta]}$ ) cannot be simplified further than shown in (H.6).

*MLP System.* The MLP systems are built upon an MLP-based deterministic input-output relationship affected by additive noise. In this case, the MLP consists of a single hidden layer with two hidden units; the nominal parameters were chosen randomly from a fixed random seed. The expression for the function induced by the  $\delta$ -disturbed MLP,  $\eta_{\theta,\delta}(\cdot)$ , is  $\forall \mathbf{x} \in \mathbb{R}^2$ ,

$$\eta_{\theta,\delta}(\mathbf{x}) = \mathbf{w}_{\text{hidden}}^T \cdot \sigma((\mathbf{W}_{\text{in}} + \delta_{\mathbf{W}}) \cdot \mathbf{x} + \mathbf{b}_{\text{in}}) + b_{\text{hidden}}, \quad (\text{H.21})$$

Table H.1: Nominal parameters of the MLP system.

Parameter	Value	Parameter	Value
$w_{11}$	-0.66612	$w_{12}$	-0.13874
$w_{21}$	-0.33963	$w_{22}$	-0.18860
$b_1$	-0.62466	$b_2$	0.28375
$w_1^h$	-0.63385	$w_2^h$	-0.04506
$b_{\text{hidden}}$	0.24580		

where  $\sigma(\cdot)$  is a LeakyReLU activation function with positive and negative slope of 1 and 0.01, respectively [61], and  $\mathbf{W}_{\text{in}}$ ,  $\delta_{\mathbf{W}}$ ,  $\mathbf{b}_{\text{in}}$ , and  $\mathbf{w}_{\text{hidden}}$  are such that

$$\mathbf{W}_{\text{in}} = \begin{pmatrix} w_{11} & w_{12} \\ w_{21} & w_{22} \end{pmatrix}, \quad (\text{H.22})$$

$$\delta_{\mathbf{W}} = \begin{pmatrix} \delta_1 & \delta_2 \\ 0 & 0 \end{pmatrix}, \quad (\text{H.23})$$

$$\mathbf{b}_{\text{in}} = \begin{pmatrix} b_1 & b_2 \end{pmatrix}^T, \quad (\text{H.24})$$

$$\mathbf{w}_{\text{hidden}} = \begin{pmatrix} w_1^h & w_2^h \end{pmatrix}^T. \quad (\text{H.25})$$

The values of the nominal parameters shown in (H.21)–(H.25) for the fixed random seed we used in our numeric analysis can be found (up to five decimals) in Table H.1.

With respect to the noise model,  $h(\cdot)$  is the identity function, i.e.,  $\forall w \in \mathbb{R}, h(w) = w$ . In conclusion, the (actual) output (H.26), nominal output (H.27) and residual (H.28), correspond  $\forall j \in \{1, 2, \dots, n\}$  to

$$Y_j^{[\delta]} = \mathbf{w}_{\text{hidden}}^T \cdot \sigma((\mathbf{W}_{\text{in}} + \delta_{\mathbf{W}}) \cdot X_j + \mathbf{b}_{\text{in}}) + b_{\text{hidden}} + W_j, \quad (\text{H.26})$$

$$\eta_{\theta}(X_j) = \mathbf{w}_{\text{hidden}}^T \cdot \sigma(\mathbf{W}_{\text{in}} \cdot X_j + \mathbf{b}_{\text{in}}) + b_{\text{hidden}}, \quad (\text{H.27})$$

$$R_j^{[\delta]} = \mathbf{w}_{\text{hidden}}^T \cdot \left[ \sigma((\mathbf{W}_{\text{in}} + \delta_{\mathbf{W}}) \cdot X_j + \mathbf{b}_{\text{in}}) - \sigma(\mathbf{W}_{\text{in}} \cdot X_j + \mathbf{b}_{\text{in}}) \right] + W_j. \quad (\text{H.28})$$

### Appendix H.1.2. Autoregressive Systems

Autoregressive (AR) systems treated in our experiments are a modification of Def. 4 that is described by the following recursive formula  $\forall j \in \{1, 2, \dots, n\}$ :<sup>30</sup>

$$D_j^{[\delta]} = \eta_{\theta,\delta}(D_{j-1}^{[\delta]}, U_j) + H_j, \quad (\text{H.29})$$

$$Y_j^{[\delta]} = D_j^{[\delta]} + W_j, \quad (\text{H.30})$$

where the r.v.s  $U$ ,  $H$ , and  $W$  are the exogenous input, model noise, and measurement noise, respectively. Let us note that the system output is  $Y_j^{[\delta]}$ , so the inner state of the system ( $D_j^{[\delta]}$ ) is not accessible without measurement noise contamination; hence, our input for the nominal model,  $\eta_{\theta}(\cdot)$ , corresponds to

<sup>30</sup>We consider the special cases  $D_0 \equiv d_0$  (see Table H.2) and  $W_0 \equiv 0$ .

$X_j^{[\delta]} = (Y_{j-1}^{[\delta]}, U_j)$ . This said, the nominal output corresponds to  $\eta_\theta(X_j^{[\delta]})$ ; hence, the residual corresponds to

$$R_j^{[\delta]} \equiv Y_j^{[\delta]} - \eta_\theta(X_j^{[\delta]}) = \eta_{\theta,\delta}(D_{j-1}^{[\delta]}, U_j) - \eta_\theta(Y_{j-1}^{[\delta]}, U_j) + H_j + W_j. \quad (\text{H.31})$$

*ARX System.* The linear autoregressive system with exogenous input (ARX) is similar to the Linear system, but rather than a full exogenous input, one component of its input is a previous step of the system state. The expression of  $\eta_{\theta,\delta}(\cdot)$  is as follows  $\forall (d, u) \in \mathbb{R}^2$ :

$$\eta_{\theta,\delta}(d, u) = (c_1 + \delta_1)d + (c_2 + \delta_2)u. \quad (\text{H.32})$$

In consequence, the (actual) output (H.33), nominal output (H.34), and residual (H.35) correspond  $\forall j \in \{1, 2, \dots, n\}$  to

$$Y_j^{[\delta]} = (c_1 + \delta_1)D_{j-1}^{[\delta]} + (c_2 + \delta_2)U_j + H_j + W_j, \quad (\text{H.33})$$

$$\eta_\theta(X_j^{[\delta]}) = c_1(D_{j-1}^{[\delta]} + W_{j-1}) + c_2U_j, \quad (\text{H.34})$$

$$R_j^{[\delta]} = \delta_1 D_{j-1}^{[\delta]} + \delta_2 U_j - c_1 W_{j-1} + H_j + W_j. \quad (\text{H.35})$$

*NARX System.* The non-linear autoregressive system with exogenous input (NARX) is a system with a non-linear relationship between the current output and the AR input (previous output and exogenous input). The expression of  $\eta_{\theta,\delta}(\cdot)$  is as follows  $\forall (d, u) \in \mathbb{R}^2$ :

$$\eta_\delta(d, u) = (c_3 + \delta_1 + c_4 \exp(-d^2)) \cdot d + (c_5 + \delta_2) \cdot u^2. \quad (\text{H.36})$$

In consequence, the (actual) output (H.37) and nominal output (H.38), correspond  $\forall j \in \{1, 2, \dots, n\}$  to

$$Y_j^{[\delta]} = (c_3 + \delta_1 + c_4 \exp(-(D_{j-1}^{[\delta]})^2)) \cdot D_{j-1}^{[\delta]} + (c_5 + \delta_2) \cdot U_j^2 + H_j + W_j, \quad (\text{H.37})$$

$$\eta_\theta(X_j^{[\delta]}) = (c_3 + c_4 \exp(-(D_{j-1}^{[\delta]} + W_{j-1})^2)) \cdot (D_{j-1}^{[\delta]} + W_{j-1}) + c_5 \cdot U_j^2. \quad (\text{H.38})$$

The residual expression ( $R_j^{[\delta]}$ ) can be obtained by replacing (H.37) and (H.38) in (H.31).

## Appendix H.2. Model Drift Quantification Methods

Here, we describe the methods we use for quantifying model drift; these methods were applied to all systems, as seen in Fig. 3 and Fig. 4. One of these methods corresponds to our MI-based RIV method, and the other two are baselines we use to compare our method. To quantify model drift, the RIV and Correlation methods have the input-residual sampling ( $\mathbf{J}_n^{[\delta]}$ ) as their own input, while the RMSE method only considers the residual sampling ( $\mathbf{R}_n^{[\delta]}$ ) as its input.

### Appendix H.2.1. RIV Method

This method is our methodological contribution, and as detailed in Sec. 4, a RIV corresponds to the MI estimation between the input and the residual with the MI estimator presented in [40]. An explanation of how this MI estimation is computed is shown in Sec. 4.2. Formally, given a sampling  $\mathbf{J}_n^{[\delta]}$ , we compute  $I_{b_n, d_n}^{\lambda, n}(\mathbf{J}_n^{[\delta]})$ , where  $\lambda = 2.3 \cdot 10^{-5}$ ,  $d_n = \exp(n^{-1/3})$ ,  $b_n = wn^{-l}$  with  $w = 5 \cdot 10^{-2}$  and  $l = 0.167$ , and  $n = 2000$ .

Table H.2: Constant coefficient values for the numerical analysis.

Coefficient	Value	Coefficient	Value
$a_U$	-2.0	$c_3$	0.8
$b_U$	2.0	$c_4$	-0.5
$\mu_S$	0.5	$c_5$	1.0
$\sigma_S$	$2\sqrt{3}/3$	$A$	1.0
$\mu_H$	0.0	$\phi$	0.0
$\sigma_H$	0.1	$d_0$	0.0
$a_W$	-0.1	$k$	1.0
$b_W$	0.1	$A_W$	1.5
$c_1$	0.6	$f_W$	1.0
$c_2$	-0.4	$\phi_W$	0.0

### Appendix H.2.2. Correlation Method

This method corresponds to the maximum absolute value of the Pearson correlation coefficient of the residual with both coordinates of the input; we denote this as

$$\text{MAPC}(\mathbf{J}_n^{[\delta]}) \equiv \max\{|\text{corr}(\mathbf{X}_{n,(1)}^{[\delta]}, \mathbf{R}_n^{[\delta]})|, |\text{corr}(\mathbf{X}_{n,(2)}^{[\delta]}, \mathbf{R}_n^{[\delta]})|\}, \quad (\text{H.39})$$

where we denote  $\forall j \in \{1, 2, \dots, n\}$ ,  $X_j^{[\delta]} \equiv (X_{j,(1)}^{[\delta]}, X_{j,(2)}^{[\delta]})$ ,  $\mathbf{X}_{n,(1)}^{[\delta]} \equiv (X_{j,(1)}^{[\delta]})_{j=1}^n$ , and  $\mathbf{X}_{n,(2)}^{[\delta]} \equiv (X_{j,(2)}^{[\delta]})_{j=1}^n$ ; and  $\text{corr}(\cdot, \cdot)$  is a mapping such that for two arbitrary vectors  $\mathbf{x} = (x_j)_{j=1}^n \in \mathbb{R}^n$  and  $\mathbf{r} = (r_j)_{j=1}^n \in \mathbb{R}^n$ , their Pearson correlation coefficient is expressed by

$$\text{corr}(\mathbf{x}, \mathbf{r}) \equiv \frac{\sum_{j=1}^n (x_j - \bar{x})(r_j - \bar{r})}{\left[ \left( \sum_{j=1}^n (x_j - \bar{x})^2 \right) \cdot \left( \sum_{j=1}^n (r_j - \bar{r})^2 \right) \right]^{1/2}}, \quad (\text{H.40})$$

where  $\bar{x} = \frac{1}{n} \sum_{j=1}^n x_j$  and  $\bar{r} = \frac{1}{n} \sum_{j=1}^n r_j$ .

### Appendix H.2.3. RMSE Method

This method corresponds to the empirical root mean squared error computed from the residual; we denote this as  $\text{RMSE}(\mathbf{R}_n^{[\delta]})$ , which can be expressed as

$$\text{RMSE}(\mathbf{R}_n^{[\delta]}) \equiv \sqrt{\frac{1}{n} \sum_{j=1}^n (R_j^{[\delta]})^2}. \quad (\text{H.41})$$

## Appendix H.3. Summary of Figure 3 and Figure 4

With all the elements described in this section, we summarize the description of Fig. 3 and Fig. 4. These figures contain 12 and 6 colormaps, respectively. Each figure is divided into 3 rows; Fig. 3 and Fig. 4 are divided into 4 and 2 columns, respectively. The rows correspond to results for each one of the methods described in Sec. Appendix H.2, and the columns correspond to results for each one of the systems described in Sec. Appendix H.1. The correspondence is made clear in the labels of each row and column.

Each colormap is a visualization of a matrix. Each cell of these matrices is related to a single  $\delta = (\delta_1, \delta_2)$  value where both  $\delta_1$  and  $\delta_2$  range from -0.15 to 0.15 with a step of 0.0015;

i.e., each matrix has  $201 \cdot 201 = 40\,401$  cells. The value of the cell corresponds to the average value of applying the corresponding method to a sampling  $\mathbf{J}_n^{[\delta]}$  or  $\mathbf{R}_n^{[\delta]}$ , respectively, of the corresponding  $\delta$ -drifted system; this average value is obtained over 10 different random seeds.

## Appendix I. Error-Bar Analysis of Model Drift Experiment on Synthetic Distribution Drifts

In this section, we perform an error-bar analysis for the experiment conducted in Sec. 7. This error analysis is summarized in Fig. I.1, which contains figures analogous to Fig. 3 and Fig. 4 (Fig. I.1a and Fig. I.1b, respectively) with the only difference of reporting the standard deviation instead of the average value.

First, we can see that all the colormaps shown in Fig. I.1 display standard deviation values of at least one order of magnitude smaller than the average values reported in Fig. 3 and Fig. 4; this validates the consistency of our results over different seeds, and in consequence, validates our discussion and interpretation of the results. Moreover, this consistency strengthens the numerical validation of our RIV method for detecting model drift.

We remark on two elements seen in Fig. I.1 regarding our method. First, we can see regions of zero empirical standard deviation at the regions where zero average estimated MI was reported in Fig. 3 and Fig. 4; this has to do with the exponentially fast decision convergence of our method on the null hypothesis (Theorem 3). Second, we highlight that outside the regions with zero estimated MI, there is no clear increase or decrease of standard deviation as we go farther from  $\delta = \mathbf{0}$ ; we understand this as a display of uniform consistency of our method regardless of the drift characteristics.

## Appendix J. Supporting Result — Proof of Lemma 2

Lemma 2 states that if any random variable ( $U$ ) has a degenerate distribution, i.e., the measure it induces only takes values in 1 or 0, then this r.v. is collapsed to a single mass point, i.e., it is deterministic in the sense that  $\exists \mathbf{c} \in \mathbb{R}^r : \mathbb{P}(U = \mathbf{c}) = 1$ .

**PROOF OF LEMMA 2.** Before starting this proof, we need to state some minor definitions. Let us consider a pair of arbitrary vectors  $\mathbf{a} = (a_j)_{j=1}^r \in \mathbb{R}^r$  and  $\mathbf{b} = (b_j)_{j=1}^r \in \mathbb{R}^r$  such that  $\forall j \in \{1, 2, \dots, r\}$ ,  $a_j < b_j$  for an arbitrary  $r \in \mathbb{N}$ , and let us define the rectangle whose main opposite vertices are  $\mathbf{a}$  and  $\mathbf{b}$  as  $I_{\mathbf{a}, \mathbf{b}} \equiv \times_{j=1}^r [a_j, b_j] \in \mathcal{B}(\mathbb{R}^r)$ .

The idea of this proof is to build a sequence of nested rectangle-based partitions and note that we can define a sequence of sets that converges to a singleton such that each of its elements has a probability measure of 1. The value in the singleton of convergence of the sequence will correspond to the single deterministic point to which the r.v. is almost surely equal.

We start by partitioning  $I_{\mathbf{a}, \mathbf{b}}$  in dyadic rectangles. For this purpose, let us consider any pair  $(a, b) \in \mathbb{R}^2$  which defines an interval such that  $a < b$ ; then, we can get the set that contains both pair of values that define each dyadic sub-intervals

of the original interval by using a mapping  $d_y : \mathbb{R}^2 \rightarrow \mathcal{B}(\mathbb{R}^2)$  such that  $d_y(a, b) = \{(a, (a+b)/2), ((a+b)/2, b)\}$ ;<sup>31</sup> using this mapping, we can define the partition of  $I_{\mathbf{a}, \mathbf{b}}$  as  $P_{\mathbf{a}, \mathbf{b}} \equiv \{\times_{j=1}^r [x_j, y_j] : \forall j \in \{1, 2, \dots, r\}, (x_j, y_j) \in d_y(a_j, b_j)\}$ . Let us note that  $P_{\mathbf{a}, \mathbf{b}}$  partitions the rectangle  $I_{\mathbf{a}, \mathbf{b}}$  into  $2^r$  smaller rectangles with half the side of the original.

Another definition we are interested in for operating in our sequence of sets is their *generalized diagonal*. If we consider  $d_E$  as the Euclidean distance, then  $(\mathbb{R}^r, d_E)$  is a metric space, and we can define the generalized diagonal (GD) of every non-empty set  $S \subseteq \mathbb{R}^r$  as  $\text{diag}(S) \equiv \sup_{(x, y) \in S^2} d_E(x, y)$ . Let us note that  $\text{diag}(I_{\mathbf{a}, \mathbf{b}}) = \sqrt{\sum_{j=1}^r (b_j - a_j)^2}$ , and that for every  $S \in P_{\mathbf{a}, \mathbf{b}}$ ,

its GD is  $\text{diag}(S) = \sqrt{\sum_{j=1}^r ((b_j - a_j)/2)^2} = \text{diag}(I_{\mathbf{a}, \mathbf{b}})/2$ .

As we are dealing with a r.v. ( $U$ ) such that  $\forall A \in \mathcal{B}(\mathbb{R}^r)$ ,  $\mathbb{P}(U \in A) \in \{0, 1\}$ ; we need to note that if we have an arbitrary set  $I$  and a partition  $P$  of it, then<sup>32</sup>

$$[\mathbb{P}(U \in I) = 1] \Rightarrow [\exists! B \in P : \mathbb{P}(U \in B) = 1]. \quad (\text{J.1})$$

Moving now to the core of our proof, if we denote  $\mathbf{1} \equiv (1)_{j=1}^r \in \mathbb{R}^r$ , we can see that  $\{I_{\mathbf{k}, \mathbf{k}+\mathbf{1}}\}_{\mathbf{k} \in \mathbb{Z}^r}$  is a partition of  $\mathbb{R}^r$ , and from (J.1), there exists a unique  $\mathbf{m} \in \mathbb{Z}^r$  such that  $\mathbb{P}(I_{\mathbf{m}, \mathbf{m}+\mathbf{1}}) = 1$ . Then, we can build a sequence of rectangles  $(I_{\mathbf{a}_n, \mathbf{b}_n})_{n \in \mathbb{N}}$  such that  $(\mathbf{a}_1, \mathbf{b}_1) = (\mathbf{m}, \mathbf{m} + \mathbf{1})$  and  $(\mathbf{a}_{n+1}, \mathbf{b}_{n+1})$  corresponds to the unique element in the singleton  $\{(\mathbf{x}, \mathbf{y}) \in \mathbb{R}^{r+r} : [I_{\mathbf{x}, \mathbf{y}} \in P_{\mathbf{a}_n, \mathbf{b}_n} \wedge \mathbb{P}(U \in I_{\mathbf{x}, \mathbf{y}}) = 1]\}$ . This means that the  $(n+1)$ -th term of the sequence corresponds to the unique rectangle with a probability measure of 1 within the ones generated by the dyadic partition of the rectangle that corresponds to the  $n$ -th term.

We are interested in defining a sequence of closed sets such that each element has a probability measure of 1. The idea for this sequence is to converge to a singleton and use the continuity of the probability measure to conclude that this singleton has a probability measure of 1. To deal with closed sets, we will consider the closed rectangle as the closure of an (open) rectangle, i.e.,  $\text{cl}(I_{\mathbf{a}, \mathbf{b}}) \equiv \times_{j=1}^r [a_j, b_j] \in \mathcal{B}(\mathbb{R}^r)$ . Then, it is possible to define the sequence of sets  $(C_n)_{n \in \mathbb{N}}$ , where  $\forall n \in \mathbb{N}$ ,  $C_n = \text{cl}(I_{\mathbf{a}_n, \mathbf{b}_n})$ ; this sequence satisfies the following properties  $\forall n \in \mathbb{N}$ :

$$[\mathbb{P}(U \in C_n) = 1] \wedge [C_{n+1} \subseteq C_n] \wedge [C_n \text{ is a closed set}]. \quad (\text{J.2})$$

One additional property of  $(C_n)_{n \in \mathbb{N}}$ , is that  $\text{diag}(C_1) = \sqrt{r}$  and  $\text{diag}(C_{n+1}) = \text{diag}(C_n)/2$  as  $I_{\mathbf{a}_{n+1}, \mathbf{b}_{n+1}} \in P_{\mathbf{a}_n, \mathbf{b}_n}$ . In consequence,  $\forall n \in \mathbb{N}$ ,  $\text{diag}(C_n) = \sqrt{r}/2^{n-1}$ , and in particular, we have that

<sup>31</sup>We remark, to avoid confusion, that both  $(a, (a+b)/2)$  and  $((a+b)/2, b)$  in  $d_y(a, b)$  are coordinate pairs in  $\mathbb{R}^2$  and not open intervals. Moreover, it is easy to see that any interval defined by  $(a, b)$  has length  $b - a$ , and any interval defined by  $(x, y) \in d_y(a, b)$  has length  $(b - a)/2$ .

<sup>32</sup>Equation (J.1) can be proven by noting that  $\mathbb{P}(U \in I) = \sum_{S \in P} \mathbb{P}(U \in S)$ . Existence of  $B$  can be proven easily, as else it would be satisfied that  $\forall S \in P, \mathbb{P}(S \in U) = 0$ , which, in turn, would imply that  $\mathbb{P}(U \in I) = 0$ , and consequently, contradicting  $\mathbb{P}(U \in I) = 1$ . Uniqueness can be proven by contradiction; if we consider  $B_1 \in P$  and  $B_2 \in P$  such that  $\mathbb{P}(U \in B_1) = \mathbb{P}(U \in B_2) = 1$ , this would imply that  $\mathbb{P}(U \in I) \geq \mathbb{P}(U \in B_1) + \mathbb{P}(U \in B_2) = 2$ , which is a contradiction.

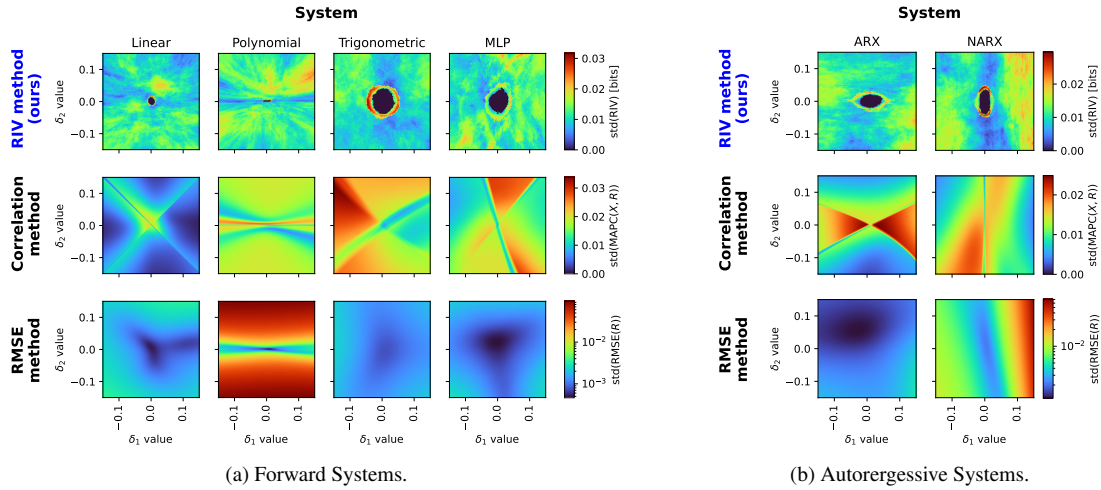


Figure I.1: Standard deviations for the numerical results of our RIV method and baselines on parametrized drifts.

$\lim_{n \rightarrow \infty} \text{diag}(C_n) = 0$ . This last limit, in addition to  $(C_n)_{n \in \mathbb{N}}$  being a sequence of nested closed non-empty sets – see (J.2) – enables us to infer from Cantor’s Intersection Theorem [62, Theorem C, Sec. 2.12] that there exists  $\mathbf{c} \in \mathbb{R}^r$  such that  $\bigcap_{i=1}^{\infty} C_i = \{\mathbf{c}\}$ . Then, we can see that

$$\mathbb{P}(U = \mathbf{c}) = \mathbb{P}(U \in \{\mathbf{c}\}) = \mathbb{P}\left(U \in \bigcap_{k=1}^{\infty} C_k\right), \quad (\text{J.3})$$

where the last term, due to the continuity of the probability measure  $\mathbb{P}$  and the set-theoretic definition of limit [60], can be expressed as

$$\mathbb{P}\left(U \in \bigcap_{k=1}^{\infty} C_k\right) = \mathbb{P}\left(U \in \lim_{n \rightarrow \infty} \bigcap_{k=1}^n C_k\right) = \lim_{n \rightarrow \infty} \mathbb{P}\left(U \in \bigcap_{k=1}^n C_k\right). \quad (\text{J.4})$$

From the nested property of  $(C_n)_{n \in \mathbb{N}}$  shown in (J.2), it is implied that  $\forall n \in \mathbb{N}$ ,

$$\bigcap_{k=1}^n C_k = C_n. \quad (\text{J.5})$$

As a last step, let us note that

$$\begin{aligned} & \mathbb{P}(U = \mathbf{c}) \\ &= \mathbb{P}\left(U \in \bigcap_{k=1}^{\infty} C_k\right) \end{aligned} \quad (\text{J.6})$$

$$= \lim_{n \rightarrow \infty} \mathbb{P}\left(U \in \bigcap_{k=1}^n C_k\right) \quad (\text{J.7})$$

$$= \lim_{n \rightarrow \infty} \mathbb{P}(U \in C_n) \quad (\text{J.8})$$

$$= \lim_{n \rightarrow \infty} 1 = 1, \quad (\text{J.9})$$

where (J.6), (J.7), (J.8), and (J.9) come from (J.3), (J.4), (J.5) and the first property shown in (J.2), respectively.

At this point, we have shown the existence of  $\mathbf{c} \in \mathbb{R}^r$  such that  $\mathbb{P}(U = \mathbf{c}) = 1$ , which was precisely what is stated in Lemma 2. Hence, concluding our proof.  $\square$

## Acknowledgements

This material is based on work supported by grants of CONICYT-Chile, Fondecyt 1210315, and the Advanced Center for Electrical and Electronic Engineering, Basal Project FB0008. Camilo Ramírez is supported by ANID-Subdirección de Capital Humano/Magíster-Nacional/2023 - 22230232 master’s scholarship. The work of Marcos Orchard is supported by grants of CONICYT-Chile, Fondecyt 1210031. We thank Diane Greenstein and Sebastián Espinoza for editing and proofreading all this material.

## References

- [1] M. Kordestani, M. Saif, M. E. Orchard, R. Razavi-Far, K. Khorasani, Failure prognosis and applications—a survey of recent literature, *IEEE transactions on reliability* 70 (2) (2019) 728–748. doi:10.1109/TR.2019.2930195.
- [2] V. Atamuradov, K. Medjaher, P. Dersin, B. Lamoureux, N. Zerhouni, Prognostics and health management for maintenance practitioners—review, implementation and tools evaluation, *International Journal of Prognostics and Health Management* 8 (3) (2017) 1–31. doi:10.36001/ijphm.2017.v8i3.2667.
- [3] C. Song, K. Liu, X. Zhang, Integration of data-level fusion model and kernel methods for degradation modeling and prognostic analysis, *IEEE Transactions on Reliability* 67 (2) (2017) 640–650. doi:10.1109/TR.2017.2715180.
- [4] A. Abid, M. T. Khan, J. Iqbal, A review on fault detection and diagnosis techniques: basics and beyond, *Artificial Intelligence Review* 54 (2021) 3639–3664. doi:10.1007/s10462-020-09934-2.
- [5] D. Miljković, Fault detection methods: A literature survey, in: 2011 Proceedings of the 34th international convention MIPRO, IEEE, 2011, pp. 750–755.
- [6] R. J. Patton, J. Chen, Robust fault detection of jet engine sensor systems using eigenstructure assignment, *Journal of Guidance, Control, and Dynamics* 15 (6) (1992) 1491–1497. doi:10.2514/3.11413.
- [7] P. M. Frank, Fault diagnosis in dynamic systems using analytical and knowledge-based redundancy: A survey and some new results, *Automatica* 26 (3) (1990) 459–474. doi:10.1016/0005-1098(90)90018-D.
- [8] T. Escobet, L. Travé-Massuyès, Parameter estimation methods for fault detection and isolation, in: *Bridge Workshop Notes*, Vol. 40, 2001, pp. 1–11.

- [9] H. Li, Y. Gao, P. Shi, H.-K. Lam, Observer-based fault detection for nonlinear systems with sensor fault and limited communication capacity, *IEEE Transactions on Automatic Control* 61 (9) (2015) 2745–2751. doi:10.1109/TAC.2015.2503566.
- [10] M. Said, R. Fazai, K. Ben Abdellafou, O. Taouali, Decentralized fault detection and isolation using bond graph and PCA methods, *The international journal of advanced manufacturing technology* 99 (2018) 517–529. doi:10.1007/s00170-018-2526-4.
- [11] M. P. Fantì, A. M. Mangini, W. Ukovich, Fault detection by labeled petri nets in centralized and distributed approaches, *IEEE Transactions on Automation Science and Engineering* 10 (2) (2012) 392–404. doi:10.1109/TASE.2012.2203596.
- [12] S. M. Tabatabaeipour, Active fault detection and isolation of discrete-time linear time-varying systems: a set-membership approach, *International Journal of Systems Science* 46 (11) (2015) 1917–1933. doi:10.1080/00207721.2013.843213.
- [13] C. Jauberthie, N. Verdière, L. Travé-Massuyès, Fault detection and identification relying on set-membership identifiability, *Annual Reviews in Control* 37 (1) (2013) 129–136. doi:10.1016/j.arcontrol.2013.04.002.
- [14] S. M. Tabatabaeipour, P. F. Odgaard, T. Bak, J. Stoustrup, Fault detection of wind turbines with uncertain parameters: A set-membership approach, *Energies* 5 (7) (2012) 2424–2448. doi:10.3390/en5072424.
- [15] B. Mu, X. Yang, J. K. Scott, Comparison of advanced set-based fault detection methods with classical data-driven and observer-based methods for uncertain nonlinear processes, *Computers & Chemical Engineering* 166 (2022) 107975. doi:10.1016/j.compchemeng.2022.107975.
- [16] F. Tamssaouet, K. T. Nguyen, K. Medjaher, M. E. Orchard, System-level failure prognostics: Literature review and main challenges, *Proceedings of the Institution of Mechanical Engineers, Part O: Journal of Risk and Reliability* 237 (3) (2023) 524–545. doi:10.1177/1748006X221118448.
- [17] K. T. P. Nguyen, Feature engineering and health indicator construction for fault detection and diagnostic, in: K. P. Tran (Ed.), *Control Charts and Machine Learning for Anomaly Detection in Manufacturing*, Springer, 2022, pp. 243–269. doi:10.1007/978-3-030-83819-5\_10.
- [18] S. Cheng, M. H. Azarian, M. G. Pecht, Sensor systems for prognostics and health management, *Sensors* 10 (6) (2010) 5774–5797. doi:10.3390/s100605774.
- [19] X. Ding, P. M. Frank, Frequency domain approach and threshold selector for robust model-based fault detection and isolation, in: *Fault Detection, Supervision and Safety for Technical Processes 1991*, Elsevier, 1992, pp. 271–276. doi:10.1016/B978-0-08-041275-7.50041-7.
- [20] S.-A. Raka, C. Combastel, Fault detection based on robust adaptive thresholds: A dynamic interval approach, *Annual Reviews in Control* 37 (1) (2013) 119–128. doi:10.1016/j.arcontrol.2013.04.001.
- [21] Z. Wang, H. Shang, Kalman filter based fault detection for two-dimensional systems, *Journal of Process Control* 28 (2015) 83–94. doi:10.1016/j.jprocont.2015.03.002.
- [22] S. Yoon, J. F. MacGregor, Statistical and causal model-based approaches to fault detection and isolation, *AIChE Journal* 46 (9) (2000) 1813–1824. doi:10.1002/aic.690460910.
- [23] J. Guo, X. Wang, Y. Li, kNN based on probability density for fault detection in multimodal processes, *Journal of Chemometrics* 32 (7) (2018) e3021. doi:10.1002/cem.3021.
- [24] P. Santos, L. F. Villa, A. Reñones, A. Bustillo, J. Maudes, An SVM-based solution for fault detection in wind turbines, *Sensors* 15 (3) (2015) 5627–5648. doi:10.3390/s150305627.
- [25] A. A. A. Mohd Amiruddin, H. Zabiri, S. A. A. Taqvi, L. D. Tufa, Neural network applications in fault diagnosis and detection: an overview of implementations in engineering-related systems, *Neural Computing and Applications* 32 (2020) 447–472. doi:10.1007/s00521-018-3911-5.
- [26] R. Iqbal, T. Maniak, F. Doctor, C. Karyotis, Fault detection and isolation in industrial processes using deep learning approaches, *IEEE Transactions on Industrial Informatics* 15 (5) (2019) 3077–3084. doi:10.1109/TII.2019.2902274.
- [27] R. Zhao, R. Yan, Z. Chen, K. Mao, P. Wang, R. X. Gao, Deep learning and its applications to machine health monitoring, *Mechanical Systems and Signal Processing* 115 (2019) 213–237. doi:10.1016/j.ymsp.2018.05.050.
- [28] L. E. Holloway, B. H. Krogh, Fault detection and diagnosis in manufacturing systems: a behavioral model approach, in: [1990] *Rensselaer's Second International Conference on Computer Integrated Manufacturing*, IEEE Computer Society, 1990, pp. 252–253. doi:10.1109/CIM.1990.128107.
- [29] J. Gama, P. Medas, G. Castillo, P. Rodrigues, Learning with drift detection, in: *Advances in Artificial Intelligence—SBIA 2004*, Springer, 2004, pp. 286–295. doi:10.1007/978-3-540-28645-5\_29.
- [30] M. H. Ardakani, M. Askarian, G. Escudero, M. Graells, A. Espuna, Toward online explore of concept drift for fault detection of chemical processes, in: *Computer Aided Chemical Engineering*, Vol. 40, Elsevier, 2017, pp. 1657–1662. doi:10.1016/B978-0-444-63965-3.50278-6.
- [31] J. Gama, I. Žliobaitė, A. Bifet, M. Pechenizkiy, A. Bouchachia, A survey on concept drift adaptation, *ACM computing surveys* 46 (4) (2014) 1–37. doi:10.1145/2523813.
- [32] J. Lu, A. Liu, F. Dong, F. Gu, J. Gama, G. Zhang, Learning under concept drift: A review, *IEEE transactions on knowledge and data engineering* 31 (12) (2018) 2346–2363. doi:10.1109/TKDE.2018.2876857.
- [33] M. Lima, M. Neto, T. S. Filho, R. A. de A. Fagundes, Learning under concept drift for regression—a systematic literature review, *IEEE Access* 10 (2022) 45410–45429. doi:10.1109/ACCESS.2022.3169785.
- [34] J. G. Moreno-Torres, T. Raeder, R. Alaiz-Rodríguez, N. V. Chawla, F. Herrera, A unifying view on dataset shift in classification, *Pattern recognition* 45 (1) (2012) 521–530. doi:10.1016/j.patcog.2011.06.019.
- [35] Y. Yamanaka, T. Iwata, H. Takahashi, M. Yamada, S. Kanai, Autoencoding binary classifiers for supervised anomaly detection, in: *PRICAI 2019: Trends in Artificial Intelligence*, Springer, 2019, pp. 647–659. doi:10.1007/978-3-030-29911-8\_50.
- [36] M. A. Bansal, D. R. Sharma, D. M. Kathuria, A systematic review on data scarcity problem in deep learning: Solution and applications, *ACM Computing Surveys* 54 (10s) (2022) 1–29. doi:10.1145/3502287.
- [37] A. Bifet, R. Gavaldà, Learning from time-changing data with adaptive windowing, in: *Proceedings of the 2007 SIAM international conference on data mining*, SIAM, 2007, pp. 443–448. doi:10.1137/1.9781611972771.42.
- [38] K. Nishida, K. Yamauchi, Detecting concept drift using statistical testing, in: *International conference on discovery science*, Springer, 2007, pp. 264–269. doi:10.1007/978-3-540-75488-6\_27.
- [39] T. M. Cover, J. A. Thomas, *Elements of Information Theory*, 2nd Edition, Wiley Interscience, New York, 2005. doi:10.1002/047174882X.
- [40] J. F. Silva, S. Narayanan, Complexity-regularized tree-structured partition for mutual information estimation, *IEEE transactions on information theory* 58 (3) (2012) 1940–1952. doi:10.1109/TIT.2011.2177771.
- [41] M. Arias Chao, C. Kulkarni, K. Goebel, O. Fink, Aircraft engine run-to-failure detection under real flight conditions for prognostics and diagnostics, *Data* 6 (1) (2021) 5. doi:10.3390/data6010005.
- [42] S. Verron, T. Tiplica, A. Kobi, Fault detection and identification with a new feature selection based on mutual information, *Journal of Process Control* 18 (5) (2008) 479–490. doi:10.1016/j.jprocont.2007.08.003.
- [43] M. M. Rashid, J. Yu, A new dissimilarity method integrating multidimensional mutual information and independent component analysis for non-gaussian dynamic process monitoring, *Chemometrics and Intelligent Laboratory Systems* 115 (2012) 44–58. doi:10.1016/j.chemolab.2012.04.008.
- [44] B. Jiang, W. Sun, R. D. Braatz, An information-theoretic framework for fault detection evaluation and design of optimal dimensionality reduction methods, *IFAC-PapersOnLine* 51 (24) (2018) 1311–1316. doi:10.1016/j.ifacol.2018.09.565.
- [45] F. Lv, S. Yu, C. Wen, J. C. Principe, Interpretable fault detection using projections of mutual information matrix, *Journal of the Franklin Institute* 358 (7) (2021) 4028–4057. doi:10.1016/j.jfranklin.2021.02.016.
- [46] M. M. Lazarescu, S. Venkatesh, H. H. Bui, Using multiple windows to track concept drift, *Intelligent data analysis* 8 (1) (2004) 29–59. doi:10.3233/IDA-2004-8103.
- [47] W. K. Newey, D. McFadden, Large sample estimation and hypothesis testing, *Handbook of econometrics* 4 (1994) 2111–2245. doi:10.1016/S1573-4412(05)80005-4.
- [48] E. L. Lehmann, J. P. Romano, *Testing statistical hypotheses*, 4th Edition,

- Springer, 2022. doi:10.1007/978-3-030-70578-7.
- [49] C. E. Shannon, A mathematical theory of communication, The Bell system technical journal 27 (3) (1948) 379–423. doi:10.1002/j.1538-7305.1948.tb01338.x.
- [50] R. Steuer, J. Kurths, C. O. Daub, J. Weise, J. Selbig, The mutual information: Detecting and evaluating dependencies between variables, Bioinformatics 18 (suppl\_2) (2002) S231–S240. doi:10.1093/bioinformatics/18.suppl\_2.S231.
- [51] T. Austin, Exchangeable random measures, Annales de l’Institut Henri Poincaré, Probabilités et Statistiques 51 (3) (2015) 842–861. doi:10.1214/13-AIHP584.
- [52] N. R. Draper, H. Smith, Applied regression analysis, 3rd Edition, John Wiley & Sons, 1998. doi:10.1002/9781118625590.
- [53] O. Kallenberg, Foundations of modern probability, Springer, 1997. doi:10.1007/b98838.
- [54] J. M. Mendel, Lessons in estimation theory for signal processing, communications, and control, Pearson Education, 1995.
- [55] K. J. Keesman, System identification: An introduction, Springer London, 2011. doi:10.1007/978-0-85729-522-4.
- [56] D. K. Frederick, J. A. DeCastro, J. S. Litt, User’s guide for the commercial modular aero-propulsion system simulation (C-MAPSS), Tech. Rep. E-16205, NASA (2007).
- [57] D. P. Kingma, J. Ba, Adam: A method for stochastic optimization, arXiv preprint arXiv:1412.6980 (2014). doi:10.48550/arXiv.1412.6980.
- [58] M. E. Gonzalez, J. F. Silva, M. Videla, M. E. Orchard, Data-driven representations for testing independence: Modeling, analysis and connection with mutual information estimation, IEEE Transactions on Signal Processing 70 (2021) 158–173. doi:10.1109/TSP.2021.3135689.
- [59] V. I. Bogachev, Measure theory, Springer, 2007. doi:10.1007/978-3-540-34514-5.
- [60] A. Gut, Probability: A graduate course, 2nd Edition, Springer, 2013. doi:10.1007/978-1-4614-4708-5.
- [61] A. L. Maas, A. Y. Hannun, A. Y. Ng, et al., Rectifier nonlinearities improve neural network acoustic models, in: Proceedings of the 30th International Conference on Machine Learning, Vol. 28, 2013, p. 3.
- [62] G. F. Simmons, Introduction to topology and modern analysis, McGraw Hill Book Company, 1963.